CATALYTIC OZONATION OF ACETONE AND TOLUENE ON ALUMINA-SUPPORTED MANGANESE OXIDE

A Thesis Submitted to the College of

Graduate and Postdoctoral Studies

In Partial Fulfillment of the Requirements

For the Degree of Doctor of Philosophy

In the Department of Chemical and Biological Engineering

University of Saskatchewan

Saskatoon

By

MOSTAFA AGHBOLAGHY

Permission to Use

In presenting this thesis in partial fulfillment of the requirements for a Postgraduate degree from the University of Saskatchewan, I agree that the Libraries of this University may make it freely available for inspection. I further agree that permission for copying of this thesis in any manner, in whole or in part, for scholarly purposes may be granted by the professor or professors who supervised my thesis work or, in their absence, by the Head of the Department or the Dean of the College in which my thesis work was done. It is understood that any copying or publication or use of this thesis or parts thereof for financial gain shall not be allowed without my written permission. It is also understood that due recognition shall be given to me and to the University of Saskatchewan in any scholarly use which may be made of any material in my thesis.

Requests for permission to copy or to make other uses of materials in this thesis in whole or part should be addressed to:

Head of the Department of Chemical and Biological Engineering
57 Campus Drive
University of Saskatchewan
Saskatoon, Saskatchewan S7N 5A9
Canada

OR

Dean
College of Graduate and Postdoctoral Studies
University of Saskatchewan
116 Thorvaldson Building, 110 Science Place
Saskatoon, Saskatchewan S7N 5C9
Canada

Abstract

Volatile organic compounds (VOCs) are important air pollutants that can have adverse health effects. Ozone-assisted catalytic oxidation (catalytic ozonation) is an effective technique for removal of VOCs from air. In this thesis, catalytic ozonation was used to remove two VOCs (acetone and toluene) from air by using γ-alumina-supported manganese oxide catalyst. This study addresses the nature and role of reaction intermediates, role of support, reaction kinetic and pathway, and removal of a binary mixture of VOCs. A combination of in situ diffuse reflectance infrared Fourier transform spectroscopy, X-ray spectroscopy techniques, and a number of temperature programmed analyses were used to achieve objectives of this investigation. Catalyst characterization showed that Mn_2O_3 was the dominant manganese phase of the catalyst. It was found that surface carboxylate intermediates were essential for an effective oxidation process, and they did not directly cause catalyst deactivation. Despite different chemical properties of acetone and toluene, surface carboxylates formed on alumina sites of the catalyst during catalytic ozonation of both VOCs. The presence of manganese sites was necessary for further oxidation of the surface carboxylates. At low reaction temperatures (e.g. 25 °C), undesired products such as acetic acid and formic acid accumulated on the surface of the catalyst and reduced the activity of the catalyst. Deactivation caused by these compounds could be reversed by heating the spent catalyst to 425 °C (under nitrogen flow) and desorbing the undesired products. Apparent activation energies of 33 and 40 kJ $mole^{-1}$ were obtained for catalytic ozonation of toluene and acetone, respectively. Catalytic ozonation of the binary mixture of acetone and toluene was favourable for toluene conversion, and repressive for acetone conversion. Increase of reaction

temperature (up to 90 °C) improved catalyst stability, increased removal of both VOCs, enhanced CO_x yield, and decreased the gap between toluene and acetone conversions. Findings from this work were used to propose possible reaction pathways for catalytic ozonation of acetone and toluene.

Acknowledgments

First, I would like to express my sincere gratitude to my PhD supervisor, Dr. Jafar Soltan, for his continuous encouragement, guidance, and support during my PhD studies. I acknowledge I would not be able to pursue the PhD program to completion without scholarly and financial supports of Dr. Soltan. His patience and encouragement during difficulties of the research are greatly appreciated.

I warmly thank my advisory committee members (alphabetic order: Dr. Ning Chen, Dr. Mehdi Nemati, Dr. Catherine Niu, and Dr. Hui Wang) for their valuable comments and feedback. Their suggestions greatly helped to improve the quality of this research.

I appreciate valuable assistance of the technical staff in the Department of Chemical and Biological Engineering, especially Mr. RLee Prokopishyn and Mr. Richard Blondin who helped me with maintenance of the analyses instruments. Also, I would like to express my appreciation to Dr. Ebrahim Rezaei for exchanges of knowledge and skills during the first year of my PhD program.

I acknowledge the College of Graduate and Postdoctoral Studies, and the Department of Chemical and Biological Engineering of the University of Saskatchewan, the Natural Sciences and Engineering Research Council of Canada, and the Government of Saskatchewan for providing financial support for this research.

Last but not least, my deep appreciation and love goes to my mother, father, and wife, whose unconditional encouragements and support has made it possible for me to pursue my goals and overcome difficulties.

Table of Contents

Page

List of Tables

Page

List of Figures

Page

Nomenclature

Abbreviations

BET	Brunauer–Emmett–Teller
CLS	Canadian light source
CN	coordination number
DDT	dichlorodiphenyltrichloroethane
DFT	density functional theory
DLaTGS	deuterated L-alanine doped triglycine sulfate
DRIFTS	diffuse reflectance infrared Fourier transform spectroscopy
EPA	environmental protection agency
EXAFS	extended X-ray absorption fine-structure
FTIR	Fourier transform infrared
GC	gas chromatograph
HXMA	hard X-ray microanalysis
ICP-MS	inductively coupled plasma mass spectrometry
LCF	linear combination fitting
MCT	mercuric cadmium telluride
MS	mass spectrometer
NO_x	nitrogen oxide
PCB	polychlorinated biphenyl
PMs	particulate matters

REIXS	resonant elastic and inelastic X-ray scattering
SBS	sick building syndrome
SO_x	sulfur oxides
SVOC	semi-volatile organic compound
TPD	temperature programmed desorption
TPO	temperature programmed oxidation
UV	ultra violet
VOC	volatile organic compound
VVOC	very volatile organic compound
WHO	world health organization
WHSV	weight hour space velocity (L h^{-1} g^{-1})
XAFS	X-ray absorption fine structure
XANES	X-ray absorption near-edge structure
XPS	X-ray photoelectron spectroscopy

Parameters

A	frequency factor (pre-exponential factor)
D	reactor internal diameter (mm)
d_p	catalyst particle size (mm)
E_a	apparent activation energy (KJ $mole^{-1}$)
ΔE_o	change in energy scale in EXAFS analyses (eV)
F	molar flow rate (mole s^{-1})
k′	reaction rate constant

r'	reaction rate (mole kg^{-1} s^{-1})
R	distance of the neighboring atoms (Å)
R_f	absolute percentage misfit between data and EXAFS model
ΔR	change in interatomic distance (Å)
R^2	coefficient of determination of the regression analysis
S_o^2	amplitude reduction factor (-)
T	reaction temperature (K or °C)
W	catalyst weight (kg)
X	conversion (-)

Greek letters/prefixes

α	reaction order of toluene in catalytic ozonation of toluene
β	reaction order of ozone in catalytic ozonation of toluene
ν	reaction order of ozone in catalytic ozonation of acetone
π	pi bond
σ	sigma bond
σ^2	mean-square displacement of the bond length ($Å^2$)
o	ortho
ω	reaction order of acetone in catalytic ozonation of acetone

Superscripts

▲	alumina site
■	active site of a catalyst

●	silica site
*	manganese site
	graphene site

Subscripts

a	apparent
ace	acetone
in	inlet
tol	toluene

Chapter 1:
Introduction

In this chapter, a brief research background and motivation of this work will be discussed. Then, the structure of the thesis will be presented.

1.1. Research background and motivation

Nowadays, the problem of air pollution is growing fast because of the emission of pollutants from industrial plants, exhaust of cars and change in our lifestyle due to more urbanization. There are concerns about the quality of air in metropolitan cities leading to decrease in quality of life. Materials such as NO_x, SO_x, particulate matters (PMs) and volatile organic compounds (VOCs) are among the principal pollutants of environment with adverse health impacts on people [1,2]. The concern about air pollution is not restricted to the outdoor environment. It has been observed that even people inside buildings are prone to air pollution problems. It has been indicated that indoor air pollution in urban areas is responsible for about 14 times more deaths than outdoor air pollution [3].

VOCs are one of the predominant indoor air pollutants [4]. VOCs may include a wide range of organic molecules such as aliphatic and cyclic hydrocarbons, aromatic hydrocarbons, aldehydes, alcohols, esters, halocarbons, ketones, alkanes, and ethers [5]. VOCs are considered a potent narcotic that alter the central nervous system. They can cause loss of coordination and

irritation of eyes, skin and lungs [6,7]. In addition, long-term exposure to some VOCs increases the risk of cancer [8].

A number of techniques have been used for removal of VOCs from air. They include techniques such as adsorption [9], biological treatment [10], non-thermal plasma [11], catalytic oxidation [12] and ozone-assisted catalytic oxidation (i.e. catalytic ozonation) [13]. Adsorption is an efficient technique for the removal of VOCs from indoor air. However, VOCs are merely transferred from the gas phase to an adsorbent; this makes it necessary to frequently regenerate the adsorbent [14]. Another deficiency of adsorbents is that they cannot remove molecules with high vapor pressure [9,14]. Non-thermal plasma generates highly active chemical species that react with VOCs, however, this technique has a high energy consumption and its reactors operate unsteadily [15]. Biological techniques are environmentally friendly and exhibit robust performance, but they suffer from low bioavailability and slow oxidation of VOCs, making the biofilters large and uncompetitive [16]. Catalytic oxidation can rapidly decompose VOCs, however, it requires reaction temperatures higher than 200 °C for an effective oxidation process [12,17]. Catalytic ozonation is a promising technique for rapid oxidation of VOCs, and its reaction temperature is significantly lower than catalytic oxidation [18]. In addition, efficient VOC removal can be achieved by using transition metal oxide catalysts in catalytic ozonation. Whereas, expensive noble metals are commonly used in catalytic oxidation of VOCs by oxygen [19].

Manganese oxides (MnO_x) are the most active metal oxides for gas phase VOC removal in the presence of ozone [20]. Manganese oxides supported on different supports have been used for catalytic ozonation of a number of VOCs such as benzene, formaldehyde, cyclohexane, and

chlorobenzene [21–24]. It has been shown that catalytic ozonation can oxidize the listed VOCs at temperatures below 100 °C. Supported manganese oxide possesses higher catalytic activity than unsupported manganese oxide [25]. In addition, studies on catalytic ozonation of VOCs, using manganese oxide supported on γ-alumina, silica, titania, and zirconia, found that VOC removal rates normalized by surface area of the catalysts were comparable or slightly lower than those with the γ-alumina supported catalysts [26–28].

Despite recent developments, the required temperature for stable operation of catalytic ozonation systems is still higher than the room temperature, since catalyst deactivation is a serious impediment. Investigating reaction intermediates that are formed on the surface of the catalyst can help to develop a better understanding of the catalyst stability. Therefore, this study aims to investigate the nature and role of reaction intermediates in catalytic ozonation of VOCs over γ-alumina-supported manganese oxide catalyst. VOCs are usually present as mixtures of different compounds. Studies of catalytic ozonation of single VOC compounds do not represent the catalyst application thoroughly. Therefore, in this thesis, catalytic ozonation of single acetone and toluene, and a binary mixture of these compounds was investigated. Acetone and toluene were chosen as model compounds since they have different chemical properties and both are common VOCs in indoor and outdoor environments [29–31].

1.2. Structure of the thesis

This thesis consists of seven chapters. In Chapter 1 (current chapter), the problem of air pollution and potential hazards of VOCs are briefly introduced. Also, motivation of this research to investigate catalytic ozonation of VOCs is explained.

Chapter 2 contains an extensive literature review on air quality, VOC removal techniques, and catalytic ozonation of VOCs. In addition, knowledge gaps in the field of catalytic ozonation are discussed and objectives of the research are identified. Experimental details including experimental setup, catalyst preparation, reaction conditions, characterization of the fresh and spent catalysts, and data analysis will be discussed in Chapter 3.

Results of catalyst characterization and catalytic ozonation of toluene over γ-alumina-supported manganese oxide are presented and discussed in Chapter 4. Similarly, results of catalytic ozonation of acetone are presented and discussed in Chapter 5. Identifying the nature of carbonaceous surface spices and differentiating their role in the reaction pathway are also discussed in these chapters. Results of catalytic ozonation of mixture of toluene and acetone are presented and discussed in Chapter 6. Moreover, the results of catalytic ozonation of the mixture of VOCs will be compared with the results of catalytic ozonation of single toluene and acetone. In addition, catalyst regeneration will be discussed in this chapter. Overall summary and conclusions, and recommendations for the future works will be presented in Chapter 7.

In addition, the thesis has five appendices. Appendix A contains results and discussion of preliminary experiments comparing catalytic ozonation of toluene, acetone and benzene. Calibration data for gas analyses are given in Appendix B. Mass transfer calculations and effect of particle size are presented in Appendix C. FTIR bands and their corresponding functional groups are provided in Appendix D. Also, permissions to use the materials from published papers are presented in Appendix E.

The described structure helps to clearly deliver the core findings of this research. However, it should be noted that field application, catalyst improvement/optimization, and

technology development of catalytic ozonation of VOCs are out of scope of this work and can be investigated in the future works.

Major parts of this thesis have been published/presented in the following publications/conference presentations:

1) M. Aghbolaghy, J. Soltan, N. Chen, Role of Surface Carboxylates in the Gas Phase Ozone-Assisted Catalytic Oxidation of Toluene, Catalysis Letters, 147 (2017) 2421–2433. https://doi.org/10.1007/s10562-017-2143-0.

2) M. Aghbolaghy, J. Soltan, R. Sutarto, The Role of Surface Carboxylates in Catalytic Ozonation of Acetone on Alumina-Supported Manganese Oxide, Chemical Engineering Research and Design, 128 (2017) 73–84. https://doi.org/10.1016/j.cherd.2017.10.002.

3) M. Aghbolaghy, N. Chen, J. Soltan, Ozone-Assisted Catalytic Oxidation of a Binary Mixture of Volatile Organic Compounds in Air, 67th Canadian Chemical Engineering Conference, Edmonton, Oral Presentation, 22-25 October, (2017).

4) M. Aghbolaghy and J. Soltan, Catalytic Oxidation of Toluene by Ozone on MnO_x/γ-Al_2O_3, 65th Canadian Chemical Engineering Conference, Calgary, Poster, 4-7 October, (2015).

5) M. Aghbolaghy and J. Soltan, Catalytic Ozonation of Mixture of Benzene and Acetone on MnO_x/γ-Al_2O_3, 65th Canadian Chemical Engineering Conference, Calgary, Oral Presentation, 4-7 October, (2015).

6) M. Aghbolaghy, Catalytic Removal of Volatile Organic Compounds (VOCs) in Air, Graduate Research Conference, Saskatoon, Oral Presentation, 4-6 March, (2015).

7) M. Aghbolaghy, E. Rezaei, J. Soltan, Comparative Catalytic Ozonation of VOCs on MnO_x/γ-Al_2O_3, 23rd Canadian Symposium on Catalysis, Edmonton, Oral Presentation, 11-14 May, (2014).

8) M. Aghbolaghy and J. Soltan, Treatment of Environmental Pollutants Using Catalytic Ozonation, Graduate Research Conference, Saskatoon, Oral Presentation, 6-8 March, (2014).

In addition, the following manuscripts are in preparation:

- M. Aghbolaghy, J. Soltan, N. Chen, Low temperature catalytic removal of a binary mixture of toluene and acetone.
- M. Aghbolaghy, and J. Soltan, Comparison of catalytic ozonation of toluene, benzene and acetone on alumina-supported manganese oxide catalyst.

Permissions to use the published papers were obtained from the publishers and are presented in Appendix E. Therefore, further citation will not be made to the mentioned published papers.

Chapter 2:
Literature review

2.1. Volatile organic compounds

Organic chemical compounds can be found everywhere in either indoor or outdoor environments. Volatile organic compounds or VOCs are organic chemical compounds that evaporate in a certain of temperature range. Volatility of an organic compound is often correlated to its boiling point. Therefore, European Union defines a VOC as any organic compound with boiling point of less than or equal to 250 °C at 1 atm [32].

World Health Organization (WHO) classifies organic pollutants to three groups based on their ease of emission. These groups are semi-volatile organic compounds (SVOCs), volatile organic compounds (VOCs), and very volatile organic compounds (VVOCs) [33]. These groups are defined in Table 2.1.

Table 2.1. Classification of organic pollutants by WHO [33].

Group	Boiling point range (°C)	Examples
SVOC	240-260 to 380-400	DDT, chlordane, phthalates, PCBs
VOC	50-100 to 240-260	formaldehyde, toluene, ethanol, acetone, isopropyl alcohol, hexanal
VVOC	<0 to 50-100	methyl chloride, propane, butane

VVOCs are almost always found as gases rather than in other materials or on surfaces. Contrarily, SVOCs are usually found in solids or liquids or on surfaces such as furnishings. Despite their differences, often all these volatile organic pollutants are referred to as VOCs [34].

The total number of VOCs is determined to be 320, in which 261 VOCs belong to outdoor and 66 VOCs belong to indoor environments [2,35]. The concern about VOC are different in indoor and outdoor environments. VOCs are considered as pollutants in indoor environments mainly due to their direct health effects on humans. However, the main concern in the outdoor environments is ability of VOCs to cause photochemical smog [1,34].

Consideration of indoor exposures to VOCs is important, since humans spend more than 80% of their lifetime indoors [36]. Many household products are sources of VOCs. VOCs are widely used as ingredients of paints, solvents, cosmetics, varnishes, cleaning and disinfecting products, and adhesives [8,30,31]. VOCs are concerning for pharmaceutical and food packaging industries as well, since some VOCs are found in the synthetic polymers that are used for packaging [37]. Table 2.2 presents potential sources of some indoor VOCs.

According to the United States environmental protection agency (EPA) [6], users of VOC-containing products can expose themselves and others to dangerous levels of VOCs. Importantly, the VOCs can persist in air even a long time after using the VOC-containing products [6]. VOCs can be adsorbed by mucous membranes and skin. This can adversely affect metabolic systems and organs [4]. Also, exposure to VOCs contributes to the sick building syndrome (SBS), which is responsible for the development of some allergies and chronic diseases [3,38,39].

Table 2.2. Sources of some VOCs found in indoor environments [4,40].

VOC	Sources
Toluene	Flooring materials, wood preservatives, paints, insulating materials, combustion sources, adhesives
Acetone	Resins, coatings, paints, polymers, varnishes
Paradichlorobenzene	Wood preservatives, ceiling materials
Formaldehyde	Paints, coatings, insulating materials, flooring materials, wood-based materials
Ethylbenzene	Adhesives, furniture, paints, combustion sources
Chloroethylene	Paints, coatings, flooring materials, dry-cleaned clothes
Acetaldehyde	Flooring materials, wood preservatives, HVAC system

In addition to loss of coordination and irritation of eyes, skin and lungs, some VOCs cause impaired neurobehavioral function [6,7]. They can cause headache, drowsiness, fatigue and confusion [6]. Benzene, vinylidine chloride, p-dichlorobenzene, chloroform, ethylene dibromide, methylene chloride and carbontetrachloride are proven to be carcinogenic for animals but not completely so for humans. Benzene, styrene, tetrachloroethylene, 1,1,1-trichloroethane, trichloroethylene, dichlorobenzene, methylene chloride and chloroform are also considered as mutagenic compounds [7]. Early life exposure to VOCs may have impact on the developing fetal and infant immune system and increase the risk of allergic diseases in young children. Also, domestic exposure to VOCs can increase the risk of asthma-like wheeze in preschool children. Among different VOCs, acetaldehyde, benzene, toluene, tetrachloroethylene and trichloroethylene have been put on priority list of health criteria [4,7].

2.2. VOC removal techniques

The important steps to reduce VOCs in the indoor environments are control of emission from the sources, increasing air ventilation, and using VOC removal technologies [4]. There are a number of traditional and newly-developed techniques for VOC removal from air. Each technique has certain advantages and disadvantages.

One of the most efficient and well-known techniques for removal of VOCs is adsorption. Activated carbon, zeolites, activated alumina, silica gel and molecular sieves are used for adsorption of VOCs. The main problem with adsorbents is that they will become deactivated after a while and they need to be regenerated. Also, adsorbents are not effective in removal of molecules with high vapor pressure such as formaldehyde and acetaldehyde [9,14]. On the other hand, regeneration of some adsorbents (e.g. activated carbon) is hard for the solvents with high boiling point. In addition, adsorbents may promote polymerization of adsorbed molecules [4]. Despites these, adsorption is the most commonly used VOC removal technique [41].

Non-thermal plasma is another technique for removal of VOCs. In this technique, electrons with high energy are discharged in a way that background gas does not heat up. These high energy electrons excite, dissociate and ionize gas molecules such as oxygen and water, to produce species such as atomic oxygen, hydroxyl radicals, and ozone which are chemically very active [15]. These active species react with VOCs and microbes. However, energy consumption of this method is fairly high, its reactors operate unsteadily, and some undesirable products can be generated [15,42,43].

Bio-based technologies including bio-scrubbers, bio-trickling filters, and bio-filters are

another category of VOC removal techniques. Biotechnologies usually have little or no energy consumption in the form of heat or radiation [44]. In addition, these techniques are environmentally friendly, have moderate capital and operation costs, exhibit robust performances, and need low maintenance [16,44]. However, strict control of parameters such as pH and nutrient concentration is required. Moreover, biotechnologies suffer from low bioavailability and slow oxidation of VOCs, which leads to large space requirements for the biological reactors [16].

Photocatalytic oxidation is a recently-developed VOC removal technique. Mechanism of photocatalytic oxidation is based on activity of semiconductor catalysts. High levels of conversion of VOCs are easily achievable by this technique. However, harmful products are formed by photocatalytic oxidation as a result of partial oxidation reactions. In addition, photocatalysts may be deactivated by adsorption of byproducts on their surface; or some species may be polymerized during photocatalytic process [45]. TiO_2 is the most commonly used catalyst in photocatalytic oxidation. Photocatalytic activity of TiO_2 is limited to UV irradiation, which restricts application of this technique in air treatment. Therefore, development of new catalysts, capable of functioning with visible light, is desired [4].

Ozonation (non-catalytic) has been used as a potential method for removal of VOCs. Although ozone is a good oxidant for odor removal, its reaction rate with hydrocarbons is low [46]. This implies using high concentration of ozone if fast reactions are required.

Incineration of VOCs is a technique that is used to remove VOCs from exhaust gases of industrial plants [47]. Even though this method is efficient, it is highly energy consuming which

leads to a high operating cost. Effectiveness of incineration decreases by decrease in concentration of VOCs [48,49].

Effectiveness of simple oxidation of VOCs can be improved by using heterogeneous catalysts. Catalytic oxidation is very efficient and has a wide range of applications. Catalytic oxidation of VOCs reduces the reaction temperature of incinerators from 1000 ^{o}C to below 600 ^{o}C, but still temperatures higher than 200 °C are required for an effective catalytic oxidation [1,12,17,50]. A further decrease in reaction temperature can be achieved by adding ozone, as a strong oxidant, to the reaction system. This process is called ozone catalytic oxidation or catalytic ozonation [18]. Decrease in reaction temperature and energy demand for air quality control is the main advantage of catalytic ozonation of VOCs [18,19]. In addition, catalysts based on transition metal oxides have high efficiencies in removal of VOCs by catalytic ozonation, eliminating the need for expensive noble metals that are commonly used in catalytic oxidation of VOCs by oxygen [19].

2.3. Ozone

2.3.1. Properties of ozone

Ozone is a chemical species that has significant effects on the life on earth. Depending on the conditions and applications, ozone can be considered harmful and undesirable or helpful and necessary. Ozone is well known for its protective role against solar UV lights. However, ground-level ozone, also called bad ozone, is associated with the formation of secondary pollutants such as smog [1,35]. On the other hand, ozone is widely used in wastewater treatment, odor

abatement, and pulp processing [46].

Concentrated ozone has an undesirably strong odor and a pale blue color [46]. Ozone has three oxygen atoms with resonance structure and equal bond distances of 0.128 nm. It has a strong oxidation potential of 2.07 eV. Fig. 2.1 shows resonance structure and electron distribution of ozone [46]. Electrophilic properties of ozone have been explained by using forms 1 and 4 of ozone [51]. Interactions of π and σ between *sp*2-hybridized atoms make the bonding of oxygen molecules possible [52].

(a)

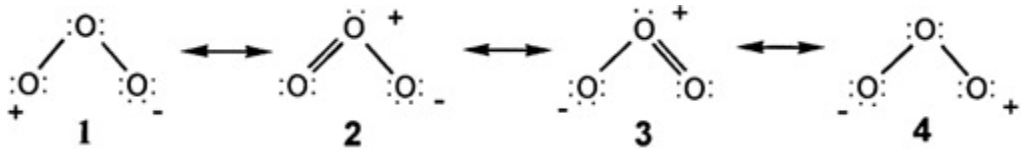

(b)

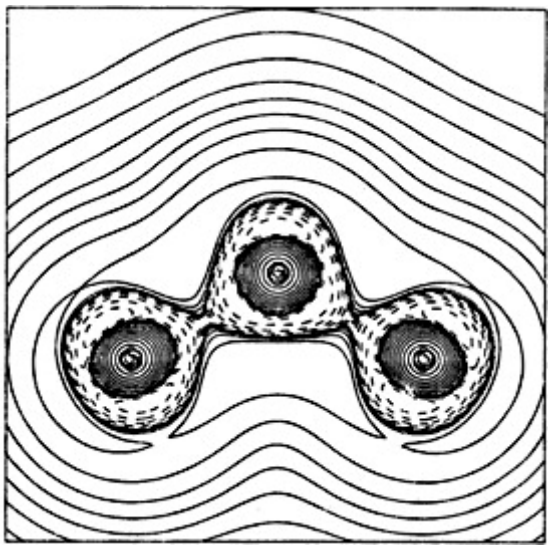

Fig. 2.1. (a) Resonance structure and (b) Electron distribution of ozone; courtesy of Taylor & Francis [46].

Ozone is naturally generated from reaction of oxygen molecules under solar UV light with wavelength of 240 to 300 nm. However, synthetic concentrated ozone was first produced in 1857 using an electrical discharge [53]. Ozone is thermodynamically unstable and is exothermally decomposed to oxygen molecules. However, non-catalytic ozone decomposition in the absence of UV light is very slow at temperatures below 100 °C. Half-life of ozone in the gas phase is about 160 hours at room temperature and atmospheric pressure. Ozone is decomposed more rapidly in the liquid phase. Its half-life is 7 minutes in the distilled water, and ozone decomposition rate increases by increase in pH of the solution [54].

2.3.2. Non-catalytic reaction of ozone with hydrocarbons in gas phase

Ozone reacts with most elements with the exception of noble gases and Fluorine. Ozone also reacts homogenously with almost all organic and organometallic compounds. However, its reaction rate depends on structure of the organic/organometallic compound. Since ozone is primarily an electrophile, it reacts faster with compounds that have electron-donating groups. Therefore, homogenous gas phase reaction of ozone with alkenes is much faster than its reaction with alkanes [46,55].

Although aromatics have high electron density, their gas phase reaction with ozone is slow. This is probably because of stable resonance structure of the aromatic ring. Moreover, homogenous reaction of ozone with aromatics such as *o*-xylene and toluene generates products such as methylglyoxal and glyoxal [56].

Oxygen containing compounds that do not have unsaturated carbon to carbon bond are

almost unreactive with ozone in the gas phase and at a temperature range of 25 – 100 °C. Even C_1 to C_3 oxygen containing alkenes have very lower reaction rates compared to other alkenes [55]. Also, reactions of ozone with larger alkenes do not lead to a complete oxidation to carbon dioxide and water vapor. Rather, these reactions produce oxygen containing products such as oxalic acid and acetic acid, which are unreactive with the gas phase ozone [46].

2.3.3. Catalytic decomposition of ozone

Ozone decomposition can be catalyzed by noble metals such as palladium and platinum, or transition metals (usually in the form of metal oxides) such as manganese, nickel, cobalt, and silver [57]. Noble metals are the most active catalysts for ozone decomposition. On the other hand, supported manganese oxide has shown the highest activity towards ozone decomposition among transition metals [46,58].

Materials such as silica, titania, γ-alumina, zirconia, activated carbon and zeolites are the commonly used supports for catalytic decomposition of ozone [58]. Although activated carbon has a very high surface area, it is not a stable support for ozone decomposition applications. It has been reported that in the presence of ozone, activated carbon is oxidized to carbon dioxide and carbon monoxide [59].

Proposed mechanism for ozone decomposition is as follows [58,60]:

$$O_3 + {}^{\blacksquare} \rightarrow O_2 + {}^{\blacksquare}O \quad (2.1)$$

$$ {}^{\blacksquare}O + O_3 \rightarrow O_2 + {}^{\blacksquare}O_2 \quad (2.2)$$

$$\blacksquare O_2 \rightarrow O_2 + \blacksquare \quad (2.3)$$

where, ■ is a catalyst active site. Eq. (2.1) occurs very quickly, while Eqs. (2.2) and (2.3) are slower. $\blacksquare O_2$ has been identified as peroxide species (O_2^{2-}) [60].

The catalysts designed for catalytic decomposition of ozone are used in the aircraft environmental control systems. The oxygen inside the aircraft comes from the surrounding atmosphere. During the high-altitude flights, the aircraft passes through ozone layer, and the intake gas contains high levels of ozone. Therefore, catalytic reactors are used to decompose ozone to oxygen molecules that can be safely breathed by passengers [61]. Other applications of catalytic ozone decomposition are photocopiers, wastewater treatment units, and sterilization units, where residual (unreacted) ozone should be removed [46,61].

2.4. Catalytic ozonation of VOCs

As mentioned earlier, in order to reduce the oxidation temperature of VOCs, it is possible to use a stronger oxidizing agent such as ozone instead of oxygen. Ozone alone does not react with most VOCs at low concentrations and it needs appropriate catalysts to become active. A number of research groups have used catalytic ozonation for oxidation of VOCs at relatively low temperatures. Catalysts used for catalytic ozonation of VOCs, reaction mechanism, and commercial applications of catalytic ozonation will be discussed in the following sections.

2.4.1. Different catalytic systems

Table 2.3 presents a summary of the main catalytic ozonation studies on removal of VOCs in gas phase. Topics such as effect of operating conditions, comparison of transition metal oxides, comparison of supports, and effect of water vapor have been studied extensively [22–24,26–28,62–72]. Naydenov and Mehandjiev were among the first researchers who investigated catalytic ozonation of VOCs. They used manganese oxide for complete oxidation of benzene by ozone at temperatures between 20 and 80 ºC [62]. It was observed that activation energy of benzene oxidation is greatly reduced when ozone is used as an oxidant instead of oxygen leading to decrease in reaction temperature. They proposed that oxygen species formed on the surface of the catalyst as a result of ozone decomposition are responsible for benzene decomposition. Mehandjiev et al. also studied low temperature oxidation of benzene over Ni-Mn catalyst and observed that application of ozone can reduce the oxidation temperature from 150-200 ºC range to 20-80 ºC [73]. Alumina supported Cu-Cr and Co-Cr oxides were used to oxidize benzene and CO using oxygen or ozone [74]. Complete oxidation of benzene was achieved at around 100 ºC by ozone. It was argued that decomposition of ozone on the surface of the catalyst facilitates the reaction and decreases the reaction temperature compared to that of conventional catalytic oxidation [74]. Andreeva et al. investigated performance of Au-V_2O_5/titania catalyst for either catalytic oxidation or catalytic ozonation [65]. In the absence of ozone, complete oxidation of benzene was achieved at 250 ºC. However, in the presence of ozone, 50% of benzene was converted at low temperature of 40 ºC. The authors suggested that most probably the oxygen activation proceeds on gold particles, while the vanadium oxide surface species are responsible for the oxidation of benzene.

Table 2.3. Main studies on catalytic ozonation for removal of VOCs.

Focus	Active metal(s)	Support(s)	VOC(s)	Ref.
Effect of operating conditions	Mn	-	Benzene	[62]
Effect of operating conditions	Ag	Alumina	Benzene	[63]
Effect of operating conditions	Mn	USY	Benzene	[64]
Effect of operating conditions	Au-V	Titania	Benzene	[65]
Effect of operating conditions	Ni, Co	Alumina	Isopropanol	[66,67]
Effect of operating conditions	Mn	CNT	Chlorobenzene	[24]
Effect of operating conditions	Mn, Fe	-	Chlorobenzene	[68]
Comparison of transition metal oxides	Mn, Fe, Co, Ni, Cu, Ag	Alumina	Benzene, Cyclohexane	[23]
Comparison of transition metal oxides	Mn, Ni, Co, Fe, Ag	ZSM-5	Toluene	[69]
Comparison of supports	Mn	Alumina, Titania, Silica, Zirconia	Benzene, Cyclohexane	[26–28]
Performance of noble metals	Pd, Pt, Mn, Pd-Mn, Pt-Mn	Alumina	Toluene	[75]
Performance of unsupported catalysts and perovskite-type catalysts	Mn, Co–Mn, Cu–Mn, Ni–Mn, Fe-Mn, La-Mn, $La_{0.8}Sr_{0.2}Mn$	-	Benzene	[25]
Structure and oxidation state of the catalyst	Cu-Mn	Silica	Benzene	[76]
Structure and oxidation state of the catalyst	Fe	Activated carbon	Propanal	[77]
Structure and oxidation state of the catalyst	Mn	Silica	Acetone	[40]

Table 2.3. Main studies on catalytic ozonation for removal of VOCs (continued).

Focus	Active metal(s)	Support(s)	VOC(s)	Ref.
Effect of water vapor	Mn	Alumina	Benzene	[70]
Effect of water vapor	Mn	-	Formaldehyde	[22]
Effects of water vapor and manganese loading	Mn-Ag	HZSM-5	Benzene	[71,72]
Effect of manganese loading	Mn	Alumina	Benzene, Toluene	[19,78]
Effect of manganese precursor	Mn	MCM-41, Alumina	Toluene	[20]
Determining the rate controlling step	Cu-Cr, Co-Cr	Alumina	Benzene	[74]
Reaction mechanism	Mn	Alumina	Toluene	[79]
Reaction kinetics and mechanism	Mn	Graphene	Toluene	[80]
In situ spectroscopy, reaction kinetics and mechanism	Mn	Silica	Acetone	[81]
Reaction mechanism and effect of layered catalyst	Ag	ZSM-5	Toluene	[82]
Economic feasibility	Mn	Silica	Chlorobenzene	[18]

A number of metal oxides (Mn, Ag, Fe, Co, Cu, and Ni) have been studied for catalytic ozonation of benzene, cyclohexane and toluene [23,69]. Mn showed the highest activity by converting pollutants to carbon dioxide and carbon monoxide; however, deactivation was the main problem and none of the catalysts showed stable activity. Mn/Al_2O_3 catalyst lost its activity for oxidation of benzene from 80 percent conversion to 40 percent within 2 hours indicating

accumulation of some intermediates on the surface of the catalyst. It was concluded that there were a number of compounds accumulating on the surface including formic acid, 2,5-furandione, phenol, and surface formates and carboxylates [23]. It has been reported [25] that supported manganese oxide possesses higher catalytic activity than unsupported manganese oxide in catalytic ozonation of benzene.

Rezaei et al. [20,75] investigated catalytic oxidation of toluene by ozone over MnO_x/γ-alumina, Pt-MnO_x/γ-alumina and Pd-MnO_x/γ-alumina catalysts. It was observed that complete removal of toluene occurred at 80 ºC using MnO_x loaded on γ-alumina. The catalyst was deactivated at room temperature because of deposition of carbon species on the surface of the catalyst. A reaction temperature of 65 ºC was required as the minimum reaction temperature to obtain steady state operation of the catalysts [20]. Addition of palladium did not improve the activity of alumina supported manganese oxides catalysts; however, addition of Pt led to decrease in the required temperature for complete oxidation of toluene from 80 to 70 ˚C [75].

A number of supports have been used in catalytic ozonation studies to clarify the effect of surface area on the reaction efficiency. Manganese oxides supported on alumina, silica, titania and zirconia (BET surface areas of 168, 300, 43, and 58 m^2/g, respectively) were used in catalytic ozonation of benzene [26,28] and cyclohexane [27]. It was found that removal rates per surface area of the catalysts were comparable or slightly lower than those with the alumina supported catalysts [26,27], indicating that catalytic activity of the catalysts depended primarily on the surface area of the catalyst rather than the types of catalyst support [28]. In a related study, benzene oxidation with ozone over silica supported manganese oxide was studied at 22 ˚C. Benzene conversion decreased with time and the catalyst was deactivated due to accumulation of

byproducts on the surface. Increase in the reaction temperature suppressed catalyst deactivation and enhanced the oxidation process [28].

Kastner et al. studied removal of propanol by ozone at room temperature by using synthetic hematite (Fe_2O_3), magnetite (Fe_3O_4) and metal oxide nano particles (α-Fe_2O_3) impregnated on activated carbon [77]. It was observed that propanal is completely oxidized by this method since no partial oxidation products were detected. However, authors ignored the effect of ozone on the structure of the activated carbon. It is believed that ozone can damage the structure of the activated carbon and this can affect performance of the catalyst [59].

Effect of water vapor in catalytic ozonation has been investigated in a number of papers. Einaga et al. [70] observed that although water vapor inhibits ozone decomposition on the catalyst, it supresses catalyst deactivation and increases benzene conversion by promoting direct reaction of ozone with the surface species. Water vapor promotes oxidation of the byproducts, including formic acid and surface formates, to CO_x and improves CO_2 selectivity [70,77]. Water vapor loses its effect by increase in temperature [64].

Effect of Mn loading (1 to 20%) on activity of alumina supported manganese oxide catalysts was studied by Rezaei et al. [19] in the temperature range of 22–100 ^oC. Analyses showed that Mn_2O_3 is the dominant phase at lower catalyst loadings; whereas mixture of MnO_2 and Mn_2O_3 was observed at higher catalyst loadings. The fraction of MnO_2 and oxidation state of Mn increased with increase of Mn loading. It was shown that lower Mn loadings were more favorable in oxidation of toluene up to 80 ^oC at which temperature, the catalysts show stable activity. According to this work, activity of the catalysts is related to the oxidation state of Mn on the catalyst. Catalysts with lower Mn loadings have higher activity in transferring electrons to

ozone to initiate ozone decomposition reaction due to their lower oxidation state. This increases the rate of decomposition of ozone to atomic oxygen which consequently enhances oxidation rate of toluene [19].

It has been shown that Co–Mn mixed oxides were one of the good candidates for benzene oxidation with ozone from the standpoint of CO_2 selectivity and efficiency of ozone utilization [25]. Einaga et al. [64] investigated the structure of catalytic active sites of manganese oxides on a high Si/Al ratio USY (SiO_2/Al_2O_3 = 180). Benzene was oxidized to carbon dioxide and carbon monoxide and higher activities were obtained under either humidified or dry conditions at 40 °C and higher temperatures due to faster oxidation of byproduct on the Mn/USY catalysts. This result is promising, because it shows that more work on the catalyst and reaction condition can lead to development of methods for catalytic ozonation of VOCs even in the room temperature range.

Liang et a. [18] studied economic feasibility of catalytic ozonation of flue gas of a waste furnace (flow rate of 50 m^3 min^{-1}) using silica supported manganese oxide catalyst and compared it with economic feasibility of catalytic oxidation (without ozone) of chlorobenzene using V_2O_5-based catalysts. They found that the cost of using catalytic ozonation was US$12.8 h^{-1}, while it was US$15.9 h^{-1} for the catalytic oxidation, indicating that catalytic ozonation is more cost-effective [18].

As discussed earlier, active oxygen species are generated during catalytic ozonation. These highly reactive species make it difficult to design a selective process. The aim of catalytic ozonation of VOCs is to completely oxidize the organic compounds, and the main issue with selectivity is the formation of some carbon monoxide along with carbon dioxide. This is

acceptable if the concentration of the produced carbon monoxide is below the regulated levels. Another issue is the emission of residual (unreacted) ozone. Fortunately, residual ozone can be decomposed and carbon monoxide can be further oxidized to carbon dioxide by using a supplementary catalytic bed. There are some commercialized or pilot scale studies that have used catalytic ozonation to in design air cleaning processes [83–85].

A pilot study [84] investigated catalytic combustion of VOCs in the presence or absence of ozone. Capacity of the plant was 100 m^3 h^{-1} and the process included ozone generator, reactor, heat exchangers, carbon adsorber, and an auxiliary scrubber. A better VOC removal performance was obtained in the presence of ozone at temperatures below 250 °C.

Another pilot study was conducted by Union Carbide which led to development of the UCAIR™ technology [85]. Schematic design of this technology is shown in Fig. 2.2. This technology was designed for indoor air treatment.

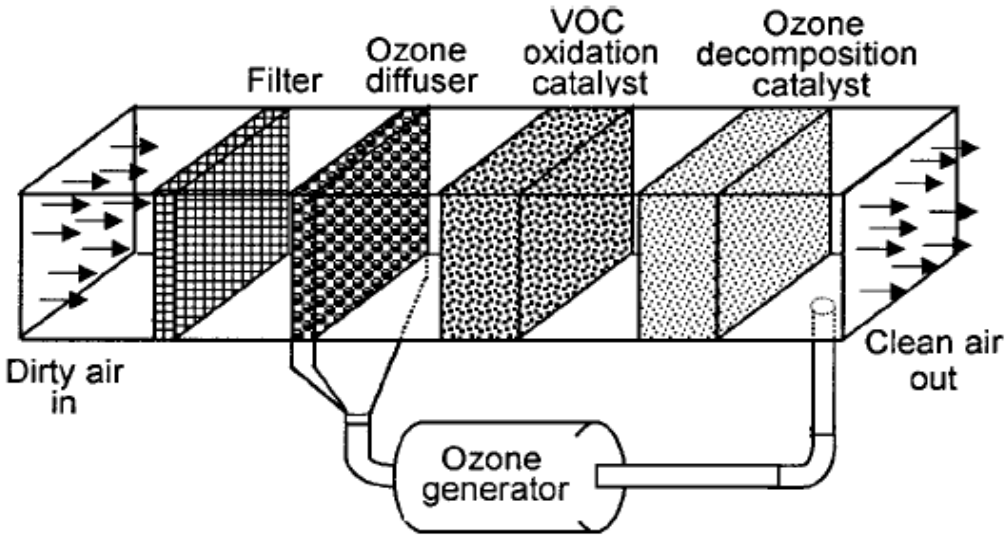

Fig. 2.2. Schematic design of the UCAIR™ indoor air treatment technology; courtesy of Taylor & Francis [46,85].

First, air passes through a filter to remove particulate matters, then ozone is added to the flow. The gas mixture passes through two catalytic beds. The first catalytic bed is for oxidation of VOCs and the second one aids with decomposition of residual ozone. The unit was claimed to be effective for removal of a wide variety of VOCs and microbiological aerosols at a relative humidity range of 25-75% [85].

Dashpure™ is another air purifier that is designed by Hitachi and commercialized in Japan [83]. Air is drawn into the purifier and passes through an ozone generator. Then it passes through a catalytic bed that oxidized the pollutants and decomposes ozone. Ozone sensors before the exhaust of the purifier detect the exhaust ozone level. If the exhaust ozone level is not safe the flow is recirculated through the catalytic bed [83].

In the field of catalytic ozonation in gas phase, a number of researchers have used X-ray absorption fine structure (XAFS) to characterize the catalysts. Rezaei et al. [75] utilized X-ray absorption near-edge structure (XANES) and extended X-ray absorption fine-structure (EXAFS) spectroscopy to study the structure of Pt-MnO_x/γ-alumina and Pd-MnO_x/γ-alumina catalysts. X-ray absorption spectra (Mn K-edge, Pd K-edge, and Pt LIII-edge) were collected at HXMA beamline of the Canadian Light Source. They used transmission mode with straight ion chamber detectors for Mn, and fluorescence mode with 32 element Ge detector for the Pt and Pd data collections. The scan step sizes for the pre-edge, XANES and EXAFS regions were 10 eV/step, 0.25 eV/step and 0.05 $Å^{-1}$, respectively. It was found that Pd does not have atomic interaction with Mn, and therefore it does not alter catalytic activity of Mn. However, XANES and EXAFS spectra of Pt and MnO_x were different from those of Pt-MnO_x implying an atomic interaction between platinum and manganese oxides. The authors inferred that interaction between Pt and

Mn occurs via surface oxygen of manganese oxides leading to formation of Mn–O–Pt bonds. This interaction increased electron occupancy of 3d orbital of manganese which led to a higher efficiency in catalytic ozonation of toluene [75].

Radhakrishnan and Oyama [86] used XAFS to characterize MnO_x (3 wt%) supported on alumina, zirconia, titania and silica. Analysis were done for all supports but strong absorption from the zirconia prevented the use of EXAFS analysis on the Mn/ zirconia catalyst. The authors argued that the interference occurred because the L-edge lines of Zr (2.2-2.5 keV) absorb strongly in front of the K-edge features of Mn (6.5 keV). However, such an interference did not occur for L-edges of Mn (0.6 keV) which appear at low energies. Einaga et al. [28] performed in situ XAFS studies in order to investigate the structural changes in manganese oxides (2.5 wt%) supported on alumina in the catalytic decomposition of ozone at room temperature. The absorption edge of MnO_x/Al_2O_3 sample was close to that of Mn_3O_4 with an average oxidation state of 2.67, and no spectral changes occurred during ozone decomposition.

2.4.2. Mechanism of catalytic ozonation of VOCs

Reed et al. [81] used in situ Raman spectroscopy to study the mechanism of catalytic ozonation of acetone on silica supported manganese oxide catalyst. They have concluded that the oxidation reaction occurs on the surface of the catalyst between atomic oxygen and adsorbed acetone molecule, leading to the following mechanism for catalytic ozonation of acetone on silica supported manganese oxide catalyst:

$$O_3 + * \rightarrow O_2 + *O \qquad (2.4)$$

$$*O + O_3 \rightarrow O_2 + *O_2 \quad (2.5)$$

$$*O_2 \rightarrow O_2 + * \quad (2.6)$$

$$A + {}^{\bullet} \leftrightarrow {}^{\bullet}A \quad (2.7)$$

$${}^{\bullet}A + * \leftrightarrow *A + {}^{\bullet} \quad (2.8)$$

$$*A + n\ *O \rightarrow \text{products} \quad (2.9)$$

where * represents a surface manganese site, $^{\bullet}$ represents a surface silica site, and A represents acetone. However, this study did not identify any reaction intermediates formed on the surface of the catalyst.

Rezaei et al. [79] studied catalytic ozonation of toluene on alumina supported manganese oxide catalyst and proposed a mechanism by assuming that C–H bond cleavage is the limiting kinetic step in the oxidation of toluene. Rezaei et al. [79] proposed the following mechanism for low temperature oxidation of toluene by ozone:

$$O_3 + * \rightarrow O_2 + O* \quad (2.10)$$

$$O* + O_3 \rightarrow O_2 + O_2* \quad (2.11)$$

$$O_2* \rightarrow O_2 + * \quad (2.12)$$

$$C_6H_5\text{-}CH_3 + * \leftrightarrow C_6H_5\text{-}CH_3* \quad (2.13)$$

$$C_6H_5\text{-}CH_3* + * \rightarrow C_6H_5\text{-}CH_2* + H* \quad (2.14)$$

$$C_6H_5\text{-}CH_2* + 7* \rightarrow C_6\text{-}C* + 7H* \quad (2.15)$$

$$H^* + O^* \leftrightarrow OH^* + * \quad (2.16)$$

$$2OH^* \leftrightarrow H_2O^* + O^* \quad (2.17)$$

$$H_2O^* \leftrightarrow H_2O + * \quad (2.18)$$

$$C_6\text{-}C^* + O^* \rightarrow C_6^* + CO^* \quad (2.19)$$

$$C_6^* + 6O^* \rightarrow 6CO^* \quad (2.20)$$

$$CO^* + O^* \rightarrow CO_2^* + * \quad (2.21)$$

$$CO^* \leftrightarrow CO + * \quad (2.22)$$

$$CO_2^* \leftrightarrow CO_2 + * \quad (2.23)$$

where, * is the manganese site. However, this mechanism ignores the role of alumina support in the reaction. Moreover, experimental evidence was not provided to support the mechanism.

Hu et al. [80] investigated catalytic ozonation of toluene on graphene supported manganese oxide catalyst. They suggested a dual site mechanism for catalytic ozonation of toluene:

$$O_3 + * \rightarrow O_2 + *O \quad (2.24)$$

$$*O + O_3 \rightarrow O_2 + *O_2 \quad (2.25)$$

$$*O_2 \rightarrow O_2 + * \quad (2.26)$$

$$C_6H_5\text{-}CH_3 + \square \leftrightarrow \square C_6H_5\text{-}CH_3 \quad (2.27)$$

$$\square C_6H_5\text{-}CH_3 + *O \rightarrow \text{products} \quad (2.28)$$

where * represents a surface manganese site, and □ represents a surface graphene site. This is similar to the mechanism proposed by Reed et al. [81] for catalytic ozonation of acetone with the difference that migration of VOC from support to manganese site is not required and the oxidation step occurs in a dual site reaction (Eq. (2.28)). Nevertheless, the mechanism of catalytic ozonation of VOCs remains an open topic and further studies are needed to elucidate the mechanism of catalytic ozonation and catalyst deactivation.

2.5. Knowledge gaps and objectives

There has been ongoing research on a number of areas related to the catalytic ozonation which were briefly reviewed in the previous section. Despite the recent developments, there are still important challenges and knowledge gaps in the process of catalytic ozonation of VOCs.

Required temperature for steady state operation of catalytic ozonation systems is still higher than the room temperature. Catalytic ozonation of VOCs at room temperature is advantageous and can reduce operating cost and energy consumption. However, catalyst deactivation is a serious impediment. There have been a number of studies aimed at understanding the nature of catalyst deactivation and formation of reaction products in catalytic ozonation. Einaga et al. used in situ Fourier transform infrared (FTIR) spectroscopy to investigate room temperature catalytic ozonation of benzene over 5 wt% Mn/USY zeolite [64] and 5 wt% MnO_2/Al_2O_3 [26]. It was observed that two types of intermediates were formed on the surface of the catalysts. These intermediates were categorized as weakly bound and strongly bound compounds. Zhao et al. [22] employed in situ FTIR spectroscopy to investigate room temperature catalytic ozonation of formaldehyde on MnO_x catalyst. Bidentate and monodentate

carbonate species were found on the catalyst surface and both increased gradually with time. Reed et al. [81] investigated catalytic ozonation of acetone on 10 wt% MnO_x/SiO_2. They suggested that ozone was more active than oxygen in oxidation of acetone. Also, in situ Raman spectroscopy at 35 °C showed that silica support was a reservoir for the physically adsorbed acetone [81]. Another study [87] by the same group showed that alumina-supported catalyst was more active than the silica-supported catalyst in acetone conversion. However, the role of the alumina support in catalytic ozonation of acetone was not clarified, due to technical limitations with Raman spectroscopy [87].

These studies have limited their investigations to ozonation operating temperatures in the range of 22-35 °C, at which severe catalyst deactivation occurs. In addition, they have not identified a mechanism for the production of the observed compounds, and therefore, have not differentiated between the roles of reaction intermediates and products. This is similar to a current knowledge gap in the field of photocatalytic oxidation of VOCs. Recent literature reviews [4,88] have indicated that understanding the reaction intermediates is key to improve catalyst stability in the photocatalytic oxidation of VOCs as well.

It is known that catalytic ozonation of VOCs at a relatively high temperature (i.e. 90 °C) shows stable activity with no or negligible catalyst deactivation [28,68,75]. Study of catalytic ozonation of VOCs at a relatively high temperature (with stable catalytic activity) and comparison of the reaction characteristics with those at the room temperature reaction (with catalyst deactivation) can provide more clear understanding of the reaction intermediates and catalyst stability. It is important to investigate the nature and roles of intermediates and products that are formed on the surface of the catalyst. This can help us develop a better understanding of

the reaction mechanism and catalyst stability.

Another important knowledge gap in the field of catalytic ozonation is removal of a mixture of VOCs. VOCs in both indoor and outdoor environments are usually present as mixtures of different compounds. Studies of catalytic ozonation of single VOC compounds do not represent the catalyst application thoroughly. This leaves an important gap between laboratory research and real-world application of the air treatment techniques in which a mixture of VOCs is to be removed. Low temperature catalytic ozonation of mixture of VOCs has not been reported in the literature. However, there are a number of reports addressing removal of mixture of VOCs using catalytic combustion with oxygen [8,89–92]. The majority of these studies have found considerable mixture effects on the activity and selectivity [89–92], indicating that the oxidation of a VOC in a mixture differs from its single component oxidation. The changes in the activity and selectivity have been either repressive [89,91] or promotive [90,92]. Significant mixture effects in catalytic combustion of VOCs with oxygen, indicates the importance of investigating catalytic ozonation of mixture of VOCs as well.

Toluene, benzene, and acetone were chosen as sample compounds for preliminary experiments (Appendix A). From the preliminary studies, very similar results were obtained for catalytic ozonation of toluene and benzene. This was probably due to highly similar structure of toluene and benzene. Therefore, acetone and toluene were chosen as model compounds for the main body of this work. Toluene and acetone have different chemical properties, and both are common VOCs in indoor and outdoor environments [29–31]. Acetone (a ketone) is an oxygen containing compound with a carbonyl group. Toluene is an aromatic compound with a methyl group attached to the aromatic ring. As mentioned earlier, in the absence of catalyst, gas phase

reaction of aromatics with ozone is slow, while oxygen containing compounds that do not have unsaturated carbon to carbon bond are unreactive with ozone at a temperature range of 25 – 100 °C [55,56]. Therefore, study of catalytic ozonation of these compounds with different chemical properties could be a good indication of generality of the results obtained in this research.

Based on the described knowledge gaps, an objective of this work is to identify the role of reaction intermediates during catalytic ozonation of VOCs at 25 °C with catalyst deactivation, and 90 °C with stable catalytic activity. Understanding the intermediates formed on the surface of the catalyst will elucidate the reaction pathway of catalytic ozonation of VOCs. For this purpose, catalytic ozonation of toluene and acetone, as single compounds, was investigated.

The other objective of this work is to study catalytic ozonation of a mixture of VOCs. This will help to better understand potentials and limitations of the catalytic ozonation in treating mixture of VOCs. For this purpose, catalytic ozonation of binary mixture of acetone and toluene was investigated and was compared with the catalytic ozonation reactions of single acetone and toluene.

As mentioned earlier in this chapter, manganese oxides (MnO_x) are the most active metal oxides for removal of VOCs in the presence of ozone [23,69]. Also, supported manganese oxide possesses higher catalytic activity than unsupported manganese oxide [25]. In addition, it was discussed that VOC removal rates normalized by surface area of the catalysts were comparable or slightly lower than those with the γ-alumina supported catalysts [26–28]. Therefore, alumina supported manganese oxide catalyst was used in this work.

A combination of in situ diffuse reflectance infrared Fourier transform spectroscopy (DRIFTS), chemical analysis of surface compounds, X-ray spectroscopy techniques, and a number of temperature programmed analyses was used to achieve objectives of this investigation.

Chapter 3:
Experimental

This chapter presents details of catalyst preparation, activity measurements, in situ DRIFTS measurements, and characterization of fresh and spent catalysts.

3.1. Catalyst preparation

Dry impregnation method was used to prepare MnO_x/γ-alumina catalyst [20]. Acetate and nitrate precursors of manganese are two commonly used precursors employed in preparing Mn-based catalysts. Alumina supported catalysts prepared from the nitrate and acetate precursors have shown comparable activity in catalytic ozonation [20].

Powdered γ-alumina (Alfa Aesar) with particle size of less than 0.208 mm was impregnated by manganese (II) nitrate tetrahydrate (Sigma Aldrich, 97%) as manganese precursor. The impregnated support was dried at 100 °C for 10 hours in air, then it was calcined at 500 °C for 4 hours. After calcination, the catalyst was crushed and sieved to produce a powder size of less than 0.208 mm. Nominal manganese loading was 10 % based on mass of metallic manganese per mass of the catalyst.

3.2. Catalyst characterization

3.2.1. BET surface area and pore volume

Brunauer–Emmett–Teller (BET) surface area and pore volume of the catalyst were determined by N_2 adsorption using ASAP 2020 (Micromeritics) instrument. The samples were degassed for 2 hours at 110 °C and 0.5 mm Hg before the surface area and pore volume measurements.

3.2.2. Inductively coupled plasma mass spectrometry

Inductively coupled plasma mass spectrometry (ICP-MS) was used for verifying manganese loading on the catalyst. ICP-MS analysis was conducted using a Nexion 300D (PerkinElmer) instrument.

3.2.3. X-ray absorption fine structure

X-ray absorption fine structure (XAFS) was used to further characterize the catalyst. One of the most important challenges in XAFS measurements is having an energy tunable X-ray source. For this reason, the X-ray source is a synchrotron, providing a full range of X-ray wavelengths. A monochromator (typically made from silicon) selects a particular energy based on Bragg diffraction, and slits are used to define the beam size [93,94]. X-ray absorption near edge structure (XANES) and extended X-ray absorption fine structure (EXAFS) of Mn *K-edge* were collected at HXMA beamline of the Canadian Light Source (CLS) [95]. During the

experiment, the CLS storage ring was operated under 250 mA operation mode, and the beamline superconducting wiggler was run at 1.9 T magnitude field. In the experiment, the second crystal of the monochromator Si(111) crystal was detuned by 50% to reduce the high harmonic components in the incident X-ray beam. The beamline was configured in its focused mode with Rh mirrors (collimating and focusing mirrors) in the X-ray beam path. Catalyst was diluted with adequate amount of boron nitride. Then, the diluted sample was ground and pressed into thin disks and protected by Kapton tape. The measurements were conducted in transmission mode with Oxford straight ion chamber detectors filled with 100% helium gas. For XANES measurements, scan step-size was 10 eV until reaching 30 eV below the edge. From that point, energy was increased in finer steps of 0.25 until 40 eV above the edge. For EXAFS measurement, 0.05k step-size was used in the range of 40 eV to 11~12k above the edge. Reference materials including Mn_2O_3 (99% bixibyite, Sigma–Aldrich), MnO_2 (99.9% pyrolusite, Alfa Aesar), MnO (99% manganosite, Alfa Aesar), and Mn_3O_4 (97% hausmannite, Sigma–Aldrich) were diluted in the same way as the catalyst sample and measured in the transmission mode as well, providing reference for different oxidation states.

Data processing including energy calibration, normalization, background removal, and linear combination fitting (LCF) of Mn *K-edge* XANES data were performed by ATHENA software [96]. Artemis software, a front-end of FEFF [97] and IFEFFIT [98], was used for R space EXAFS fittings. Parameters that were included in the EXAFS fittings were coordination number (CN), mean-square displacement of the bond length (σ^2), amplitude reduction factor (S_o^2), change in interatomic distance (ΔR) and change in energy scale (ΔE_o). S_o^2 value was found by fixing coordination numbers based on crystallography data of the reference material. k-weights of 1, 2 and 3 were simultaneously applied to remove dependency of S_o^2 to different k-

weights. Then, the fixed S_o^2 value was used with k-weight of one to find the coordination numbers at the first and second shells of the MnO_x clusters. In all cases, EXAFS data were fitted in R space in the range of 1 – 3.7 Å, and ΔR, σ^2, and ΔE_o were allowed to be floating.

3.2.4. X-ray photoelectron spectroscopy

X-ray photoelectron spectroscopy (XPS) measurements were performed using an Omicron Multiprobe system with a monochromatized Al Kα source (hν = 1486.7 eV) and Sphera EA125 hemispherical electron energy analyzer at the Surface Science Facility located at the REIXS beamline of the Canadian Light Source. Electron gun was also used to neutralize the charging effect on the catalyst surface. The operating vacuum pressure was below 2×10^{-10} mbar. The spectra were collected using a pass energy of 50 eV and steps of 0.5 eV. Data analysis was performed using the CasaXPS software [99]. Results of the catalyst characterization are presented and discussed in section "*4.1. Characterization of MnO_x/γ-alumina*".

3.3. Activity measurements

Fig. 2.1. depicts a schematic diagram of the experimental setup for the catalyst activity measurements. VOCs were supplied from gas cylinders with ppmvv level concentration of pollutant and balance of nitrogen (Praxair, accuracy of ±2%). A high purity oxygen stream (Praxair, 99.993%) passed through an ozone generator (AZCO Industries LTD, HTU-500S) to produce ozone. A high purity nitrogen stream (Praxair, 99.999%) was used for dilution and purging purposes.

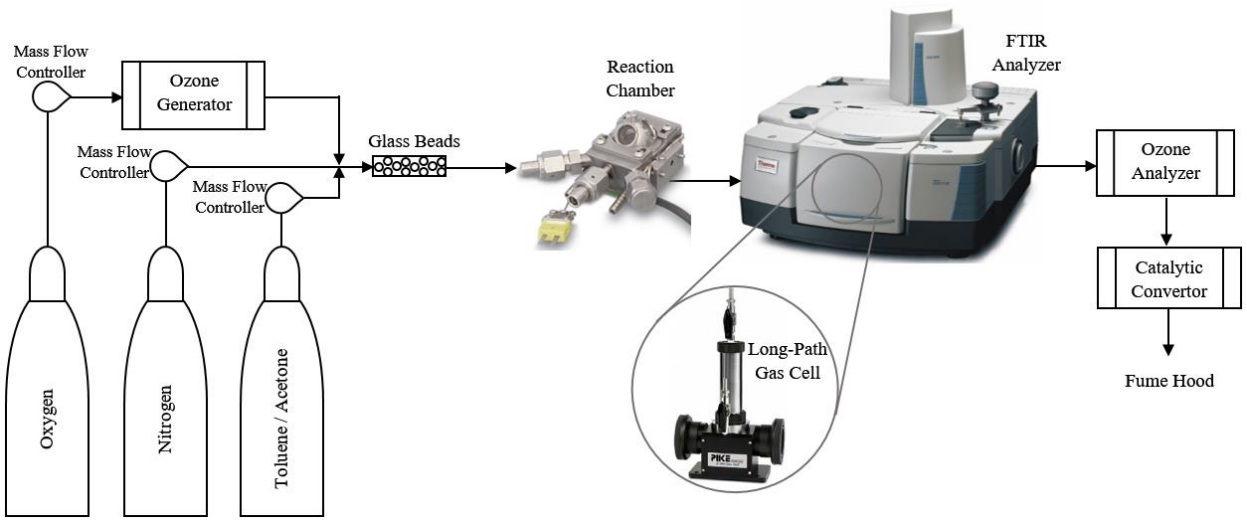

Fig. 3.1. Schematic of the experimental setup for catalyst activity measurements.

Mass flow controllers (Brooks, SLA 5850, accuracy of ±1%) were employed to control gas flow rates. Gas streams were combined and passed through a horizontal Pyrex tube. This tube, filled with glass beads, improved mixing of gas streams before entering the reactor. A reaction chamber (Harrick, HVC-DRM-5) equipped with a temperature controller was used as an atmospheric reactor to conduct most of the reaction experiments.

The reaction chamber was at atmospheric pressure and allowed high temperature operations up to 900 °C. Exhaust stream of the reactor passed through a long-path gas cell (PIKE, volume 0.1 L, 2.4 m optical length, KBr window), coupled with a Nicolet iS50 FTIR spectrometer. Deuterated L-alanine doped triglycine sulfate (DLaTGS) detector was employed. Spectra were collected at a resolution of 4 cm^{-1} in the range of 4000-400 cm^{-1}. Calibration curves for the gas analyses are presented in Appendix B.

In addition, an ozone analyzer (Teledyne API M454) was employed to measure ozone content in the exhaust stream. A gas cylinder with ppmvv level concentrations of CO_2 and CO balanced with nitrogen (Praxair, accuracy of ±2%) was employed for calibration purposes.

Activity measurement experiments were conducted at atmospheric pressure at 25 - 90 °C. Blank experiments in the absence of catalyst showed negligible non-catalytic gas phase reaction between VOCs and ozone at the mentioned temperature range. Total oxygen to nitrogen ratio in the reaction mixture was kept at 20/80 v% to resemble air composition. 0.06 g of the catalyst was used for each experiment. Total feed gas flow rate was 350 Sml/min resulting in a weight hour space velocity (WHSV) of 350 L h^{-1} g^{-1} in the reactor.

Although concentration of single VOCs in the indoor environments is only a few ppmvv, concentration of total VOCs, especially in industrial indoor environments, is much higher [50,100]. On the other hand, usually a single VOC is used as a model compound to study VOC removal techniques. Therefore, researchers in the field of catalytic oxidation and ozonation use an inlet VOC concentration of 50 - 300 ppmv [13,18,24,101] to represent maximum total VOC concentration in the indoor environments. In this work, a total VOC(s) concentration of 130 ppmv was used in the inlet stream.

Before reaction, VOCs were adsorbed on the surface of the catalyst at atmospheric pressure and the desired reaction temperature. This eliminates contribution of direct adsorption to VOCs removal during the catalytic ozonation reaction. Once the catalyst was saturated with VOCs, ozone was introduced into the reactor to start the reaction. Each reaction was repeated at least twice and standard error is reported in each figure.

3.3.1. Activity measurements for catalytic ozonation of toluene

For catalytic ozonation of toluene, toluene and ozone concentrations in the inlet stream were 130 and 1200 ppmv, respectively. CO_x yield was calculated based on Eq. (3.1):

$$CO_x\ yield = 100 \times \frac{[CO]+[CO_2]}{(7\times[C_7H_8]_{reacted})} \quad (3.1)$$

where, concentrations are in ppmv. Results of catalytic ozonation of toluene are presented and discussed in Chapter 4.

3.3.2. Activity measurements for catalytic ozonation of acetone

For catalytic ozonation of acetone, acetone and ozone concentrations in the inlet stream were 130 and 1200 ppmv, respectively. CO_x yield was calculated based on Eq. (3.2):

$$CO_x\ yield = 100 \times \frac{[CO]+[CO_2]}{(3\times[C_3H_6O]_{reacted})} \quad (3.2)$$

where, concentrations are in ppmv. Results of catalytic ozonation of acetone are presented and discussed in Chapter 5.

3.3.3. Activity measurements for catalytic ozonation of mixture of toluene and acetone

Total VOCs concentration in the inlet stream was 130 ppmv. Therefore, 65 ppmv of each VOC compound was used for catalytic ozonation of the mixture of toluene and acetone. Ozone concentration in the inlet stream was 1200 ppmv. CO_x yield was calculated based on Eq. (3.3):

$$CO_x\ yield = 100 \times \frac{[CO]+[CO_2]}{[(7\times[C_7H_8]_{reacted})+(3\times[C_3H_6O]_{reacted})]} \quad (3.3)$$

where, concentrations are in ppmv. Results of catalytic ozonation of the mixture of toluene and acetone are presented and discussed in Chapter 6.

3.4. Temperature programmed analyses

Temperature programmed oxidation (TPO) was carried out on the spent catalyst. The set-up, described in section "*3.3. Activity measurements*" and depicted in Fig. 2.1, was used for TPO analyses. After reaction, the reaction system was immediately purged with nitrogen for 10 minutes. Then, the catalyst was heated to 745 °C at a rate of 10 °C/min under 350 mL/min of 20-80 v% oxygen-nitrogen flow. The exhaust gas was analyzed by the long-path gas cell, coupled with the FTIR spectrometer.

TPO results were used to calculate the overall carbon balance. For this purpose, *total carbon in* and *total carbon out* were calculated. *Total carbon in* is the amount of carbon entering the reactor as VOCs during the saturation and reaction time. *Total carbon out* was calculated as sum of carbon out before TPO (CO_x during reaction and unreacted VOCs) and carbon evolved during TPO. Then, the overall carbon balance was calculated based on Eq. (3.4):

$$Carbon\ balance\ (\%) = 100 \times \frac{Total\ carbon\ out}{Total\ carbon\ in} \quad (3.4)$$

Temperature programmed desorption (TPD) was carried out on the spent catalyst. The set-up, described in section "*3.3. Activity measurements*" and depicted in Fig. 2.1, was used for

TPD analyses. After reaction, the reaction system was immediately purged with nitrogen for 10 minutes. Then, the catalyst was heated to 860 °C at a rate of 20 °C/min under atmospheric-pressure N_2 flow. The evolved gases were analyzed by the long-path gas cell, coupled with the FTIR spectrometer.

Temperature programmed weight loss of the spent catalyst was studied by a thermal analyzer (TGA Q500, TA Instruments) with standard furnace type. For this purpose, samples were heated to 790 °C at a rate of 20 °C/min under a pure nitrogen flow.

3.5. In situ DRIFTS measurements

A modified experimental setup (Fig. 3.2) was used for the in situ DRIFTS measurements. In this setup, the Nicolet iS50 FTIR spectrometer was coupled with a DRIFTS accessory (Harrick, Praying Mantis). Then, the reaction chamber (Harrick, HVC-DRM-5), equipped with ZnSe windows, was installed on the DRIFTS accessory. A narrow band mercuric cadmium telluride (MCT-A) detector was employed to achieve a high sensitivity for DRIFTS spectra collection. Liquid nitrogen was used for cooling the MCT-A detector. DRIFTS spectra were collected with a resolution of 4 cm^{-1} in the range of 3900-1300 cm^{-1} to achieve fast scanning and to avoid saturation of the detector. Potassium bromide (KBr) was used for background collection.

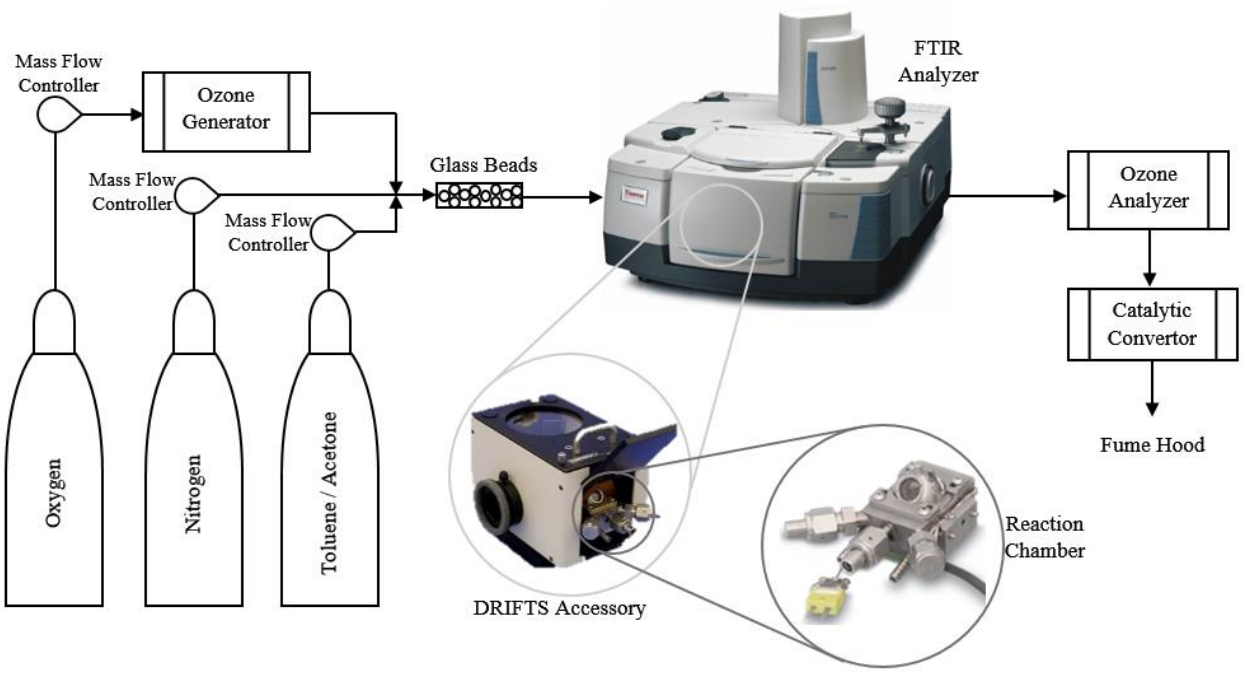

Fig. 3.2. Schematic of the experimental setup for in situ DRIFTS measurements.

In situ DRIFTS spectra were collected during reaction, TPO, and TPD. Operation conditions were the same as those for the activity measurements (see section "*3.3. Activity measurements*") or temperature programmed analyses (see section "*3.4. Temperature programmed analyses*").

3.6. Product identification by GC-MS

A gas chromatograph (Agilent, 7890A) coupled with a mass spectrometer (Agilent, 5975C) was employed to identify carbonaceous species deposited on the catalysts. An Agilent standard HP-5MS column was utilized in the gas chromatograph. For this purpose, the spent catalysts

were washed with dichloromethane, and the obtained extracts were analyzed by the gas chromatograph-mass spectrometer.

3.7. Kinetic analyses

A modified experimental setup (Fig. 3.3) was used for kinetic analyses. Experiments were conducted in a plug flow reactor at atmospheric pressure. The reactor is made of a horizontal pyrex tube with inner diameter of 0.0125 m. This system allowed to use varied amounts of the catalyst for the kinetic studies. As mentioned earlier, a catalyst powder size of less than 0.208 mm was used in the experiments. The tube was fixed in an oven (Binder, FP 115), controlling the reaction temperature. Kinetic data were obtained at three different temperatures (70, 80, and 90 °C), since catalyst activity is not stable at temperatures below 70 °C due to catalyst deactivation. The employed configuration did not exhibit mass transfer limitations for catalytic ozonation of toluene and acetone (see Appendix C).

Differential method of analysis was used to determine the reaction rates. Space time of the reactor varied from 0 to 846 kg s mole^{-1}. Data of space time versus VOC conversion were fitted to Eq. (3.5) [102] by using curve fitting tool of MATLAB 2016a:

$$X_{voc} = A(1 - \exp(-B\frac{W}{F_{voc,in}})) \quad (3.5)$$

where, W, $X_{voc,}$ and $F_{voc,in}$ are catalyst weight (kg), VOC conversion, and inlet molar flow rate of VOC (mole s^{-1}), respectively. A and B are fitting parameters.

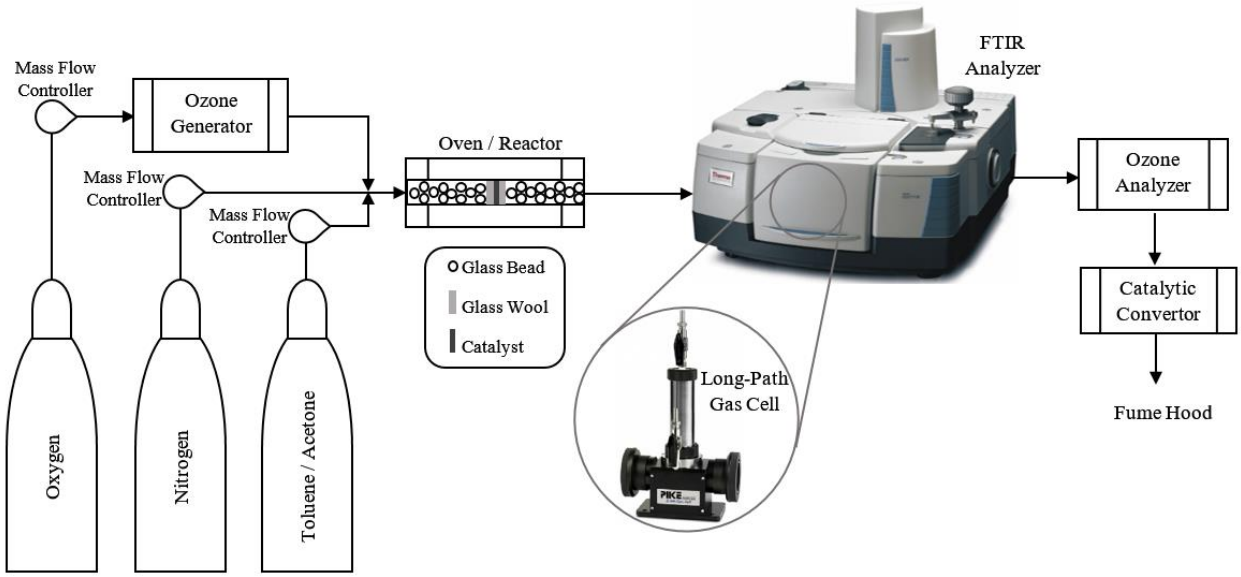

Fig. 3.3. Schematic of the experimental setup for kinetic analyses.

Then, reaction rates (r_{voc}) were calculated by Eq. (3.6):

$$-r'_{voc} = \frac{dX_{voc}}{d(W/F_{voc,in})} \tag{3.6}$$

Finally, the obtained reaction data were fitted to the power law kinetic model by using the non-linear least squares regression tool of IBM SPSS 24.

Chapter 4:
Catalytic ozonation of toluene

Results of investigation of catalytic ozonation of toluene on MnO_x/γ-alumina (10%) catalyst are presented in this chapter. First, characterization of the MnO_x/γ-alumina will be discussed. Then catalyst activity and reaction kinetics will be discussed, followed by in situ DRIFTS studies and characterization of the spent catalyst. Finally, the role of surface carboxylates in catalytic ozonation of toluene will be discussed.

Contribution of the PhD candidate:

The PhD candidate, Mostafa Aghbolaghy, was the major contributor of this chapter. All of the written text was prepared by Mostafa Aghbolaghy. Dr. Jafar Soltan supervised and provided consultation during the experimental period and thesis preparation. An earlier version of the experimental setup had been designed and constructed by Dr. Ebrahim Rezaei. The experimental setup was significantly upgraded by Mostafa Aghbolaghy. The upgrade included changes to design, tubing, flow control, and analysis systems. XANES and XAFS data were collected in the Canadian Light Source by assistance of Dr. Ning Chen. Also, XPS data were collected in the Canadian Light Source by assistance of Ronny Sutarto. Dr. Ning Chen provided general guidance for analyses of the XANES and XAFS data. In situ DRIFTS measurements, catalyst

activity measurements, temperature programmed analyses, and GC-MS analysis were performed and interpreted by Mostafa Aghbolaghy. Suggestions from advisory committee members (alphabetic order: Dr. Ning Chen, Dr. Mehdi Nemati, Dr. Catherine Niu, and Dr. Hui Wang) were used to improve the quality of this work.

4.1. Characterization of MnO_x/γ-alumina

BET surface area and pore volume of pure γ-alumina were 219 m^2/g and 0.60 cm^3/g, respectively. Addition of manganese slightly decreased the surface area and pore volume. BET surface area and pore volume of the fresh MnO_x/γ-alumina catalyst were 200 m^2/g and 0.56 cm^3/g, respectively. This indicates that the structure of γ-alumina was preserved during the catalyst preparation. ICP-MS analysis showed that the manganese loading on the catalyst was 9.8 wt%. This is close to the nominal manganese loading of 10 wt%.

X-ray absorption fine structure (XAFS) was used to further characterize the catalyst. Essentially, XAFS probes the local structure around selected atomic species and is based on the way that X-rays are absorbed by an atom at energies near and above the core level binding energies of that atom [103,104]. In other words, XAFS is a measure of the energy dependence of absorption coefficient. If energy of the incident X-ray is equal to that of the binding energy of a core-level electron, there will be a sharp rise in absorption (i.e. absorption edge). The strong dependence of absorption coefficient on atomic number and X-ray energy is a fundamental property [93,103,104].

The obtained X-ray absorption spectrum can be divided into two regimes including X-ray absorption near-edge structure (XANES) and extended X-ray absorption fine structure (EXAFS).

XANES is especially sensitive to formal oxidation state and coordination chemistry of the absorbing atom. XANES can be used as a fingerprint to identify phases, as position and shape of edge are sensitive to formal valence state, ligand type, and coordination environment. Also, owing to large signal of XANES, it might be utilized at lower concentrations and imperfect sample conditions [103,104].

Mn *K-edge* XANES spectra of the catalyst and pure reference materials were collected to investigate the manganese oxide phases of the catalyst. Fig. 4.1 shows the XANES spectra. Absorption energy of Mn *K-edge* was determined to be 6553.86 eV for the catalyst, which was very close to Mn *K-edge* absorption energy of Mn_2O_3 (6553.73 eV). Linear combination fitting of the XANES spectra showed that Mn_2O_3 was the dominant manganese oxide phase of the catalyst with 82% abundance, followed by 11% MnO_2, and 7% Mn_3O_4.

It has been reported [19] that decrease in Mn loading of catalysts decreases oxidation state of the manganese and increases catalytic activity towards catalytic ozonation of toluene. Similar studies have found that catalysts with lower oxidation state of Mn are more active in catalytic ozonation of acetone and benzene [40,78].

Therefore, among the detected Mn species in this work, Mn_3O_4 is the most active species, followed by Mn_2O_3, and MnO_2. On the other hand, Mn_2O_3 is the dominant Mn species of the catalyst with 82% abundance, while Mn_3O_4 constitutes only 7% of the Mn species. Thus, one can conclude that Mn_2O_3 was the main Mn species responsible for the catalytic ozonation of acetone in this work.

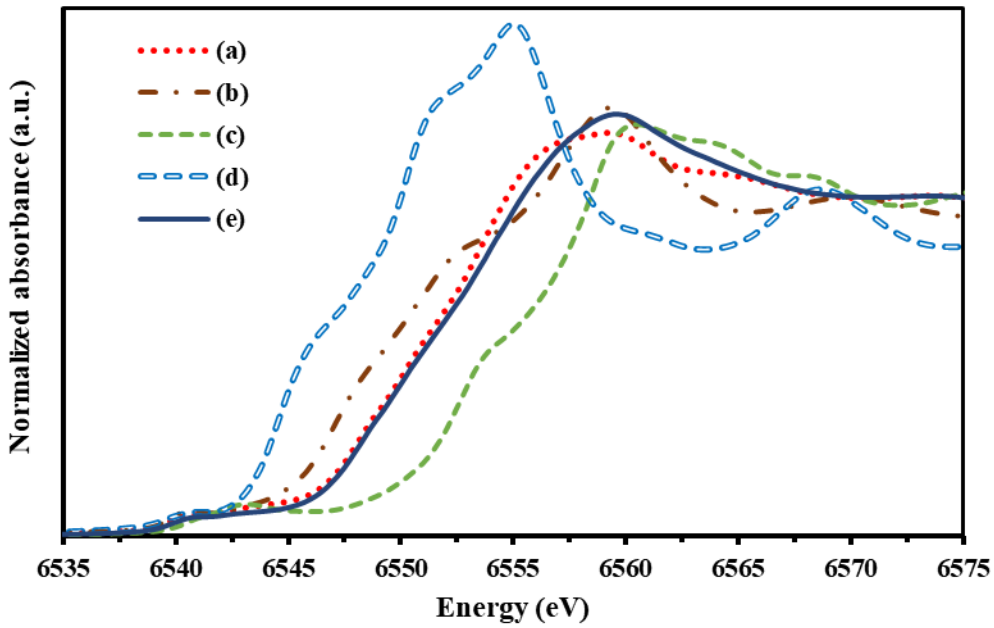

Fig. 4.1. XANES spectra of Mn *K-edge*;
(a) Mn_2O_3 (b) Mn_3O_4 (c) MnO_2 (d) MnO (e) $MnO_x\gamma$-Al_2O_3.

EXAFS is utilized to determine coordination number, distances and species of the neighboring atoms [103,104]. EXAFS can be described in terms of the wave behavior of photoelectron created in the absorption process. Since this phenomenon is an interference effect and depends on the wave nature of the photoelectron, it is better to describe it by means of photoelectron wavenumber (k) rather than X-ray energy. EXAFS model can be described by the following equation:

$$x(k) = \sum_j \frac{N_j S_0^2 f_j(k) e^{-2R_j/\lambda(k)} e^{-2k^2\sigma_j^2}}{KR_j^2} \sin[2kR_j + \delta_j(k)] \qquad (4.1)$$

where f(k), δ(k), R and N are scattering amplitude, phase-shift, distance and coordination number of the neighboring atoms. Also, σ^2, S_o^2 and λ(k) are mean square disorder of neighbor distance, amplitude reduction term and mean free path of photoelectron, respectively. The sum is over shells of similar neighboring atoms [22-24].

Mn_2O_3, the dominant manganese oxide phase of the catalyst, was used to estimate S_o^2 for EXAFS analyses. Mn_2O_3 has two Mn sites with occupancies of 25% and 75%. The site with 75% occupancy has two oxygen bonds at 1.90 Å, two oxygen bonds at 1.98 Å, and another set of two oxygen bonds at 2.25 Å. On the other hand, the site with 25% occupancy has 6 oxygen atoms at 1.99 Å, which are very close to the oxygen bond length of the other Mn site at 1.98 Å. The close atomic coordinates of oxygen in the two Mn sites make the EXAFS analysis complicated. Therefore, aggregate FEFF calculation was used to integrate the two Mn sites into one single site for EXAFS analysis. In the aggregate method, the path lists are weighted by fractional population of each site in the unit cell, before running for fuzzy degeneracy [105].

Fig. 4.2 shows the magnitude and real part of the Fourier transform of Mn *K-edge* spectra and fittings for the catalyst and Mn_2O_3. Also, Table 4.1 presents crystal structure of Mn_2O_3 and EXAFS fitting results for Mn_2O_3 and the catalyst. An amplitude reduction factor of 0.754 was obtained for Mn_2O_3. This is comparable with S_o^2 of 0.740 found by Longo et al. [106] for Mn_2O_3. Fitting EXAFS data of Mn_2O_3 based on the aggregate method locates the first shell oxygen atoms at interatomic distances of ca. 1.87, 1.96 and 2.22 Å with coordination numbers of 1.5, 3.0 and 1.5, respectively. Also, Mn atom at the second shell was located at interatomic distance of ca. 3.11 Å with coordination number of 6.

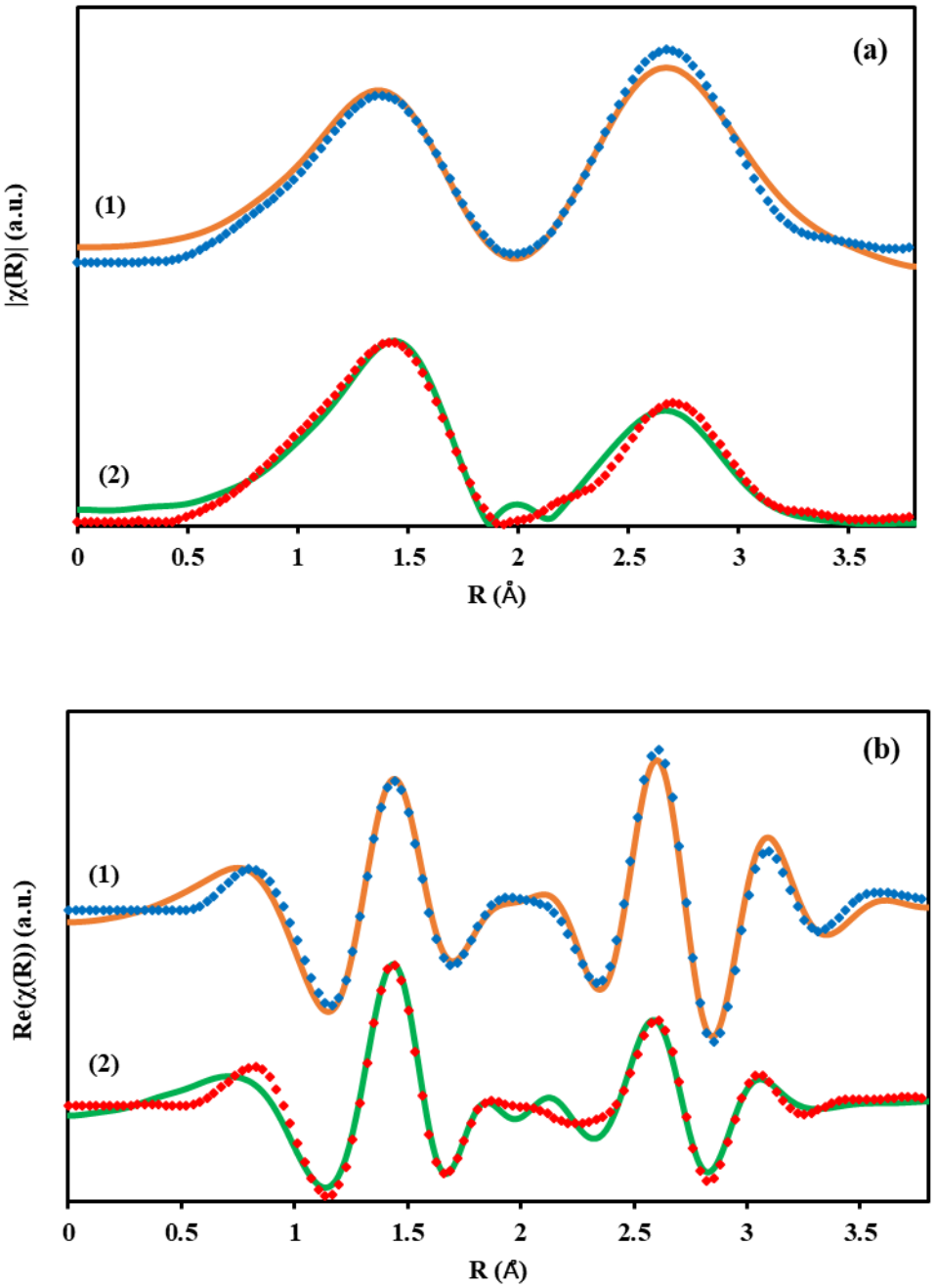

Fig. 4.2. (a) Magnitude and (b) real part of the Fourier transform of Mn K-edge data (symbols) and fitting (solid lines); (1) Mn_2O_3 (2) $MnO_x/\gamma\text{-}Al_2O_3$.

Fitting EXAFS data of the catalyst found 5.58 Mn atoms at the second Mn shell at interatomic distance of ca. 3.12 Å. This is slightly lower than the number of Mn atoms at the second Mn shell of Mn_2O_3, which can be assigned to contribution of other manganese phases as identified by LCF of the XANES spectra.

On the other hand, 1.5, 3.0, and 1.7 oxygen atoms were found at the first Mn shell at interatomic distances of ca. 1.88, 1.97 and 2.23 Å, respectively. These are in good agreement with the values obtained for Mn_2O_3. Therefore, there were 6.2 oxygen atoms at the first Mn shell of the catalyst. Absolute percentage misfit between data and model was less than 2.5% for both catalyst and Mn_2O_3 EXAFS fittings, indicating that the models were fitted closely to the EXAFS data.

Fig. 4.3 shows deconvolution of the Mn $2p_{1/2}$ and Mn $2p_{3/2}$ XPS spectra of the MnO_x/γ-alumina catalysts. Four peaks were found from deconvolution of the spectra. The peaks at 641.0 and 652.7 eV are assigned to Mn^{3+}, and the peaks at 642.1 and 653.8 eV are attribute to Mn^{4+} [71,107]. Mn^{3+} to Mn^{4+} ratio was 6.7 with Mn^{3+} abundance of 87%. Considering that Mn_2O_3 has an Mn oxidation state of +3, the XPS results confirm the XANES results that Mn_2O_3 is the dominant manganese oxide phase of the catalyst.

Table 4.1. Crystal structure and EXAFS results by using aggregate FEEF method.

	Path / Bond	CN	R (Å)	σ^2 ($\times 10^{-3}$ Å^2)	ΔE_o (eV)	S_o^2	R_f (%)[a]
Mn_2O_3 (crystal structure)	Mn–O	1.5	1.90				
	Mn–O	3.0	1.99				
	Mn–O	1.5	2.25				
	Mn–Mn	6.0	3.11				
Mn_2O_3 (EXAFS fitting)	Mn–O	1.5	1.87 ± 0.02	4.8 ± 2.9	-3.87 ± 2.29	0.754 ± 0.173	1.2
	Mn–O	3.0	1.96 ± 0.02				
	Mn–O	1.5	2.22 ± 0.02				
	Mn–Mn	6.0	3.11 ± 0.02	7.7 ± 2.5			
MnO_x/γ-Alumina	Mn–O	1.5 ± 0.3	1.88 ± 0.01	3.6 ± 2.1	-0.16 ± 1.67	0.754	2.4
	Mn–O	3.0 ± 0.6	1.97 ± 0.01				
	Mn–O	1.7 ± 0.7	2.23 ± 0.01				
	Mn–Mn	5.6 ± 1.9	3.12 ± 0.02	12.0 ± 3.9			

[a] Absolute percentage misfit between data and model

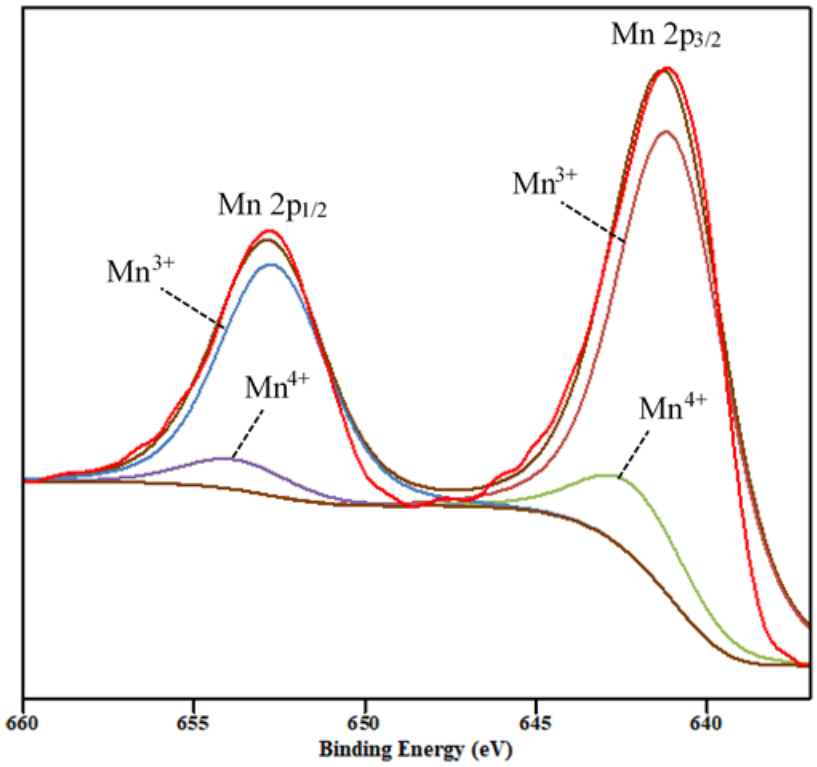

Fig. 4.3. Mn $2p_{1/2}$ and $Mn2p_{3/2}$ XPS spectra of the MnO_x/γ-alumina catalyst and their deconvoluted peaks.

4.2. Catalytic activity of MnO_x/γ-alumina in catalytic ozonation of toluene

Catalytic ozonation of toluene was carried out over MnO_x/γ-alumina catalyst at 25 and 90 °C. Toluene and ozone conversion profiles as a function of reaction time are presented in Fig. 4.4 (a). Also, Fig. 4.4 (b) shows CO and CO_2 concentrations in the product stream during the catalytic ozonation.

At 90 °C, a stable reaction was observed with high conversions of about 91% for toluene and 92% for ozone. However, at 25 °C operation, a decline in toluene and ozone conversions

was observed. After 150 minutes of the reaction at 25 °C, toluene and ozone conversions dropped to 64% and 37%, respectively. At 90 °C, carbon monoxide and carbon dioxide concentrations increased gradually with reaction time and reached constant concentrations of 200 and 500 ppmv, respectively. On the other hand, at 25 °C, carbon monoxide and carbon dioxide concentrations increased initially and reached maximum values of 75 and 235 ppmv, respectively, followed by a decline in CO_2 concentration.

It has been suggested [86,87] that ozone decomposition on the surface of the catalyst generates highly reactive oxygen species that rapidly oxidize the adsorbed VOCs in catalytic ozonation processes. Ozone decomposition on manganese oxide occurs as follows [58,60]:

$$O_3 + Mn^{n+} \rightarrow O_2 + O^{2-} + Mn^{(n+2)+} \quad (4.2)$$

$$O_3 + O^{2-} + Mn^{(n+2)+} \rightarrow O_2 + O_2^{2-} + Mn^{(n+2)+} \quad (4.3)$$

$$O_2^{2-} + Mn^{(n+2)+} \rightarrow O_2 + Mn^{n+} \quad (4.4)$$

The similarity of VOC and ozone conversion profiles can suggest that higher ozone conversion may lead to higher VOC conversion. However, a study [75] showed that Pd/γ-Al_2O_3 (1 wt%), which is very active for ozone decomposition (without VOCs), fails in catalytic ozonation of toluene and experiences a severe deactivation. Therefore, higher ozone conversion by a catalyst does not necessarily enhance VOC conversion, although ozone decomposition remains an essential part of all gas phase catalytic ozonation systems and is strongly linked to the overall oxidation process.

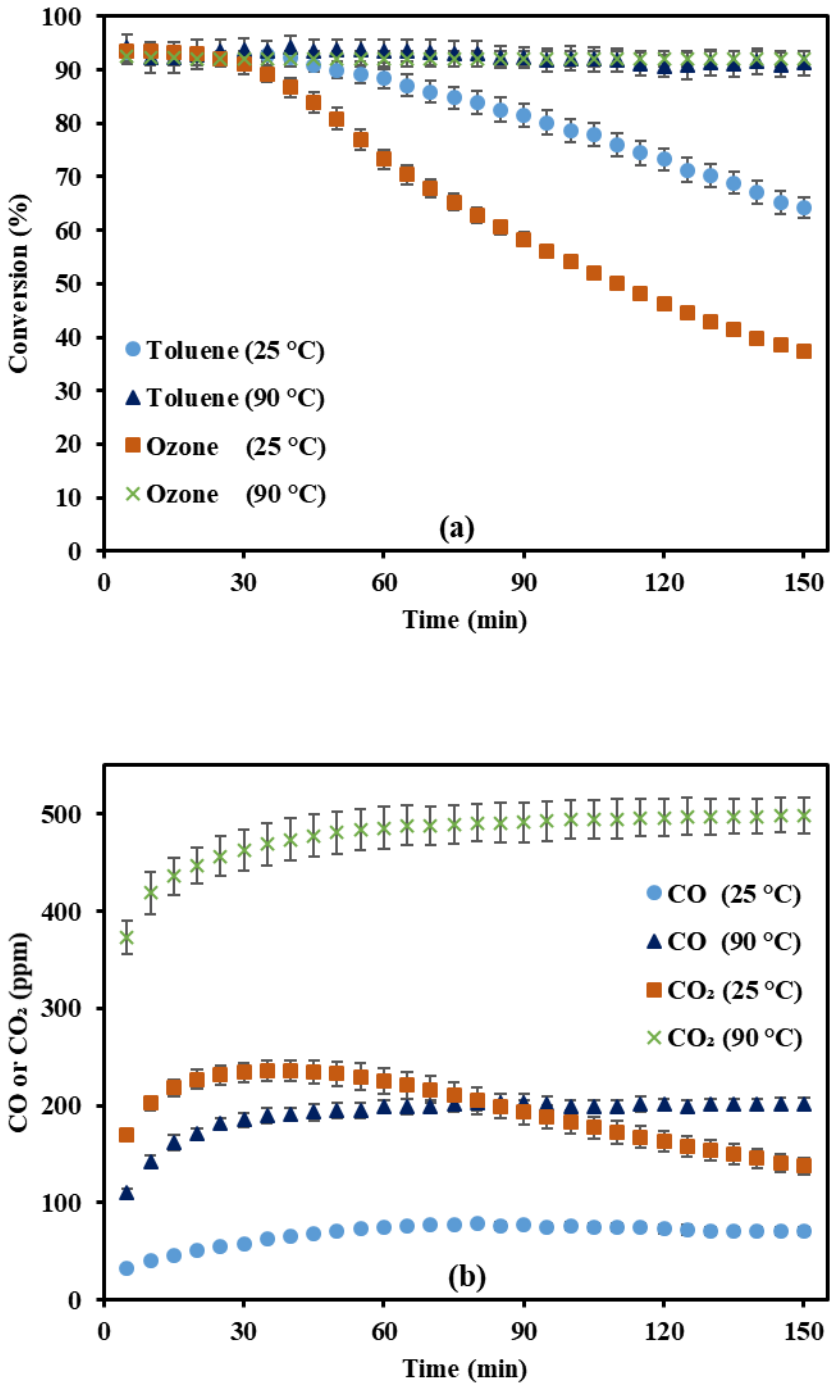

Fig. 4.4. Catalytic ozonation of toluene at 25 and 90 °C on MnO_x/γ-alumina, (a) toluene and ozone conversions; (b) CO and CO_2 concentrations in the exhaust stream; WHSV = 350 L h^{-1} g^{-1}, [O_3] = 1200 ppmv, and [toluene] = 130 ppmv; error bars are standard errors.

4.3. Catalytic activity of γ-alumina in catalytic ozonation of toluene

Similar experiments were conducted by using γ-alumina to investigate its role in catalytic ozonation of toluene. Toluene and ozone conversion profiles along with the produced CO and CO_2 concentrations are presented in Fig. 4.5.

Rapid catalyst deactivation was observed at both 25 and 90 °C, however, toluene and ozone conversions were relatively higher at 90 °C compared to those at the 25 °C reaction. After only 40 minutes of reaction at 90 °C, toluene and ozone conversions dropped to 50% and 37%, respectively. At 25 °C, toluene and ozone conversions plunged to 21% and 7%, respectively. Similarly, produced carbon monoxide and carbon dioxide concentrations for reactions over γ-alumina were significantly lower than those for reactions over $MnO_x/\gamma\text{-}Al_2O_3$ catalyst.

This observation emphasizes the important role of the Mn sites in the catalytic activity of the $MnO_x/\gamma\text{-}Al_2O_3$ catalyst. Moreover, this observation suggests that $\gamma\text{-}Al_2O_3$ is not an inert support and it can oxidize toluene in the presence of ozone, although the reaction is not stable and a rapid catalyst deactivation occurs. Studies on catalytic ozonation of VOCs, using manganese oxide supported on γ-alumina, silica, titania, and zirconia, found that VOC removal rates normalized by surface area of the catalysts were comparable or slightly lower than those with the γ-alumina supported catalysts [26,27].

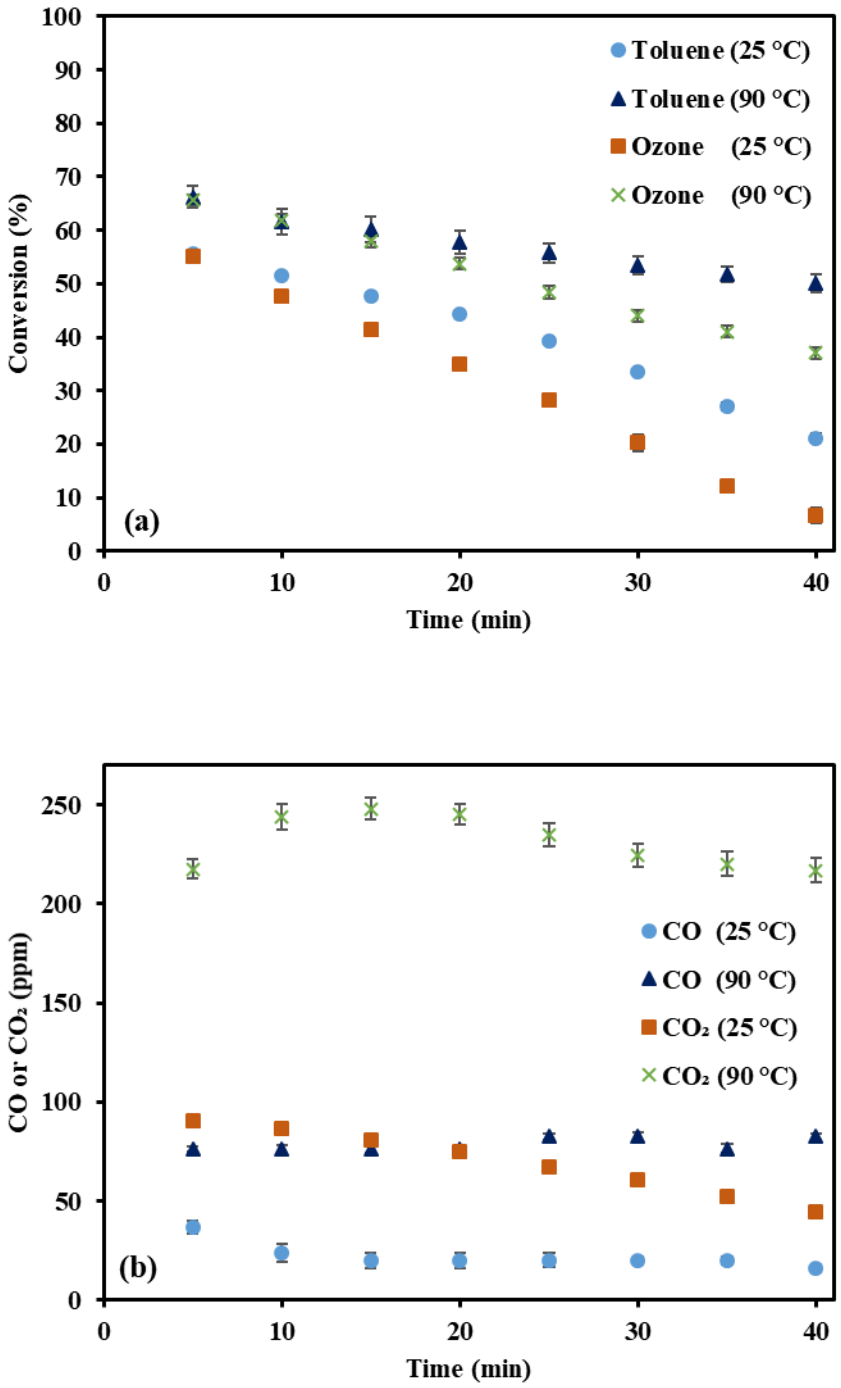

Fig. 4.5. Catalytic ozonation of toluene at 25 and 90 °C on γ-alumina, (a) toluene and ozone conversions; (b) CO and CO_2 concentrations in the exhaust stream; WHSV = 350 L h^{-1} g^{-1}, [O_3] = 1200 ppmv, and [toluene] = 130 ppmv; error bars are standard errors.

4.4. Reaction kinetics of catalytic ozonation of toluene on MnO_x/γ-alumina

Kinetic data were obtained at three different temperatures (70, 80, and 90 °C), since catalyst activity is stable at temperatures above 60 °C and catalyst deactivation occurs at lower temperatures. Homogeneous reaction between ozone and toluene (in the absence of catalyst) was negligible at these temperatures. Similar observation has been reported by other researchers [108]. As mentioned in Chapter 3, the employed catalyst powder size, reaction conditions and reactor configurations inhibited mass transfer limitations. Reaction rates were obtained using differential method of analysis as discussed in section "*3.7. Kinetic analyses*". Table 2.1 presents the obtained reaction rates for catalytic ozonation of toluene on MnO_x/γ-alumina. The power law model has been used in several kinetic studies of catalytic ozonation [80,81] of VOCs. This model is expressed by Eq. (4.5):

$$-r'_{tol} = k' C_{tol}^{\alpha} C_{O_3}^{\beta} \tag{4.5}$$

where, r'_{tol} is toluene reaction rate (mole kg^{-1} s^{-1}), C_{tol} is concentration of toluene (mole L^{-1}), and C_{O_3} is concentration of ozone (mole L^{-1}). In addition, there are three unknown parameters (α, β, and k). α and β are orders of reaction with respect to toluene and ozone, respectively. k' is the reaction rate constant, which can be expressed as:

$$k' = A(\exp(\frac{-E_a}{RT})) \tag{4.6}$$

where, R is the universal gas constant (8.314 J K^{-1} $mole^{-1}$), A is frequency factor (i.e. pre-exponential factor), E_a is the apparent activation energy, and T is the reaction temperature (K).

Table 4.2. Reaction rates for catalytic ozonation of toluene on MnO_x/γ-alumina.

Temperature (K)	Toluene [a] ($\times 10^6$ mole L^{-1})	Ozone [b] ($\times 10^6$ mole L^{-1})	$-r_{tol}$ ($\times 10^4$ mole kg^{-1} s^{-1})
363	5.3	49.1	26.9
363	4.7	42.4	24.6
363	4.3	40.6	23.7
363	3.5	36.0	21.6
363	2.1	20.8	15.4
363	1.1	10.8	10.2
363	0.3	1.5	3.2
353	5.3	49.1	18.8
353	4.8	43.9	16.8
353	4.3	39.9	15.1
353	2.9	29.2	10.8
353	2.1	23.4	8.3
353	1.0	10.3	4.1
343	5.3	49.1	11.8
343	4.7	43.0	10.9
343	4.0	39.2	10.1
343	3.5	34.7	9.4
343	2.3	22.0	7.0

[a] Standard error within ± 3%.
[b] Standard error within ± 1.5%.

Combining Eqs. (4.5) and (4.6) results in Eq (4.7):

$$-r'_{tol} = A(\exp(\frac{-E_a}{RT}))C_{tol}^{\alpha}C_{O_3}^{\beta} \quad (4.7)$$

Reaction data were fitted to Eq. (4.7) by using the non-linear least squares regression. This allows non-isothermal fitting of the data. Results of fitting are presented in Table 4.3. Also, Fig. 4.6 compares the experimental and predicted rates of toluene removal in catalytic ozonation.

The obtained apparent activation energy (33 kJ $mole^{-1}$) is comparable to the apparent activation (29 kJ $mole^{-1}$) of catalytic ozonation of toluene over MnO_2/graphene [80]. Also, the obtained activation energy is lower than the activation energy (56 kJ $mole^{-1}$) of homogenous gaseous reaction of toluene with ozone [109], indicating that a heterogenous reaction occurs on MnO_x/γ-alumina. In addition, apparent activation energy (83 - 107 kJ $mole^{-1}$) of catalytic oxidation of toluene (in the absence of ozone) [110,111] is significantly higher than the obtained apparent activation energy for catalytic ozonation.

The obtained reaction orders for toluene and ozone were positive, fractional, and between zero and one. Similar reaction orders were obtained for catalytic ozonation of toluene over MnO_2/graphene [80]. Positive reaction orders for both toluene and ozone mean that an increase in concentration of toluene or ozone enhances the reaction rate.

Table 4.3. Fitting results of the kinetic model for catalytic ozonation of toluene.

A ($mole^{0.348}$ $L^{0.652}$ kg^{-1} s^{-1})	E_a (kJ $mole^{-1}$)	α	β	R^2 [a]
1.580×10^5	33	0.183	0.469	0.955

[a] Coefficient of determination of the regression analysis.

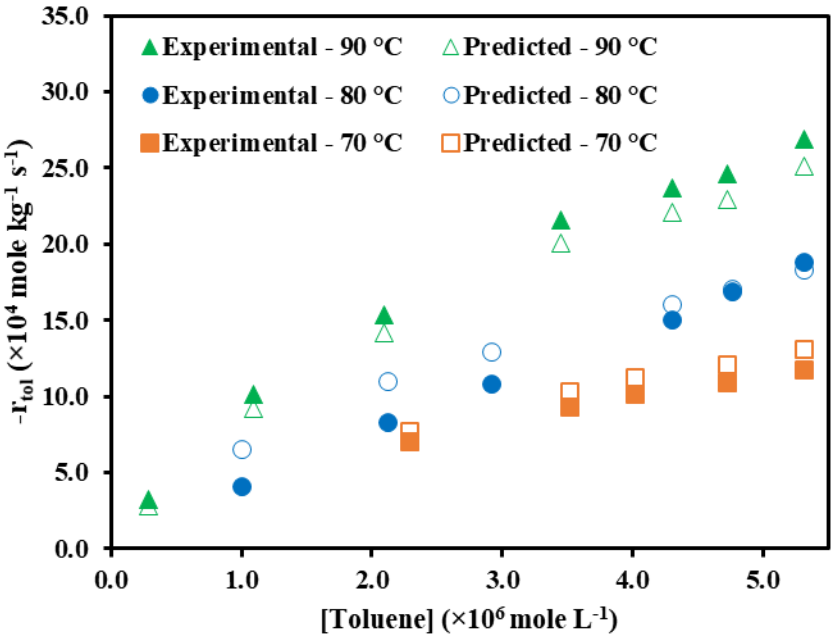

Fig. 4.6. Comparison of the experimental and predicted rates of toluene removal in catalytic ozonation.

4.5. In situ DRIFTS of catalytic ozonation of toluene

To better understand the effect of temperature on catalyst activity, in situ DRIFTS studies were conducted. Fig. 4.7a and Fig. 4.7b show in situ DRIFTS spectra of the catalytic ozonation of toluene over MnO_x/γ-Al_2O_3 catalyst at 25 °C and 90 °C, respectively.

Toluene adsorption on the catalyst did not change the spectrum of the fresh catalyst, due to low concentration of toluene in the inlet stream. Once ozone was introduced into the reactor, a number of peaks appeared. The peaks at around 1429, 1740, and 1603 cm^{-1} were the main bands corresponding to C-H asymmetric deformation vibration, C=O stretching, and overlap of aromatic ring stretching and COO^- stretching of surface carboxylates, respectively. Moreover,

there was a broad band from 2400 to 3750 cm^{-1} corresponding to the overlap of OH stretching of alcohols, carboxylic acids and water. Similar observations have been reported during in situ DRIFTS study of catalytic ozonation of benzene over $MnO_2/\gamma\text{-}Al_2O_3$ [26]. Complete list of significant bands and corresponding functional groups are presented in Appendix D [19,26,112].

The in situ spectra suggest that catalytic ozonation started with a similar mechanism at both 25 and 90 °C. This caused appearance and initial increase of similar bands at both temperatures. However, the bands corresponding to the undesired product formation (i.e. 1740, and the broad band at 2400 – 3750 cm^{-1}) were stronger at 25 °C, which is in agreement with the deactivation pattern of the catalyst at 25 ° C.

In situ DRIFTS spectra for catalytic ozonation of toluene using pure γ-alumina at 25 ° C are depicted in Fig. 4.8. The significant bands were at around 1325-1393 and 1600 cm^{-1} corresponding to COO^- stretching of the surface carboxylates, and overlap of aromatic ring stretching and another COO^- stretching, respectively. In addition, there was a broad band from 2500 to 3750 cm^{-1} corresponding to the overlap of OH stretching of alcohols, carboxylic acids and water.

The most important difference between the spectra obtained from MnO_x/γ- alumina and γ-alumina was the presence of a very strong band at around 1740 cm^{-1} (corresponding to C=O stretching) on the spectra of the MnO_x/γ-alumina catalyst. The same band appeared only as a shoulder on the spectra of the γ-alumina catalyst. This implies that the presence of manganese oxide is essential to effectively oxidize carbonaceous materials on the surface of the catalyst.

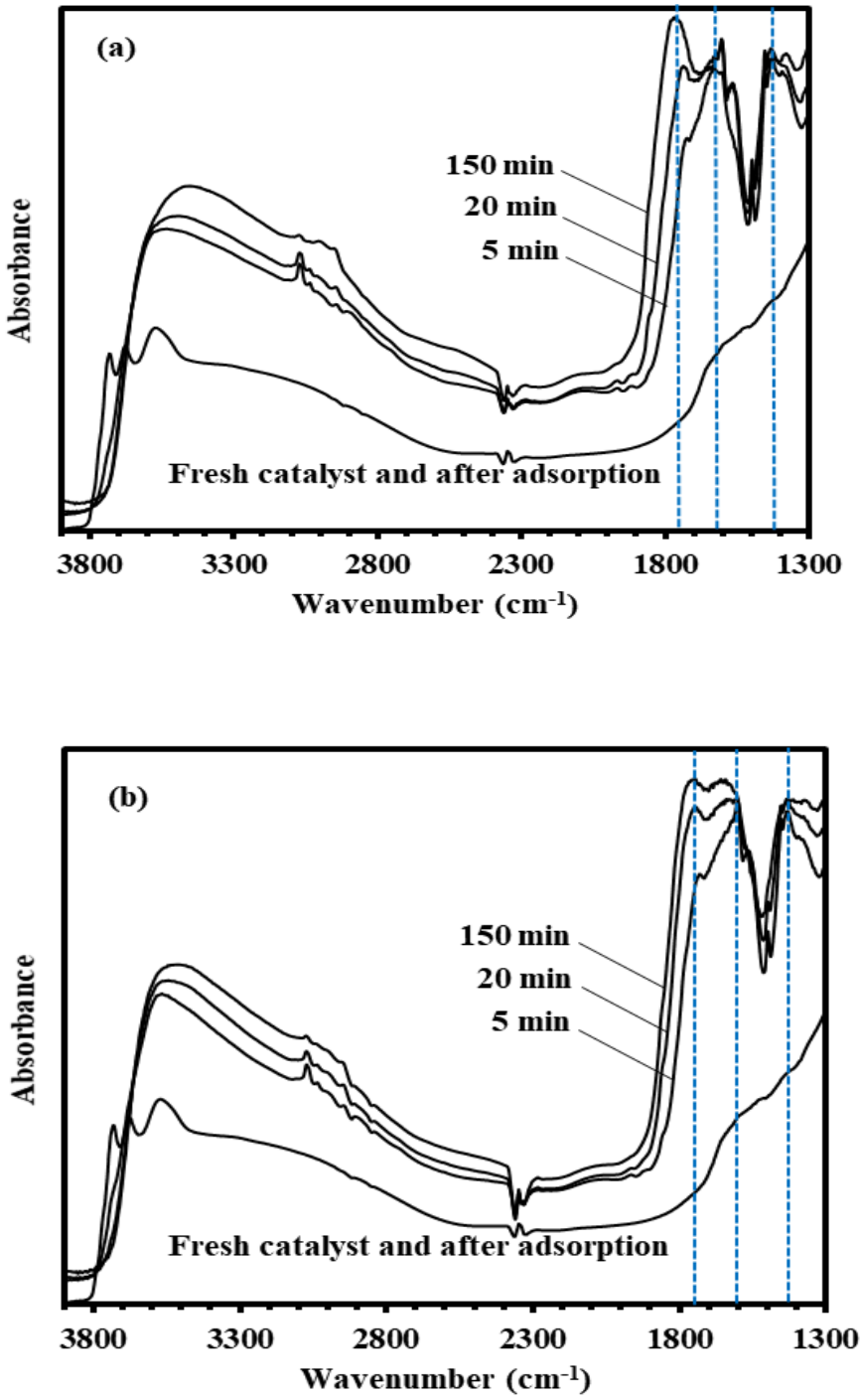

Fig. 4.7. In situ DRIFTS spectra of catalytic ozonation of toluene over MnO_x/γ-alumina at (a) 25 °C and (b) 90 °C; WHSV = 350 L h^{-1} g^{-1}, [O_3] = 1200 ppmv, and [toluene] = 130 ppmv.

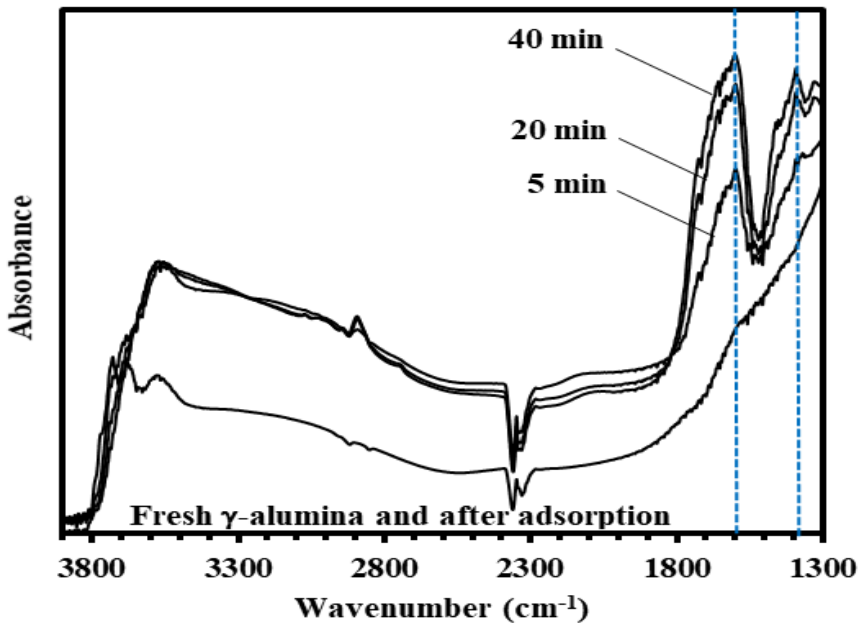

Fig. 4.8. In situ DRIFTS spectra of catalytic ozonation of toluene over γ-alumina at 25 °C; WHSV = 350 L h^{-1} g^{-1}, [O_3] = 1200 ppmv, and [toluene] = 130 ppmv.

4.6. Temperature programmed analysis on the spent catalyst

Thermo-gravimetric analysis was conducted under inert N_2 environment. Fig. 4.9 shows weight loss profile of the spent MnO_x/γ-alumina catalyst during the thermo-gravimetric analysis. After heating the spent catalysts at a rate of 20 °C/min to 790 °C, the spent catalysts of 25 and 90 °C reactions lost 27% and 11% of their weights, respectively. This indicates that higher amount of materials accumulated on the catalyst at the 25 °C operation.

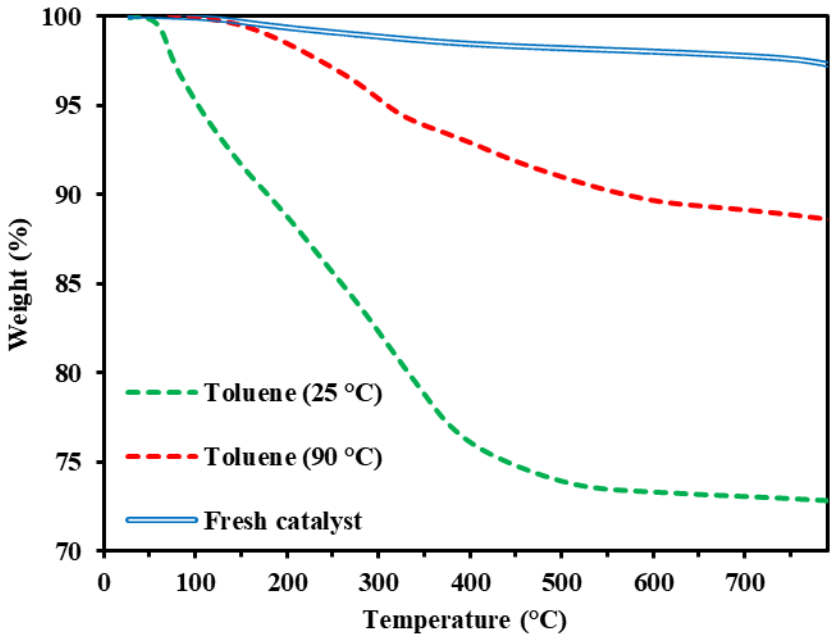

Fig. 4.9. Weight loss during thermo-gravimetric analysis of MnO_x/γ-alumina catalyst used in catalytic ozonation of toluene at 25 °C and 90 °C.

Fig. 4.10 depicts in situ DRIFTS spectra at different temperatures of 325, 525 and 870 °C during temperature programmed desorption (TPD) of the catalyst used in the 25 °C catalytic ozonation. TPD was carried out under inert N_2 flow and the spent catalyst was heated up to 870 °C at a rate of 20 °C/min. By heating the spent catalyst to 325 °C, intensities of all bands decreased to some extent. Further increase in temperature to 525 °C, reduced intensities of the band at 1740 cm^{-1} (C=O stretching) and the broad band at 2400 – 3750 cm^{-1} (OH stretching). On the other hand, it increased intensities of the bands at 1429 (C-H asymmetric deformation vibration) and 1600 cm^{-1} (overlap of aromatic ring stretching and COO^- stretching of surface carboxylates). At 525 °C, there were still two other bands at 2930 cm^{-1} and 3060 cm^{-1}

corresponding to saturated and unsaturated C-H stretching, respectively. Further increase in temperature to 870 °C, removed the bands at 1740 and 2930 cm^{-1} and reduced intensity of the bands at 1429 and 1600 cm^{-1}. Therefore, even at 870 °C, the bands at 1429, 1530 – 1600, and 3060 cm^{-1} (as indicated in Fig. 4.10) remained on the spectra.

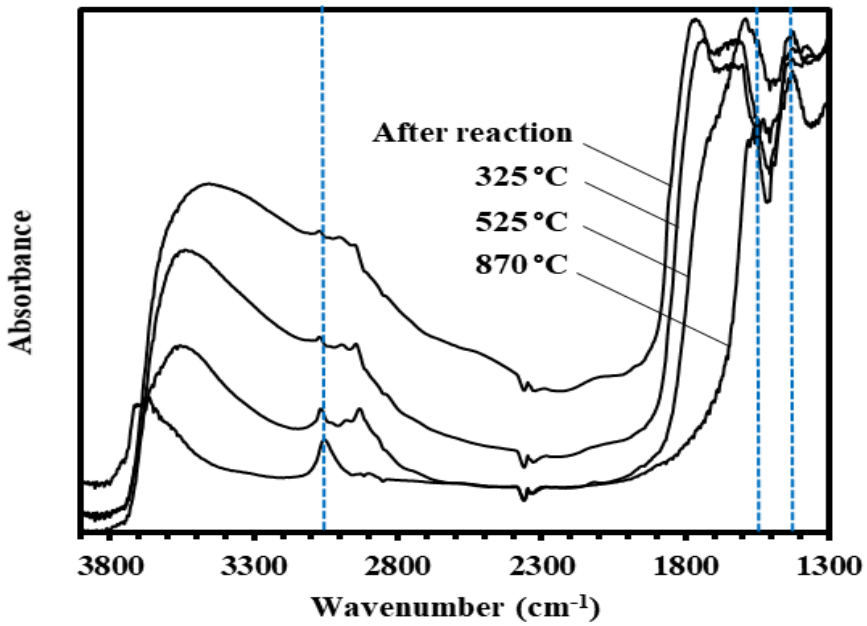

Fig. 4.10. In situ DRIFTS spectra during TPD analysis of spent MnO_x/γ-alumina catalyst used in catalytic ozonation of toluene at 25 °C.

The evolved gases during TPD were analyzed and Table 4.4 presents a summary of the detected compounds at each temperature range. CO and CO_2 were found in the exhaust gas during TPD of the spent catalyst at almost all TPD temperatures (25 - 870 °C). The presence of significant amounts of CO and CO_2 in a wide range of temperature indicates that the detected

CO_x not only originated from desorption of adsorbed CO and CO_2, but also they evolved from decomposition of larger carbonaceous compounds that were deposited on the catalyst.

During TPD of the catalyst used for the 25 °C catalytic ozonation, acetic acid, formic acid and water were desorbed by heating the spent catalyst to 325 °C. Benzene and methane were detected during TPD from 525 to 870 °C. This is the same temperature range at which the bands corresponding to saturated C-H stretching, aromatic ring stretching and COO^- stretching of surface carboxylates were decreased/removed as well (Fig. 4.10). This implies that benzene and methane evolved from decomposition of larger surface carboxylate compounds. Surface carboxylates have been found in catalytic ozonation of VOCs using SiO_2-based catalysts as well [28]. During TPD of the catalyst used for the 90 °C catalytic ozonation, benzene and methane were detected at 525 - 870 °C temperature range. This indicates that the surface carboxylates, associated with benzene and methane, were present at the 90 °C catalytic ozonation as well.

Table 4.4. Compounds detected in the exhaust gas during TPD of the spent MnO_x/γ-alumina used in catalytic ozonation of toluene.

Sample	Temperature range (°C)	Detected compounds
25 °C reaction	25 - 325	acetic acid, formic acid, water vapor, CO, CO_2
25 °C reaction	325 - 525	water vapor, CO, CO_2
25 °C reaction	525 - 870	benzene, methane, CO, CO_2
90 °C reaction	25 - 325	water vapor, CO, CO_2
90 °C reaction	325 - 525	water vapor, CO, CO_2
90 °C reaction	525 - 870	benzene, methane, CO, CO_2

Temperature programmed oxidation (TPO) of the spent catalysts was conducted under atmospheric-pressure flow of oxygen-nitrogen (20-80 v%) and heating rate of 10 °C/min. Fig. 4.11 depicts in situ DRIFTS spectra during TPO of the catalyst used in the 25 °C catalytic ozonation. By increasing temperature to 745 °C almost all bands corresponding to carbonaceous materials disappeared. Similar results have been reported for TPO of spent MnO_2/γ-alumina catalysts used for catalytic ozonation of benzene [26]. This is different from TPD (under N_2) results that even at 870 °C, some bands at 1429, 1530 – 1600, and 3060 cm^{-1} remained on the spectra.

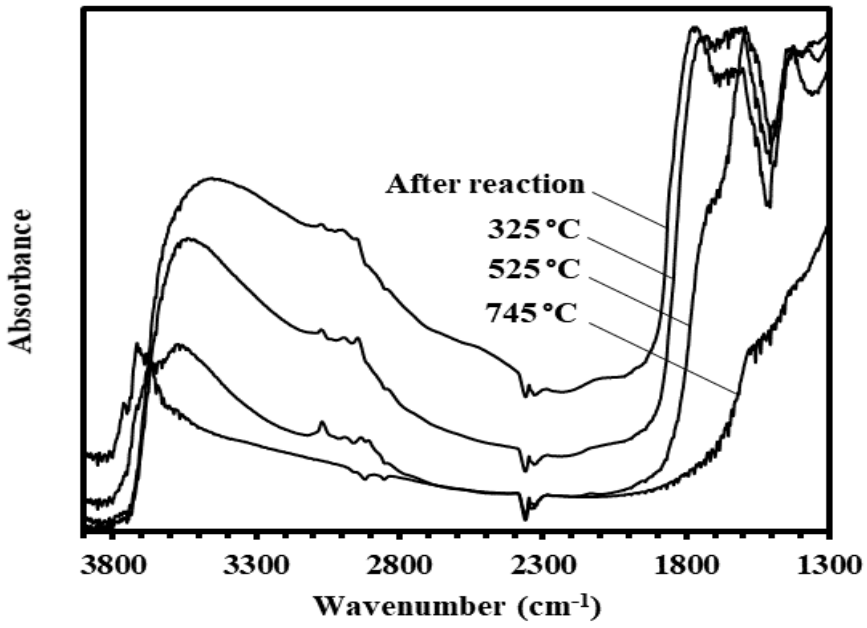

Fig. 4.11. In situ DRIFTS spectra during TPO analysis of spent MnO_x/γ-alumina catalyst used in catalytic ozonation of toluene at 25 °C.

Fig. 4.12 shows the variations in CO and CO_2 concentrations during TPO analysis. For the catalyst used in the 25 °C catalytic ozonation (Fig. 4.12a), maximum CO generation was at 342 °C with a concentration of 385 ppmv. Also, maximum CO_2 concentration was 2260 ppmv that was obtained at 372 °C. Most of the CO_2 was generated in the temperature range of 275 – 525 °C. This is in agreement with the DRIFTS spectra during TPO (Fig. 4.11) that increasing temperature to 525 °C decreased the intensity of the band at 1740 cm^{-1} (C=O stretching) significantly. Benzene and methane gases were not detected during TPO analysis. This indicates that the surface carboxylates, associated with benzene and methane, were oxidized to CO and CO_2.

Similar results were obtained for the catalyst used in the 90 °C catalytic ozonation (Fig. 4.12b), however, CO and CO_2 concentrations were relatively lower. In this case, the maximum CO concentration was 195 ppmv that was obtained at 308 °C, and CO_2 concentration reached a maximum value of 1330 ppmv at 345 °C. For the catalyst used in the 25 °C reaction, total amount of the evolved CO_x during TPO was almost 2 times higher than that of the 90 °C reaction (Table 4.5), indicating that higher amount of carbonaceous materials accumulated on the catalyst in the 25 °C reaction.

Table 4.5 shows the quantitative data for the overall carbon balance in the process. The overall carbon balance was calculated based on Eq. (3.4) as described in section "*3.4. Temperature programmed analyses*". For the 25 °C operation, about 25.57 mg carbon entered the reactor during the saturation and reaction time. On the other hand, 25.13 mg carbon was detected in the exhaust of the reactor as unreacted toluene, produced CO_x during reaction, and CO_x during TPO. This resulted in a 94.58% overall carbon balance.

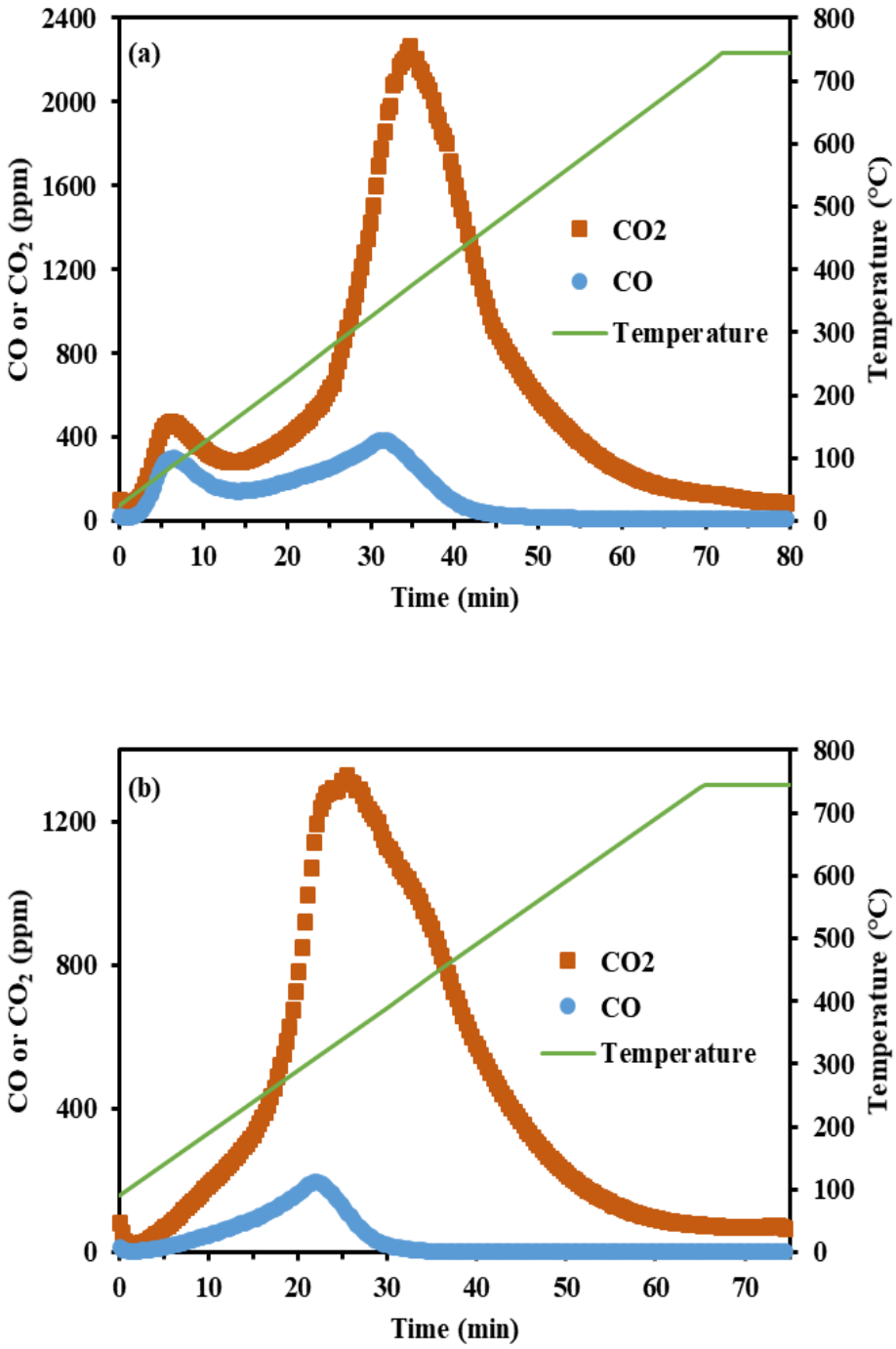

Fig. 4.12. Variation of CO and CO_2 concentrations during TPO analysis of the spent MnO_x/γ-alumina used in catalytic ozonation of toluene at (a) 25 °C (b) 90 °C.

For the 90 °C operation, about 25.01 mg carbon entered the system and the same amount was detected in the exhaust stream resulting in a 100% overall carbon balance.

Table 4.5. Breakdown of carbon (numbers are in mg) distribution and the overall carbon balance for catalytic ozonation of toluene over MnO_x/γ-alumina.

	25 °C reaction	90 °C reaction
Total carbon in [a]	26.57	25.01
Total carbon out before TPO [b]	14.72	19.70
Total carbon evolved during TPO [c]	10.41	5.31
Total Carbon out	25.13	25.01
Carbon balance (%)	94.58	100

[a] During reaction and catalyst saturation with toluene.
[b] As CO_x and unreacted toluene.
[c] As evolved CO_x during TPO.

4.7. Identification of carbonaceous deposits by GC-MS

The carbonaceous species accumulated on the spent MnO_x/γ-alumina catalyst were extracted with dichloromethane and were analyzed with GC-MS. For the catalyst used at 25 °C, a number of organic compounds such as formic acid, acetic acid, acetol, formyl acetate, acetic anhydride, acetoxyacetic acid, β-isoamylene oxide, and isopropyl methyl ketone were found. These compounds are listed in the order of increasing the number of carbon atoms in their structures. For the catalyst used at 90 °C, none of the mentioned compounds were detected by GC-MS analysis of the extract.

4.8. Role of surface carboxylates

The surface carboxylates, with the most significant band at around 1600 cm^{-1}, were observed during the catalytic ozonation of toluene over MnO_x/γ-alumina catalyst. As discussed earlier, the surface carboxylates were found in the catalytic ozonation with pure γ-alumina as well. To investigate whether the surface carboxylates form on the manganese oxide sites, catalytic ozonation of toluene using pure Mn_2O_3 was conducted. Mn_2O_3 was chosen to represent the MnO_x Since Mn_2O_3 was the major manganese phase of the MnO_x/γ-alumina catalyst with 82% abundance (see section "*4.1. Characterization of MnO_x/γ-alumina*"). In situ DRIFTS spectra for catalytic ozonation of toluene using pure Mn_2O_3 at 25 ° C are depicted in Fig. 4.13.

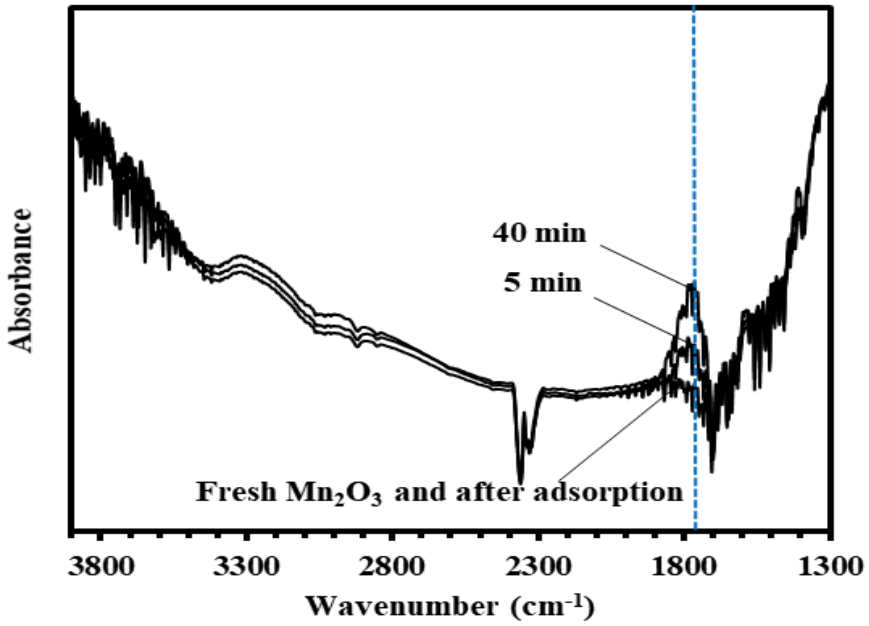

Fig. 4.13. In situ DRIFTS spectra of catalytic ozonation of toluene over Mn_2O_3 at 25 °C; WHSV = 350 L h^{-1} g^{-1}, [O_3] = 1200 ppmv, and [toluene] = 130 ppmv.

Interestingly, the only significant band was at around 1760 cm^{-1} corresponding to C=O stretching. Also, surface carboxylates, with a significant band at around 1600 cm^{-1}, were not formed on pure Mn_2O_3. Therefore, it is plausible that the surface carboxylases resided mainly on the γ-alumina part of the MnO_x/γ-alumina catalyst.

In situ DRIFTS spectra of a one-minute catalytic ozonation reaction over MnO_x/γ-alumina at 25 °C (Fig. 4.14) shows that the surface carboxylases were formed on the surface of the catalyst from the early moments of the reaction.

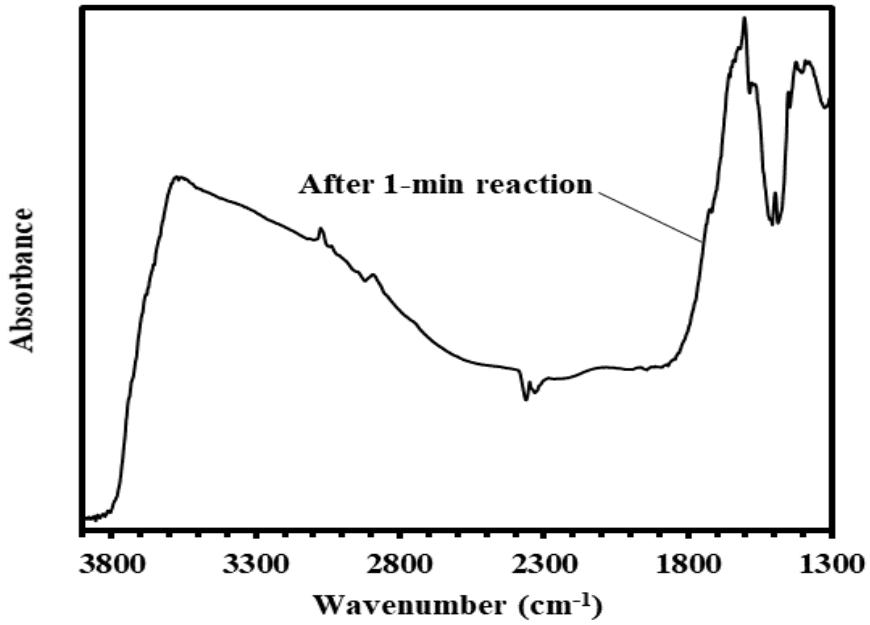

Fig. 4.14. In situ DRIFTS spectra of the one-minute catalytic ozonation of toluene at 25 °C over MnO_x/γ-alumina.

Therefore, these compounds were present from the early moments of the reaction, however, toluene and ozone conversions were not decreased in the first 20 minutes of the

reaction at 25 °C (See Fig. 4.4). The surface carboxylates were observed during the catalytic ozonation at 90 °C as well, while a stable catalytic ozonation was observed. Achieving a stable catalytic activity despite the presence of surface carboxylates indicates that surface carboxylates do not cause deactivation of the MnO_x/γ-alumina catalyst. This conclusion is different from previous studies [26,28,64,108] that have assumed all accumulated materials are detrimental to the catalytic activity, without differentiating between their roles in the reaction.

4.9. Reaction pathway of catalytic ozonation of toluene

As discussed in Chapter 2, there are two proposed reaction mechanisms for catalytic ozonation of toluene over manganese oxides supported on graphene and alumina [79,80]. The reaction mechanism proposed for alumina supported manganese oxide catalyst [79] does not have any experimental evidence to support the suggested mechanism and has ignored the role of alumina support in the reaction. The reaction mechanism proposed for graphene supported manganese oxide catalyst [80] has no experimental evidence and is an adopted version of a mechanism suggested by Reed et al. [81] for catalytic ozonation of acetone on silica supported manganese oxide catalyst. However, findings in this work showed a different possible pathway for catalytic ozonation of toluene.

As discussed earlier, ozone decomposition on the surface of the catalyst generates highly reactive atomically adsorbed oxygen species ($^{\blacksquare}O$) that rapidly oxidize adsorbed VOCs [86,87]:

$$O_3 + {}^{\blacksquare} \rightarrow O_2 + {}^{\blacksquare}O \quad (4.8)$$

$$ {}^{\blacksquare}O + O_3 \rightarrow O_2 + {}^{\blacksquare}O_2 \quad (4.9)$$

$$\blacksquare O_2 \rightarrow O_2 + \blacksquare \quad (4.10)$$

where ■ represents a catalyst active site. Ozone decomposition occurs on both γ-alumina and Mn sites of the MnO_x/γ-alumina catalyst (see Fig. 4.4 and Fig. 4.5). Therefore, ■ can be either an alumina or Mn site.

Fig. 4.15 shows the breakthrough curves of toluene adsorption on MnO_x/γ-alumina, pure γ-alumina, and pure Mn_2O_3. Adsorption breakthrough times for MnO_x/γ-alumina, and pure γ-alumina were 4 and 5 min, respectively. However, breakthrough time for pure Mn_2O_3 was very short (less than 1 min). Therefore, toluene is mainly adsorbed on γ-alumina sites of the MnO_x/γ-alumina catalyst.

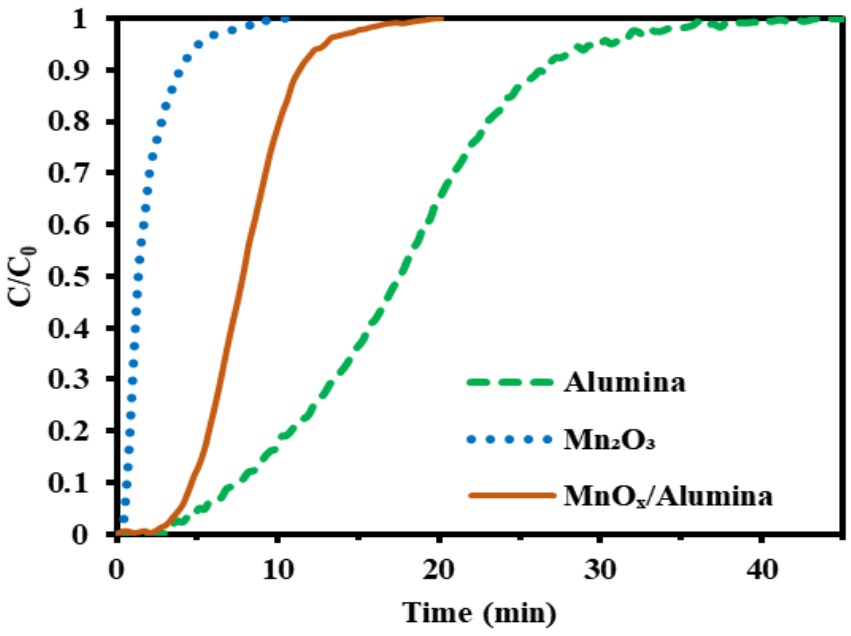

Fig. 4.15. Breakthrough curves of toluene adsorption on MnO_x/γ-alumina, γ-alumina, and Mn_2O_3 at 25 °C.

As discussed in section "*4.3. Catalytic activity of γ-alumina in catalytic ozonation of toluene*", alumina not only acts as a reservoir for toluene, but also it interacts effectively with toluene, in the presence of ozone, to create surface carboxylate intermediates. The presence of highly reactive atomic oxygen species, resulted from ozone decomposition, creates an oxidative environment. Many quick reactions can occur in this oxidative environment, which makes it difficult to identify unstable reaction intermediates.

However, studies on interaction of toluene with metal oxides have shown [113–116] that toluene interacts with the surface of metal oxides via abstraction of H atoms from the methyl group. Therefore, a possible pathway for catalytic ozonation of toluene on the MnO_x/γ-alumina catalyst is as follows:

$$C_6H_5–CH_3 + {}^{\blacktriangle} \leftrightarrow {}^{\blacktriangle}C_6H_5–CH_3 \quad (4.11)$$

$$^{\blacktriangle}C_6H_5–CH_3 + {}^{\blacktriangle} \rightarrow {}^{\blacktriangle}C_6H_5–CH_2 + {}^{\blacktriangle}H \quad (4.12)$$

$$^{\blacktriangle}C_6H_5–CH_2 + 2{}^{\blacktriangle}O \rightarrow {}^{\blacktriangle}C_6H_5–COO + 2{}^{\blacktriangle}H \quad (4.13)$$

where $^{\blacktriangle}$ represents an alumina site. Eq. (4.11) shows adsorption of toluene on the first alumina site. Eq. (4.12) is based on dissociation of one H atom from the methyl group of toluene [113–116]. Then, the unstable benzyl species ($^{\blacktriangle}C_6H_5–CH_2$) reacts with oxygen species (Eq. (4.13)) to produce adsorbed benzoate ($^{\blacktriangle}C_6H_5–COO$), which is a stable surface carboxylate intermediate. Eq. (4.13) may include multiple steps. The adsorbed protons ($^{\blacktriangle}H$) can react with the oxygen species and produce water (Eqs. (4.14 – 4.16)) [79,116]:

$$^{\blacktriangle}H + {}^{\blacktriangle}O \leftrightarrow {}^{\blacktriangle}OH \quad (4.14)$$

$$2{}^{\blacktriangle}OH \leftrightarrow {}^{\blacktriangle}H_2O + {}^{\blacktriangle}O \quad (4.15)$$

$$^{\blacktriangle}H_2O \leftrightarrow {}^{\blacktriangle} + H_2O \quad (4.16)$$

Pure γ-alumina cannot further oxidize surface carboxylates (see section "*4.3. Catalytic activity of γ-alumina in catalytic ozonation of toluene*") and the presence of Mn sites is necessary for further oxidation of the surface carboxylates (Eqs. (4.17) and (4.18)):

$$^{\blacktriangle}C_6H_5{-}COO + * \leftrightarrow *C_6H_5{-}COO \quad (4.17)$$

$$*C_6H_5{-}COO + n\ *O \rightarrow \text{products} \quad (4.18)$$

where * represents a surface Mn site. It has been reported [108] that room temperature oxidation of species with COO^- group (representing carboxylates) in the presence of ozone transforms them to species containing C=O and C–O functional groups such as carboxylic acids. As discussed earlier, formic acid and acetic acid were found during TPD of the catalyst used for catalytic ozonation at 25 °C (see Table 4.4). In addition to formic acid, acetic acid, acetol, formyl acetate, acetic anhydride, acetoxyacetic acid, β-isoamylene oxide, and isopropyl methyl ketone were detected in the extract of the spent catalyst. It is believed that these undesired products, which were found only in the 25 °C operation, accumulated on the surface of the catalyst and caused catalyst deactivation.

4.10. Summary

In this chapter, characterization of MnO_x/γ-alumina catalyst and catalytic ozonation of toluene were discussed. BET surface area and pore volume of the MnO_x/γ-alumina catalyst were 200 m^2/g and 0.56 cm^3/g, respectively. Nominal manganese loading was 10 wt%. LCF of the Mn *K-edge* XANES spectra showed that Mn_2O_3 was the dominant manganese oxide phase of the

catalyst with 82% abundance, followed by 11% MnO_2, and 7% Mn_3O_4. Absorption energy of Mn *K-edge* was determined to be 6553.86 eV for the catalyst. XPS results confirmed that Mn_2O_3 was the major manganese oxide phase of the catalyst.

Catalytic ozonation of toluene was conducted over MnO_x/γ-alumina catalyst at 25 and 90 °C. At 90 °C, a stable reaction was observed with high conversions of about 91% and 92% for toluene and ozone, respectively. However, at 25 °C operation, a decline in toluene and ozone conversions was observed. Kinetic studies over MnO_x/γ-alumina showed that reaction orders for toluene and ozone were 0.181 and 0.469, respectively. Also, an apparent activation energy of 33 kJ $mole^{-1}$ was determined. Rapid catalyst deactivation was observed at both 25 and 90 °C operation when using pure γ-alumina (without manganese) as catalyst. This emphasizes the important role of the manganese in the catalytic activity of the MnO_x/γ- alumina catalyst.

In situ DRIFTS studies, along with a number of temperature programmed analyses helped to distinguishing the role of surface carboxylates from that of undesired products such as acetic acid and formic acid. This helped to develop a better understanding of the reaction mechanism and catalyst stability. During catalytic ozonation of toluene, surface carboxylates were observed on MnO_x/γ-alumina and pure γ-alumina. However, they were not formed on pure manganese oxide.

Alumina not only acts as a reservoir for toluene, but also it interacts effectively with toluene, in the presence of ozone, to create surface carboxylate intermediates. Pure alumina cannot further oxidize surface carboxylates and hence the presence of manganese sites is necessary for further oxidation of the surface carboxylates.

It is believed that at 25 °C, undesired products such as acetic acid and formic acid accumulate on the surface of the MnO_x/γ-alumina catalyst and decrease the catalyst activity. However, at 90 °C, the undesired products are quickly oxidized to carbon dioxide and carbon monoxide. Therefore, a stable catalytic activity is observed at 90 °C.

Chapter 5:
Catalytic ozonation of acetone

Results of catalytic ozonation of acetone on MnO_x/γ-alumina are presented and discussed in this chapter. First, catalyst activity and reaction kinetics will be discussed, followed by in situ DRIFTS studies and characterization of the spent catalyst. Finally, reaction pathway of catalytic ozonation of acetone will be discussed.

Contribution of the PhD candidate:

The PhD candidate, Mostafa Aghbolaghy, was the major contributor of this chapter. All of the written text was prepared by Mostafa Aghbolaghy. Dr. Jafar Soltan supervised and provided consultation during the experimental period and thesis preparation. All experiments were designed, performed, analyzed, and interpreted by Mostafa Aghbolaghy. An earlier version of the experimental setup had been designed and constructed by Dr. Ebrahim Rezaei. The experimental setup was significantly upgraded by Mostafa Aghbolaghy. The upgrade included changes to design, tubing, flow control, and analysis systems. Suggestions from advisory committee members (alphabetic order: Dr. Ning Chen, Dr. Mehdi Nemati, Dr. Catherine Niu, and Dr. Hui Wang) were used to improve the quality of this work.

5.1. Catalytic activity of MnO_x/γ-alumina in catalytic ozonation of acetone

Catalytic ozonation of acetone was conducted over MnO_x/γ-alumina catalyst at 25 and 90 °C. Fig. 5.1a shows profiles of ozone and acetone conversion with reaction time at both temperatures. A stable catalyst activity was observed at 90 °C with acetone and ozone conversions of 90 % and 91 %, respectively. On the other hand, a gradual decline in the conversions was observed at 25 °C, so that at reaction time of 150 min, acetone and ozone conversions were 47 % and 26 %, respectively.

Fig. 5.1b shows the profiles of carbon monoxide and carbon dioxide concentrations in the exhaust gas stream with reaction time for catalytic ozonation of acetone over MnO_x/γ-alumina catalyst. At 90 °C, carbon monoxide and carbon dioxide concentrations were almost constant at 93 and 255 ppmv, respectively. However, at 25 °C, carbon monoxide and carbon dioxide concentrations decreased gradually and reached values of 38 and 127 ppmv (at 150 min), respectively.

5.2. Catalytic activity of γ-alumina in catalytic ozonation of acetone

Similar experiments were conducted by using pure γ-alumina as catalyst. The profiles of acetone and ozone conversions at 25 and 90 °C on γ-alumina are shown in Fig. 5.2a. It was observed that after 40 minutes, acetone and ozone conversions at 25 °C dropped to 18 % and 8 %, respectively. At 90 °C, not only pure γ-alumina did not show stable catalytic activity, but also acetone and ozone conversions dropped to 39 % and 34 %, respectively.

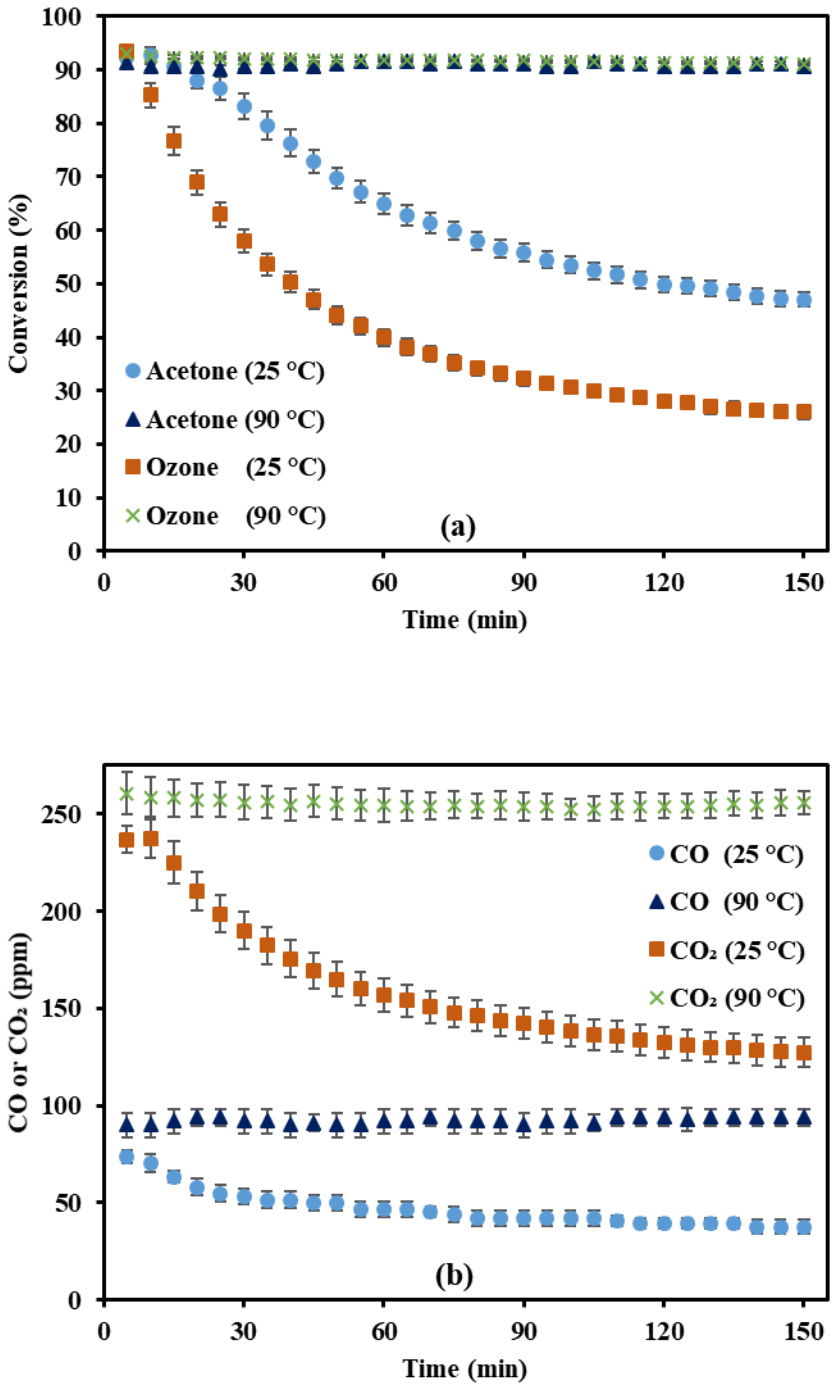

Fig. 5.1. Catalytic ozonation of acetone at 25 and 90 °C on MnO_x/γ-alumina, (a) acetone and ozone conversions; (b) CO and CO_2 concentrations in the exhaust stream; WHSV = 350 L h^{-1} g^{-1}, [O_3] = 1200 ppmv, and [acetone] = 130 ppmv; error bars are standard errors.

Carbon dioxide and carbon monoxide concentrations for catalytic ozonation over pure γ-alumina (Fig. 5.2b) were lower than those of MnO_x/γ-alumina catalyst. Although catalyst deactivation occurred rapidly for pure γ-alumina, these results suggest that γ-alumina is not an inert support and it can oxidize acetone in the presence of ozone. Moreover, these observations indicate that the presence of manganese oxide sites is necessary for an effective catalytic ozonation process.

5.3. Reaction kinetics of catalytic ozonation of acetone on MnO_x/γ-alumina

Kinetic data were obtained at three different temperatures (70, 80, and 90 °C). Blank experiments in the absence of catalyst showed negligible homogeneous non-catalytic reaction between acetone and ozone (less than 1% acetone or ozone conversion). Reed et al. [40,81] have reported that reaction between acetone and ozone follows a homogeneous path at temperatures higher than 200 °C, and a catalytic path at temperatures lower than 125 °C. As mentioned in Chapter 3, the employed catalyst powder size, reaction conditions and reactor configurations inhibited mass transfer limitations. Reaction rates were obtained using differential method of analysis as discussed in section "*3.7. Kinetic analyses*". The power law model for catalytic ozonation of acetone is expressed by Eq. (5.1):

$$-r'_{ace} = k' C_{ace}^{\omega} C_{O_3}^{\nu} \qquad (5.1)$$

where, r'_{ace} is acetone reaction rate (mole kg^{-1} s^{-1}), C_{ace} is concentration of acetone (mole L^{-1}), and C_{O_3} is concentration of ozone (mole L^{-1}).

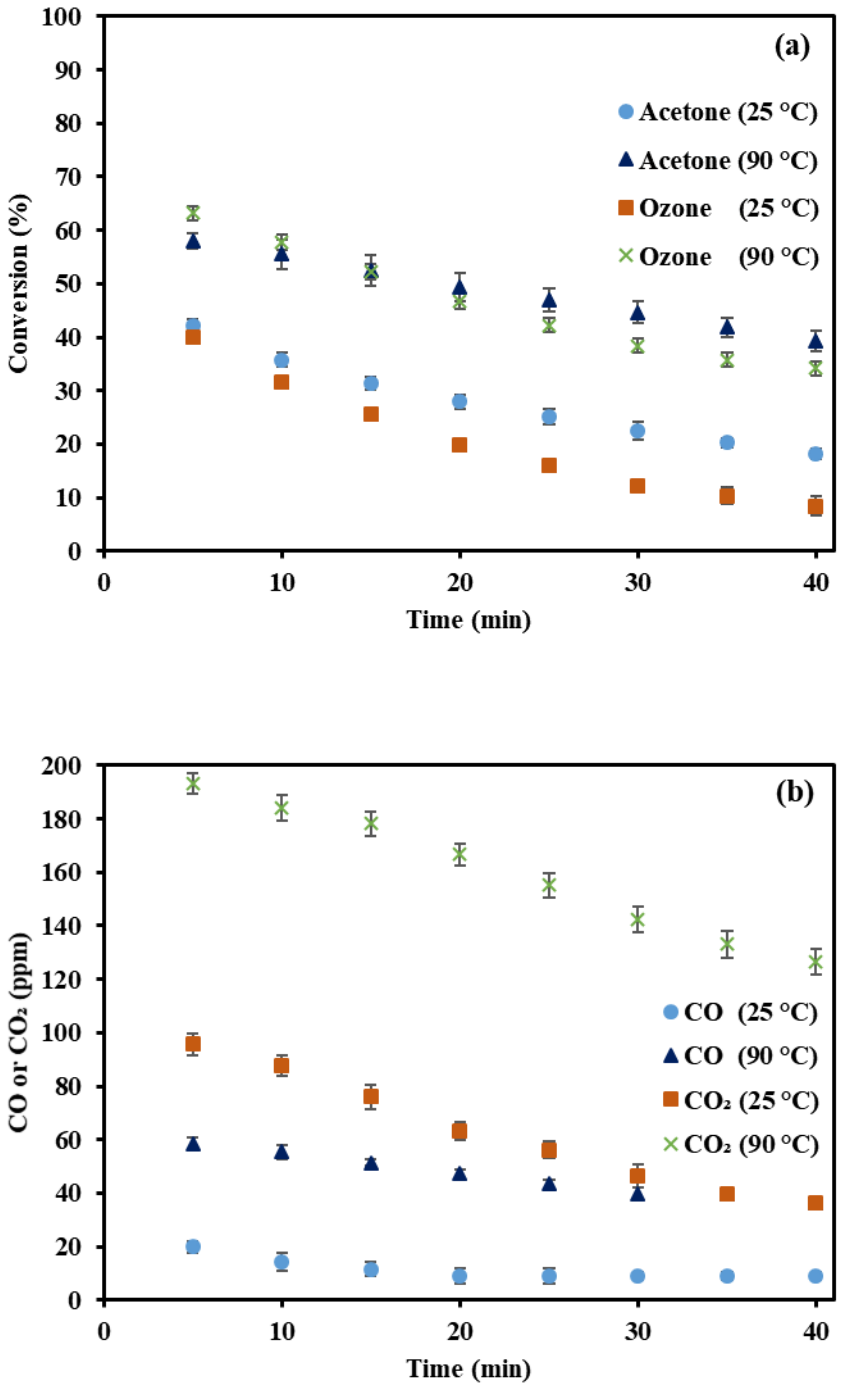

Fig. 5.2. Catalytic ozonation of acetone at 25 and 90 °C on γ-alumina, (a) acetone and ozone conversions; (b) CO and CO_2 concentrations in the exhaust stream; WHSV = 350 L h^{-1} g^{-1}, [O_3] = 1200 ppmv, and [acetone] = 130 ppmv; error bars are standard errors.

ω and v are reaction orders with respect to acetone and ozone, respectively. Also, k' is the reaction rate constant, which is expressed as:

$$k' = A(\exp(\frac{-E_a}{RT})) \quad (5.2)$$

where, R is the universal gas constant (8.314 J K^{-1} $mole^{-1}$), A is frequency factor (i.e. pre-exponential factor), E_a is the apparent activation energy, and T is the reaction temperature (K). Combining Eqs. (5.1) and (5.2) results in Eq (5.3), which allows non-isothermal fitting of the data:

$$-r'_{ace} = A(\exp(\frac{-E_a}{RT}))C_{ace}^{\omega}C_{O_3}^{v} \quad (5.3)$$

Table 5.1 presents the obtained reaction rates for catalytic ozonation of acetone on MnO_x/γ-alumina.

Reaction data were fitted to Eq. (5.3) by using non-linear least squares regression. Table 5.2 presents the fitting results. Also, Fig. 5.3 compares the experimental and predicted rates of acetone removal in catalytic ozonation.

An apparent activation energy of 40 kJ $mole^{-1}$ was obtained for catalytic ozonation of acetone. This is significantly lower than apparent activation energy of catalytic oxidation of acetone in the absence of ozone that has been reported to be in the range of 79 - 118 kJ $mole^{-1}$ [117,118].

Table 5.1. Reaction rates for catalytic ozonation of acetone on MnO_x/γ-alumina.

Temperature (K)	Acetone [a] ($\times 10^6$ mole L^{-1})	Ozone [b] ($\times 10^6$ mole L^{-1})	$-r_{ace}$ ($\times 10^4$ mole kg^{-1} s^{-1})
363	5.3	49.1	11.4
363	5.0	47.0	10.6
363	4.6	42.9	9.9
363	3.8	37.9	7.9
363	3.2	33.4	7.0
363	2.0	22.4	5.0
363	0.4	4.7	1.8
353	5.3	49.1	7.1
353	5.0	46.0	6.4
353	4.4	42.0	5.7
353	3.8	38.6	5.0
353	2.9	32.3	4.4
343	5.3	49.1	4.3
343	4.8	44.8	3.6
343	4.4	42.6	3.2
343	4.0	34.6	2.5

[a] Standard error within ± 2.6%.
[b] Standard error within ± 1.4%.

Table 5.2. Fitting results of the kinetic model for catalytic ozonation of acetone.

$\boldsymbol{A}$ (mole$^{0.385}$ $L^{0.615}$ kg^{-1} s^{-1})	$\boldsymbol{E_a}$ (kJ $mole^{-1}$)	ω	v	R^{2} [a]
2.741×10^5	40	0.109	0.506	0.914

[a] Coefficient of determination of the regression analysis.

Obtained reaction orders for acetone and ozone were 0.109 and 0.506, respectively. These are comparable to the values obtained by Reed et al. [81] for catalytic ozonation of acetone on MnO_x/SiO_2. They have reported reaction orders of 0.194 and 0.634 for acetone and ozone, respectively [81]. The positive reaction orders mean that an increase in concentration of acetone or ozone enhances the reaction rate.

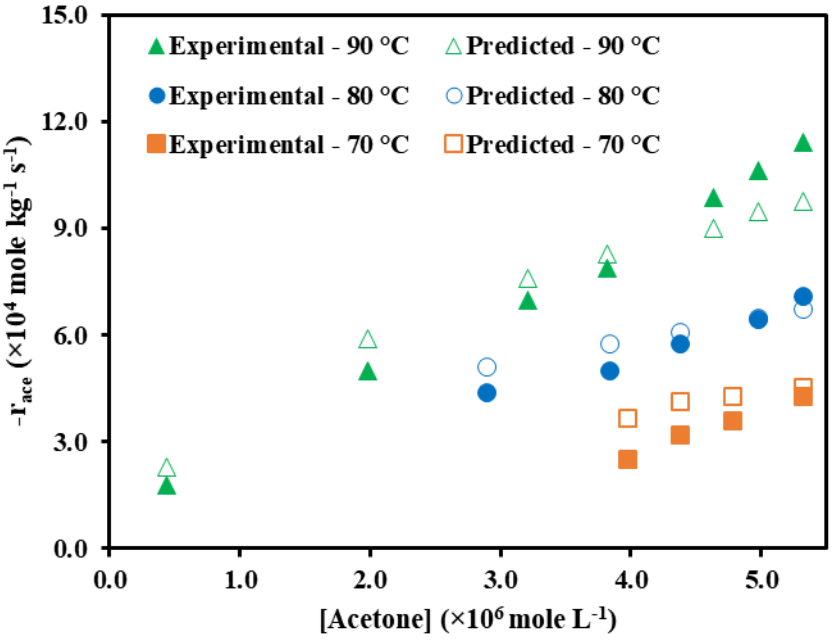

Fig. 5.3. Comparison of the experimental and predicted rates of acetone removal in catalytic ozonation.

5.4. In situ DRIFTS of catalytic ozonation of acetone

In order to better understand the formation of products during catalytic ozonation of acetone, in situ DRIFTS study was conducted. Fig. 5.4a and Fig. 5.4b show in situ DRIFTS

spectra of the catalytic ozonation of acetone over MnO_x/γ-alumina catalyst at 25 °C and 90 °C, respectively. Also, FT-IR spectrum of acetone in the gas phase is depicted in Fig. 5.5.

A number of peaks were observed after adsorption of acetone on the catalyst, suggesting that both physical and chemical adsorption mechanisms were involved in the adsorption process. The peaks at 1370, 1427, and 2973 cm^{-1} were similar to those of the gas phase acetone. However, the peak at 1702 cm^{-1} (corresponding to C=O stretching) [26,112] was different from that of the gas phase acetone at 1737 cm^{-1}. Moreover, after acetone adsorption, a new strong peak appeared at around 1600 cm^{-1}, corresponding to antisymmetric and symmetric COO^- stretching of carboxylates [112].

The shift in the peak corresponding to C=O stretching indicates that acetone interacted with the surface of the catalyst mainly via its carbonyl group. Also, appearance of the new peak corresponding to COO^- stretching of carboxylates indicates that some of the adsorbed acetone was partially oxidized by lattice oxygen [119,120].

Another observation was that the peaks at 1370 and 1702 cm^{-1} had higher intensities at 25 °C than 90 °C adsorption. However, the peak at around 1600 cm^{-1} at 90 °C was stronger than that at 25 °C adsorption, despite the shorter adsorption breakthrough time at 90 °C (Fig. 5.6.). This indicates that although physical and chemical adsorptions occurred at both operating temperatures, chemical adsorption was more dominant at 90 °C.

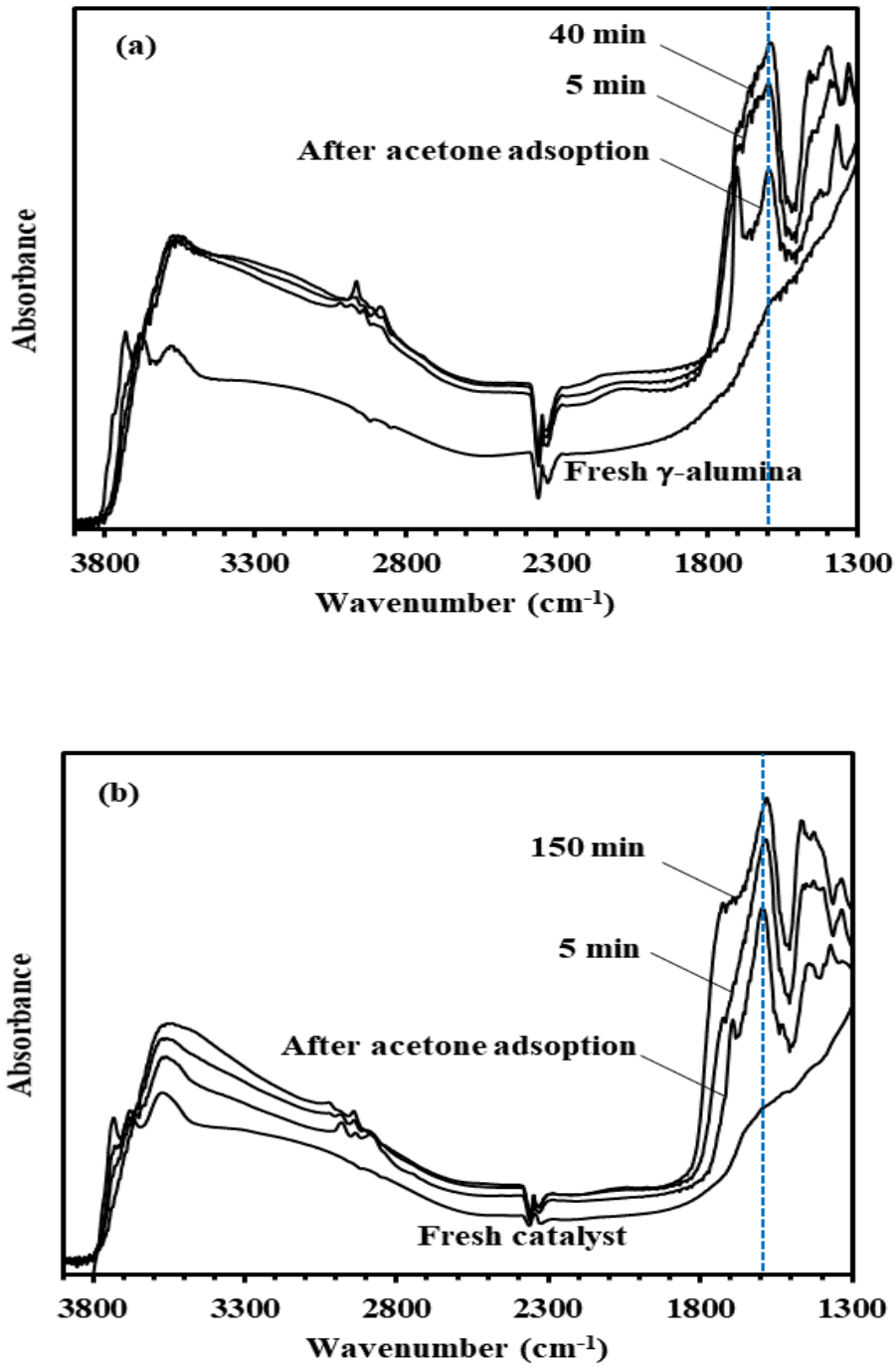

Fig. 5.4. In situ DRIFTS spectra of catalytic ozonation of acetone over MnO_x/γ-alumina at (a) 25 °C and (b) 90 °C; WHSV = 350 L h^{-1} g^{-1}, [O_3] = 1200 ppmv, and [acetone] = 130 ppmv.

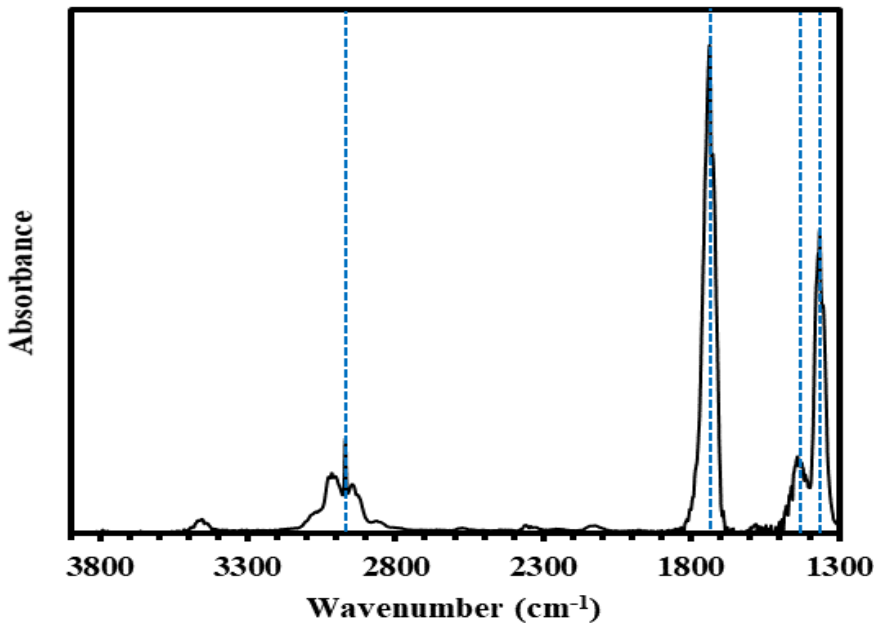

Fig. 5.5. FT-IR spectrum of acetone in the gas phase.

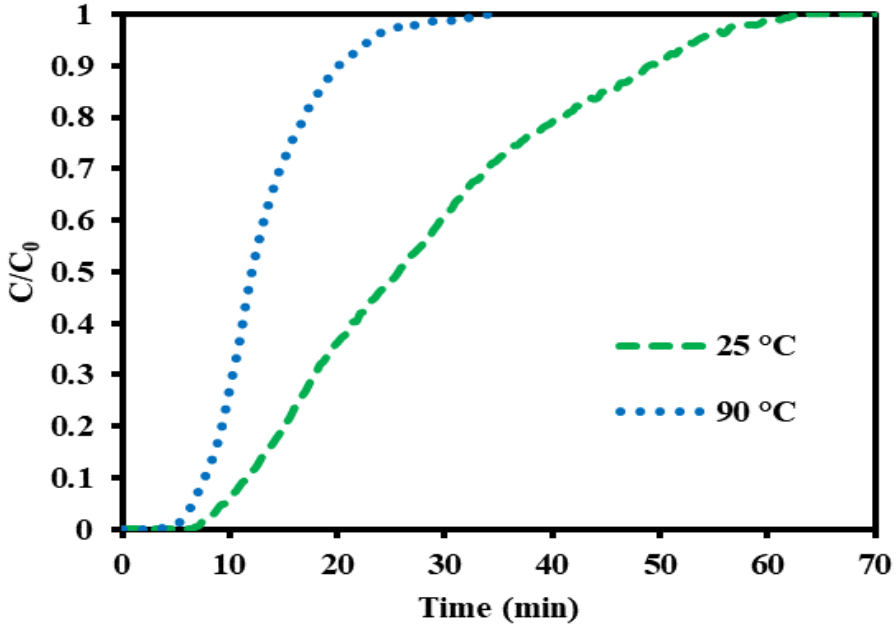

Fig. 5.6. Breakthrough curves of adsorption of acetone on MnO_x/γ-alumina at 25 and 90 °C.

Once ozone was introduced into the reaction chamber in the presence of MnO_x/γ-alumina catalyst, the peaks related to the physical adsorption of acetone disappeared and a number of new peaks emerged. The bands at around 1410, 1462, 1725 cm^{-1} were the main peaks. Moreover, addition of ozone to the system increased the intensity of the peak at around 1600 cm^{-1} (COO^- stretching of carboxylates) significantly. The list of significant peaks and their corresponding functional groups are presented in Appendix D [19,26,112].

Although the observed trends in the DRIFTS spectra after addition of ozone are generally the same at 25 and 90 °C, there was relatively stronger carboxylic acid C=O stretching peak at 25 °C. Also, there was a small peak at 1854 cm^{-1} (C=O stretching of anhydrides) that was present only at the 25 °C spectra.

Fig. 5.7a and Fig. 5.7b show in situ DRIFTS spectra of the catalytic ozonation of acetone over γ-alumina at 25 °C and 90 °C, respectively. A number of peaks were observed after adsorption of acetone on the γ-alumina. These peaks were similar to those of the acetone adsorption on MnO_x/γ-alumina catalyst. Similarly, the peak at around 1600 cm^{-1} (COO^- stretching of carboxylates) at 90 °C was stronger than that at 25 °C adsorption.

At both 25 and 90 °C, addition of ozone to the system in the presence of pure γ-alumina increased intensity of the peak at around 1600 cm^{-1}, however, it did not generate a strong C=O stretching peak at 1700-1725 cm^{-1}. The C=O stretching appeared only as a shoulder for γ-alumina at both 25 and 90 °C operations. This implies that the presence of Mn sites is necessary to effectively utilize ozone and achieve further oxidation of carboxylates on the surface of the catalyst.

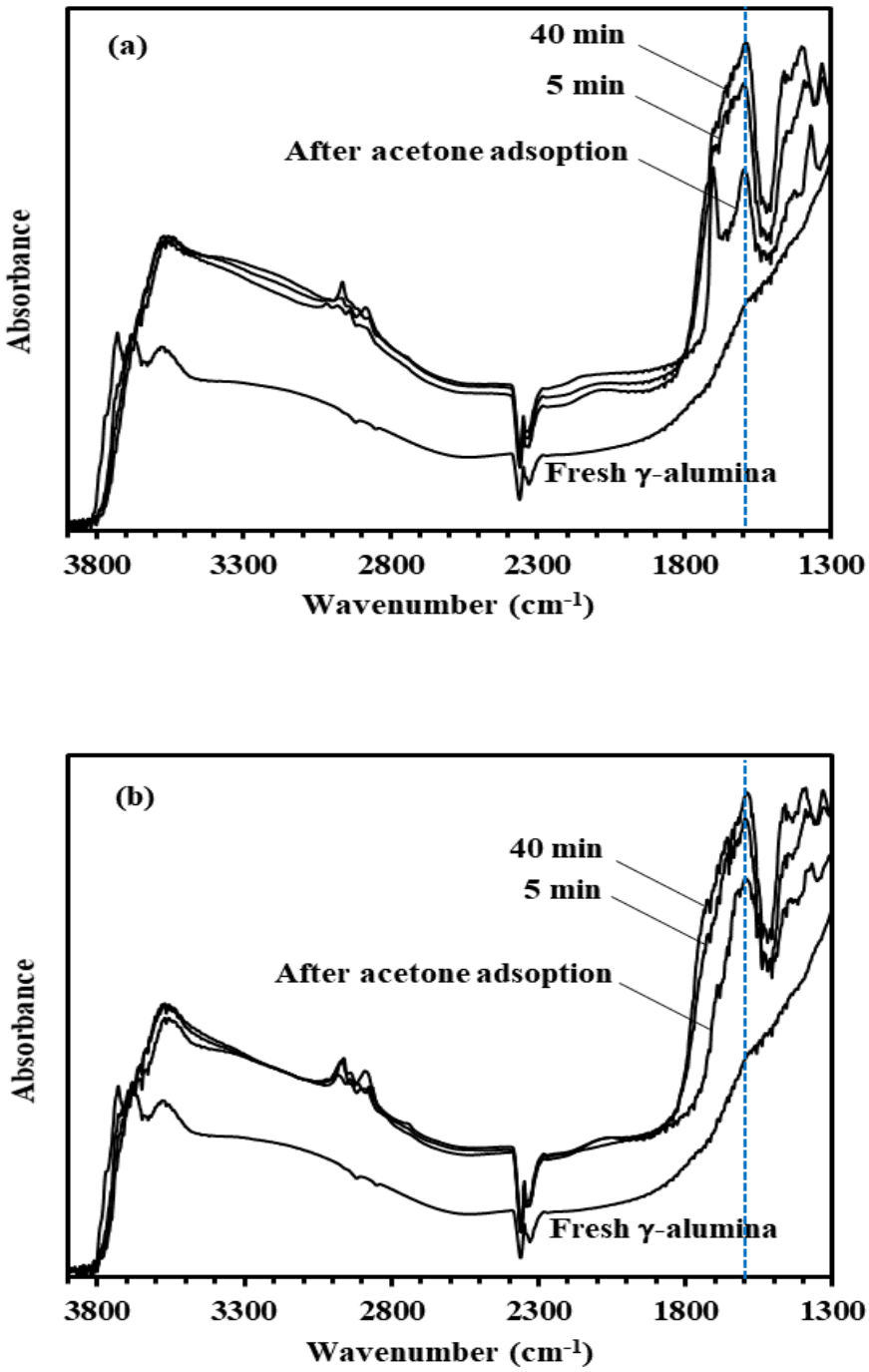

Fig. 5.7. In situ DRIFTS spectra of catalytic ozonation of acetone over γ-alumina at (a) 25 °C and (b) 90 °C; WHSV = 350 L h^{-1} g^{-1}, [O_3] = 1200 ppmv, and [acetone] = 130 ppmv.

5.5. Temperature programmed analysis on the spent catalyst

Thermo-gravimetric analysis was carried out under nitrogen flow at a heating rate of 20 °C/min. Variation in weight of the catalyst versus temperature is shown in Fig. 5.8. By heating the spent MnO_x/γ-alumina catalysts up to 790 °C, the spent catalyst of the 25 °C reaction lost 10% of its weight, whereas the spent catalyst of the 90 °C reaction lost only 5% of its weight. This indicates that the amount of reaction products deposited on the spent catalyst of the 25 °C reaction was higher than that of the 90 °C reaction.

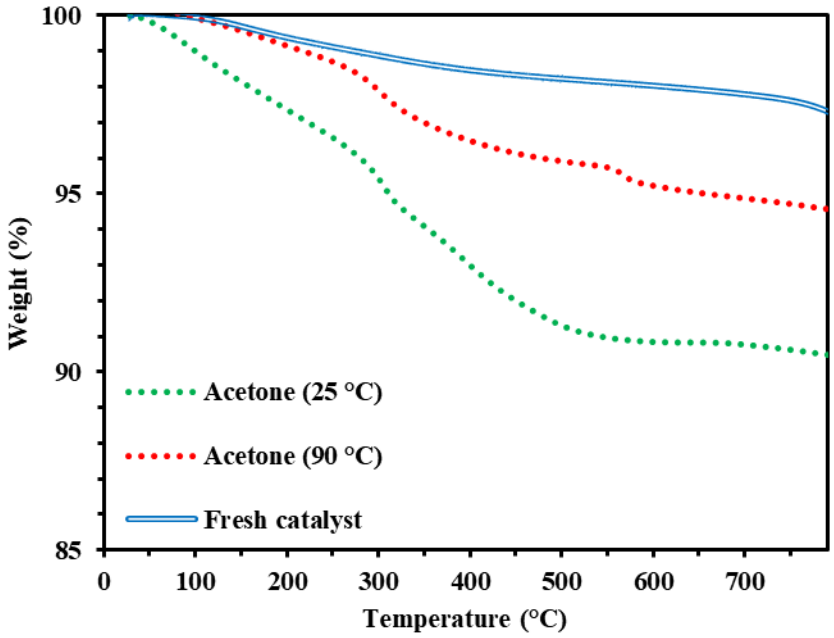

Fig. 5.8. Weight loss during thermo-gravimetric analysis of MnO_x/γ-alumina catalyst used in catalytic ozonation of acetone at 25 °C and 90 °C.

Temperature programmed desorption (TPD) was conducted on the spent catalysts under nitrogen flow at a heating rate of 20 °C/min. Fig. 5.9 shows in situ DRIFTS spectra during TPD of the spent MnO_x/γ-alumina catalyst used in the 25 °C catalytic ozonation of acetone. A significant decrease in intensities of the bands corresponding to C=O stretching and OH stretching was observed by heating the spent catalyst up to 425 °C. Increase in temperature to 625 °C, decreased the intensities of the bands corresponding to COO^- stretching of carboxylates and C-H stretching. Then, almost complete removal of these bands was observed by further increase in temperature to 860 °C. Similar results were obtained for TPD of the spent MnO_x/γ-alumina catalyst used for catalytic ozonation of acetone at 90 °C.

The evolved gases during TPD were analyzed and the compounds detected in the evolved gas stream are presented in Table 5.3. Carbon dioxide and carbon monoxide were detected as evolved gases in a wide temperature range of 25 - 860 °C. The presence of carbon dioxide and carbon monoxide in such a wide temperature range indicates that these compounds were not only desorbed from the surface of the catalyst, but they also were generated from decomposition of larger carbonaceous molecules that were accumulated on the catalyst. In addition, methane was detected in the gas phase in the same temperature range that intensities of the peaks corresponding to COO^- stretching of carboxylates and C-H stretching decreased significantly. These findings suggest that carbon dioxide, carbon monoxide, and methane were most probably evolved as a result of decomposition of a surface carboxylate such as acetate which had not desorbed at lower temperatures. On the other hand, acetic acid and physically adsorbed acetone were desorbed at relatively lower temperatures.

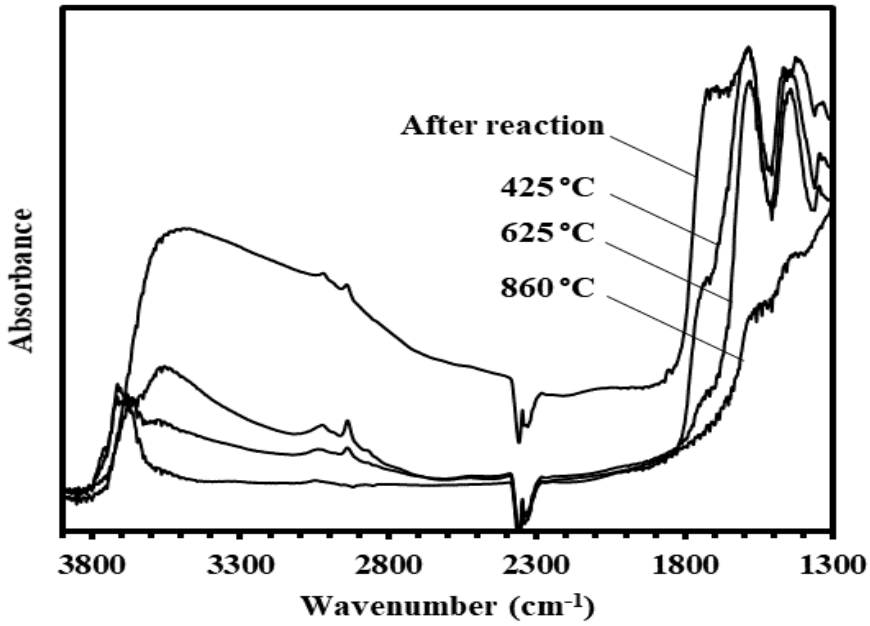

Fig. 5.9. In situ DRIFTS spectra during TPD analysis of spent MnO_x/γ-alumina catalyst used in catalytic ozonation of acetone at 25 °C.

Table 5.3. Compounds detected in the gas phase during TPD analysis of the spent MnO_x/γ-alumina catalyst used in catalytic ozonation of acetone.

Sample	Temperature range (°C)	Detected compounds
25 °C reaction	25 - 425	acetic acid, acetone, water vapor, CO, CO_2
25 °C reaction	425 - 860	methane, CO, CO_2
90 °C reaction	90 - 425	acetone, water vapor, CO, CO_2
90 °C reaction	425 - 860	methane, CO, CO_2

Temperature programmed desorption was conducted on the spent γ-alumina as well. Fig. 5.10 shows in situ DRIFTS spectra during TPD of the spent γ-alumina used in the 25 °C catalytic ozonation of acetone. Similar to the MnO_x/γ-alumina catalyst, almost complete removal of these bands was observed by further increase in temperature to 860 °C. Methane was detected in the evolved gas stream in the temperature range of 425 – 860 °C. Also, intensities of the bands corresponding to COO^- stretching of carboxylates and C-H stretching decreased in the same temperature range. This confirms that γ-alumina is not an inert support, and surface carboxylates such as acetate were formed on alumina regardless of the presence or absence of manganese sites.

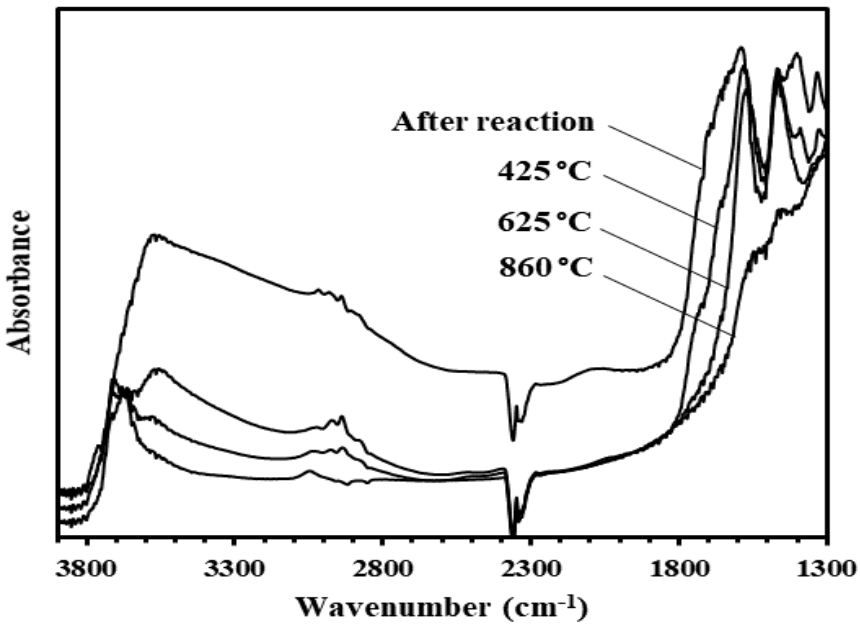

Fig. 5.10. In situ DRIFTS spectra during TPD analysis of spent γ-alumina catalyst used in catalytic ozonation of acetone at 25 °C.

Temperature programmed oxidation (TPO) was conducted on the spent catalysts. TPO analysis was performed under oxygen-nitrogen (20-80 v%) flow at a heating rate of 10 °C/min. Fig. 5.11 depicts in situ DRIFTS spectra during TPO of the spent MnO_x/γ-alumina catalyst used for 25 °C catalytic ozonation of acetone. Increase of temperature to 625 °C was enough to remove all the bands corresponding to the carbonaceous materials. This is significantly lower than the temperature required in TPD (860 °C under pure nitrogen flow) for removal of all the bands corresponding to the carbonaceous materials.

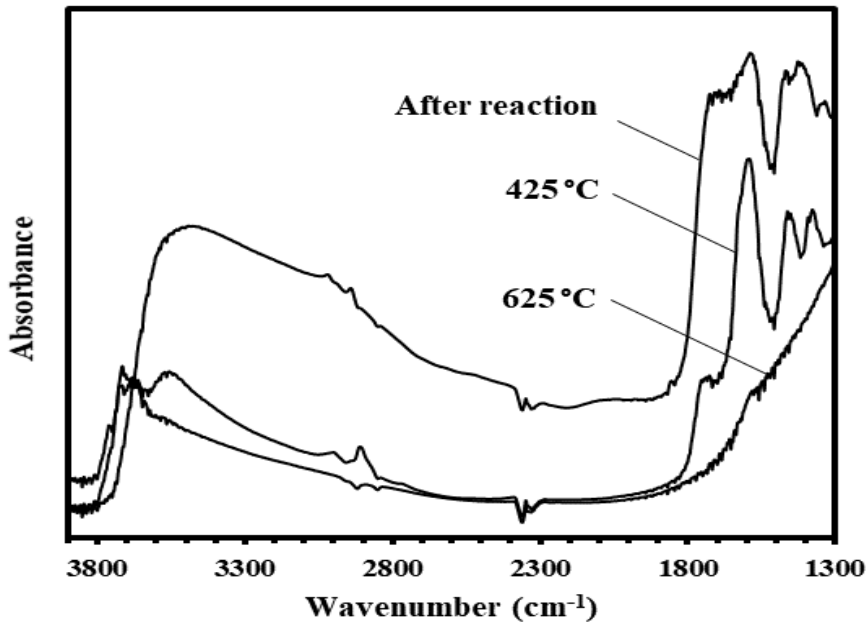

Fig. 5.11. In situ DRIFTS spectra during TPO analysis of spent MnO_x/γ-alumina catalyst used in catalytic ozonation of acetone at 25 °C.

Fig. 5.12 shows the profiles of concentration of carbon dioxide and carbon monoxide in the product gas stream during the TPO analyses. TPO of the catalyst used in the 25 °C operation,

produced maximum carbon dioxide concentration of 680 ppmv at 318 °C, and maximum carbon monoxide concentration of 55 ppmv at 308 °C.

For the catalyst used in the 90 °C operation, maximum carbon dioxide concentration of 285 ppmv at 345 °C, and maximum carbon monoxide concentration of 20 ppmv at 284 °C. Total amount of the evolved carbon during TPO of the catalyst used in the 25 °C reaction was 2.06 mg, which was almost 60% higher than that of the 90 °C reaction. This indicates that higher amount of carbonaceous materials accumulated on the spent catalyst in the 25 °C reaction compared to the 90 °C reaction. In addition, methane was not detected in the product gas stream during TPO analysis, indicating that the surface carboxylates associated with methane (e.g. acetate) were oxidized to carbon dioxide and carbon monoxide.

Table 5.4 presents the carbon distribution breakdown and overall carbon balance. The overall carbon balance was calculated based on Eq. (3.4) as described in section "*3.4. Temperature programmed analyses*".

For the 25 °C operation, the total amount of carbon entering the reactor was 14.74 mg. About 14.46 mg of carbon left the reactor in the form of unconverted acetone, CO_x produced during the ozonation reaction and CO_x during TPO. This resulted in a 98.10% overall carbon balance. For the 90 °C operation, 12.39 mg carbon entered the reactor, and 12.35 mg total carbon was detected in the product stream (ozonation and subsequent TPO). Therefore, the overall carbon balance was about 99.68%.

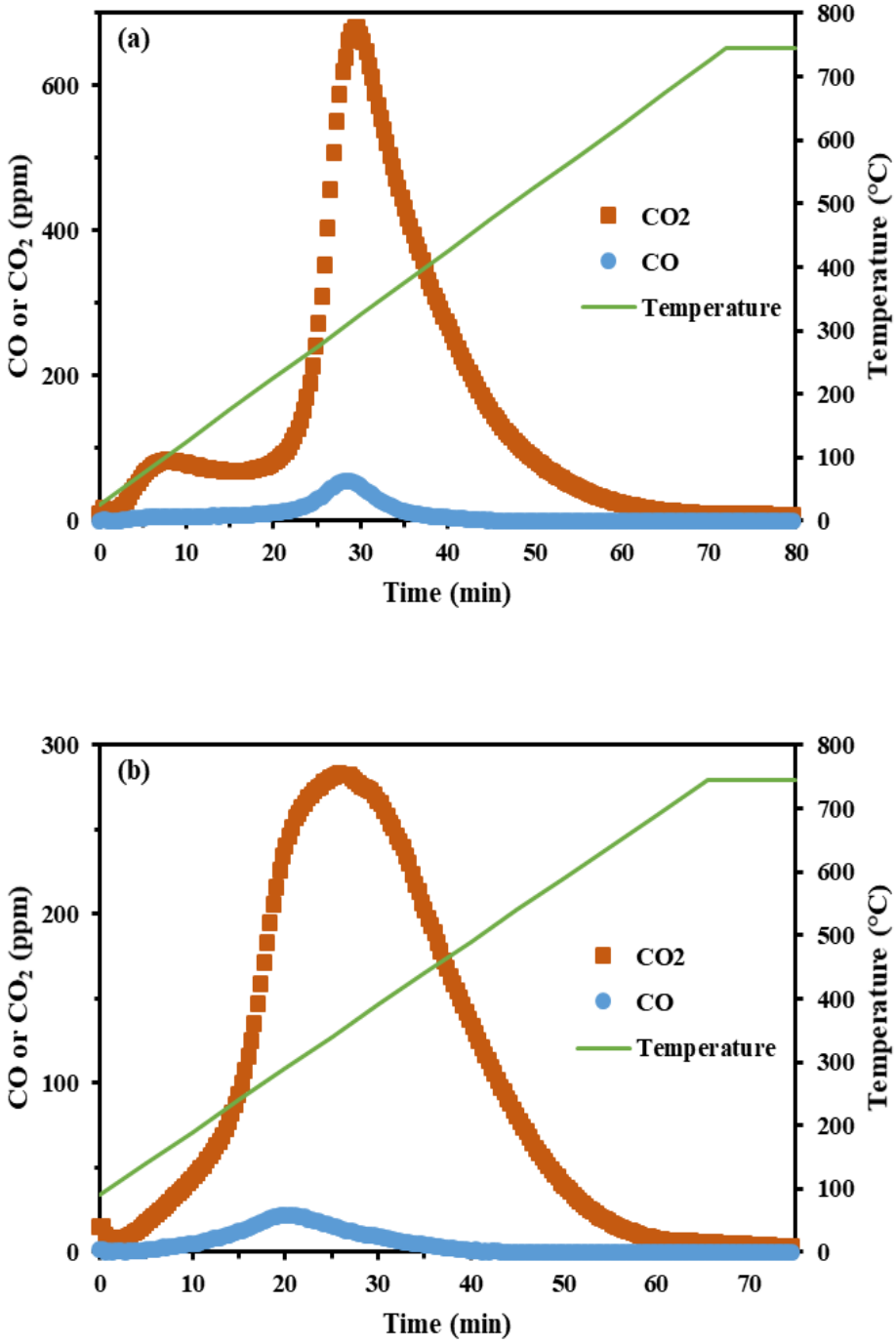

Fig. 5.12. Variation of CO and CO_2 concentrations during TPO analysis of the spent MnO_x/γ-alumina used in catalytic ozonation of acetone at (a) 25 °C (b) 90 °C.

Table 5.4. Carbon distribution breakdown (numbers are in mg) and the overall carbon balance for catalytic ozonation of acetone over MnO_x/γ-alumina.

	25 °C reaction	90 °C reaction
Total carbon in [a]	14.74	12.39
Total carbon out before TPO [b]	12.40	11.06
Total carbon evolved during TPO [c]	2.06	1.29
Total Carbon out	14.46	12.35
Carbon balance (%)	98.10	99.68

[a] During reaction and catalyst saturation with acetone.
[b] As CO_x and unreacted acetone.
[c] As evolved CO_x during TPO.

5.6. Identifying carbonaceous deposits by GC-MS

The spent MnO_x/γ-alumina catalysts were extracted with dichloromethane and were analyzed by GC-MS to identify the carbonaceous species that were deposited on the catalyst during the ozonation reaction. Compounds such as acetic acid, acetic anhydride, β-isoamylene oxide and isopropyl methyl ketone were found for the catalyst used in the 25 °C reaction. It has been reported [26] that formic acid, acetic acid, phenol, and oxalic acid were detected in catalytic ozonation of benzene over alumina-supported manganese oxide at room temperature. Also, Xi, et al. [87] have reported that compounds such as acetic acid, acetaldehyde, ethylene, and acetylene were detected in the exhaust stream of catalytic ozonation of acetone over silica-supported manganese oxide. At 25 °C, incomplete oxidation of acetone led to the formation of the partially oxidized undesired products that gradually accumulated on the catalyst. None of the mentioned

compounds were found in GC-MS analysis of the catalyst used for the 90 °C reaction. It is believed that increase of temperature led to better oxidation of carbonaceous deposits to CO_x.

5.7. Reaction pathway of catalytic ozonation of acetone

Reed et al. [81] suggested a possible reaction mechanism for catalytic ozonation of acetone on 10 wt% MnO_x/SiO_2. In this mechanism, silica support is a reservoir for the physically adsorbed acetone, and acetone molecules migrate to the Mn sites and react with highly active atomic oxygen species produced from ozone decomposition [81]:

$$CH_3–CO–CH_3 + {}^{\bullet} \leftrightarrow {}^{\bullet}CH_3–CO–CH_3 \quad (5.4)$$

$$^{\bullet}CH_3–CO–CH_3 + * \leftrightarrow * CH_3–CO–CH_3 + {}^{\bullet} \quad (5.5)$$

$$O_3 + * \rightarrow O_2 + *O \quad (5.6)$$

$$*CH_3–CO–CH_3 + m\ *O \rightarrow \text{products} \quad (5.7)$$

where * represents a surface manganese site, $^{\bullet}$ represents a surface silica site.

However, findings in this research showed a different possible pathway for the catalytic ozonation of acetone on alumina-supported manganese oxide, leading to the following scheme:

$$CH_3–CO–CH_3 + {}^{\blacktriangle} \leftrightarrow {}^{\blacktriangle}CH_3–CO–CH_3 \quad (5.8)$$

$$^{\blacktriangle}CH_3–CO–CH_3 + {}^{\blacktriangle}O \rightarrow {}^{\blacktriangle}CH_3–COO + {}^{\blacktriangle}CH_3 \quad (5.9)$$

$$^{\blacktriangle}CH_3–COO + * \leftrightarrow *CH_3–COO + {}^{\blacktriangle} \quad (5.10)$$

$$*CH_3–COO + n\ *O \rightarrow \text{products} \quad (5.11)$$

where * represents a surface manganese site, $^{\blacktriangle}$ represents a surface alumina site. As discussed in sections 5.4 and 5.5, alumina not only acts as a reservoir for acetone (Eq. (5.8)), but also it

interacts with acetone to create surface carboxylate intermediates such as surface acetate ($\blacktriangle CH_3–COO$). Although the surface carboxylates are formed during the adsorption process as well, the presence of ozone enhances formation of these intermediates significantly. Formation of the surface carboxylates is shown by (Eq. (5.9)). Pure γ-alumina is not able to further oxidize the surface carboxylates (see Fig. 5.2) and the presence of manganese sites is necessary for effective oxidation of the surface carboxylates to carboxylic acids and anhydrides, and eventually to carbon dioxide and carbon monoxide (Eqs. (5.10) and (5.11)). Unlike acetate ($\blacktriangle CH_3–COO$), $\blacktriangle CH_3$ is highly reactive and unstable [121] and can be immediately oxidized.

It has been suggested [86,87] that oxygen species such as O_2^-, O_2^{2-}, and O^{2-} may be responsible for oxidation of VOCs in catalytic ozonation processes. Other studies [63,81,122] have shown that molecular oxygen species do not contribute to the oxidation reaction and are generated due to catalytic self-decomposition of ozone (Eqs. (5.13) and (5.14)). Rather, atomic oxygen species (O^{2-}) is responsible for oxidation of VOCs/carbonaceous deposits in catalytic ozonation processes [63,81,122].

$$O_3 + \blacksquare \rightarrow O_2 + \blacksquare O \quad (5.12)$$

$$\blacksquare O + O_3 \rightarrow O_2 + \blacksquare O_2 \quad (5.13)$$

$$\blacksquare O_2 \rightarrow O_2 + \blacksquare \quad (5.14)$$

where, $\blacksquare$ can be either an alumina or Mn site.

At 90 °C, the surface carboxylates are quickly oxidized to carbon dioxide and carbon monoxide. At 25 °C, in addition to carbon dioxide and carbon monoxide, undesired products such as acetic acid are produced (see Table 5.3). It is believed that these undesired products accumulate on the surface of the MnO_x/γ-alumina catalyst and reduce the catalyst activity.

5.8. Summary

Catalytic ozonation of acetone was conducted on alumina-supported manganese oxide. A stable catalyst activity was observed at 90 °C with acetone and ozone conversions of 90 % and 91 %, respectively. On the other hand, a gradual decline in the conversions was observed at 25 °C. An apparent activation energy of 40 kJ $mole^{-1}$ was obtained for catalytic ozonation of acetone over alumina-supported manganese oxide catalyst. Also, reaction orders of 0.109 and 0.506 were obtained for acetone and ozone, respectively.

Stable activity was not achieved for catalytic ozonation of acetone over pure γ-alumina at either 25 or 90 °C. Although catalyst deactivation occurred rapidly for pure γ-alumina, γ-alumina was not an inert support and it oxidized acetone to some extent in the presence of ozone.

In situ DRIFTS studies showed that acetone interacted with the surface of the alumina-supported manganese oxide catalyst mainly via its carbonyl group. Surface carboxylates such as surface acetate were produced during acetone adsorption and catalytic ozonation on both MnO_x/γ-alumina and pure γ-alumina as a result of interaction of alumina with the adsorbed acetone. The presence of Mn sites was necessary to achieve further oxidation of carboxylates on the surface of the catalyst.

Temperature programmed oxidation of the spent MnO_x/γ-alumina catalysts showed that more carbonaceous materials accumulated on the spent catalyst in the 25 °C reaction compared to the 90 °C reaction. Increase of temperature to 625 °C under oxygen-nitrogen (without ozone) flow was enough to remove all the deposited carbonaceous materials.

At 25 °C, incomplete oxidation of acetone produced compounds such as acetic acid, acetic anhydride, β-isoamylene oxide and isopropyl methyl ketone. These undesired products accumulated on the MnO_x/γ-alumina and reduced the catalytic activity. Thus, a gradual catalyst deactivation occurred at 25 °C. However, at 90 ° carbonaceous deposits were quickly oxidized to carbon dioxide and carbon monoxide, which led to a stable catalytic activity.

Chapter 6:
Catalytic ozonation of mixture of toluene and acetone

A wide variety of VOCs with different physicochemical properties are present in indoor and outdoor environments. Performance of a catalytic ozonation system used for removal of a mixture of VOCs may differ from its performance for removal of individual VOC compounds. Therefore, investigating catalytic ozonation of mixture of VOCs can help to understand the limitations of the catalytic ozonation and can aid with potential commercialization of the catalytic ozonation technique. Despite its importance, low temperature (below 100 °C) catalytic ozonation of mixture of VOCs has not been reported in the literature. In this chapter, results of catalytic ozonation of mixture of toluene and acetone on MnO_x/γ-alumina are presented and discussed. Moreover, the results of catalytic ozonation of the mixture will be compared with the results of catalytic ozonation of single toluene and acetone. First, catalyst activity will be discussed, followed by in situ DRIFTS studies, characterization of the spent catalyst, and catalyst regeneration.

For the sake of consistency, catalytic ozonation of mixture of toluene and acetone at 25, 60, and 90 °C will be referred to as mixture-25, mixture-60, and mixture-90, respectively. Similarly, catalytic ozonation of single component VOCs will be referred to as toluene-25, toluene-60, toluene-90, acetone-25, acetone-60, and acetone-90. It should be noted that the results corresponding to toluene-25, toluene-90, acetone-25, and acetone-90 have already been

presented and discussed in Chapter 4 and Chapter 5; in this chapter, these data are referred to for comparison and further discussion.

Contribution of the PhD candidate:

The PhD candidate, Mostafa Aghbolaghy, was the major contributor of this chapter. All of the written text was prepared by Mostafa Aghbolaghy. Dr. Jafar Soltan supervised and provided consultation during the experimental period and thesis preparation. All experiments were designed, performed, analyzed, and interpreted by Mostafa Aghbolaghy. An earlier version of the experimental setup had been designed and constructed by Dr. Ebrahim Rezaei. The experimental setup was significantly upgraded by Mostafa Aghbolaghy. The upgrade included changes to design, tubing, flow control, and analysis systems. Suggestions from advisory committee members (alphabetic order: Dr. Ning Chen, Dr. Mehdi Nemati, Dr. Catherine Niu, and Dr. Hui Wang) were used to improve the quality of this work.

6.1. Catalytic activity of MnO_x/γ-alumina in catalytic ozonation of mixture of VOCs

Fig. 6.1 shows VOCs and ozone conversions, and carbon dioxide and carbon monoxide concentrations for catalytic ozonation of mixture of toluene and acetone. Total VOCs concentration in the inlet stream was 130 ppmv. Therefore, 65 ppmv of each toluene and 65 ppmv of acetone were used for catalytic ozonation of the mixture of toluene and acetone.

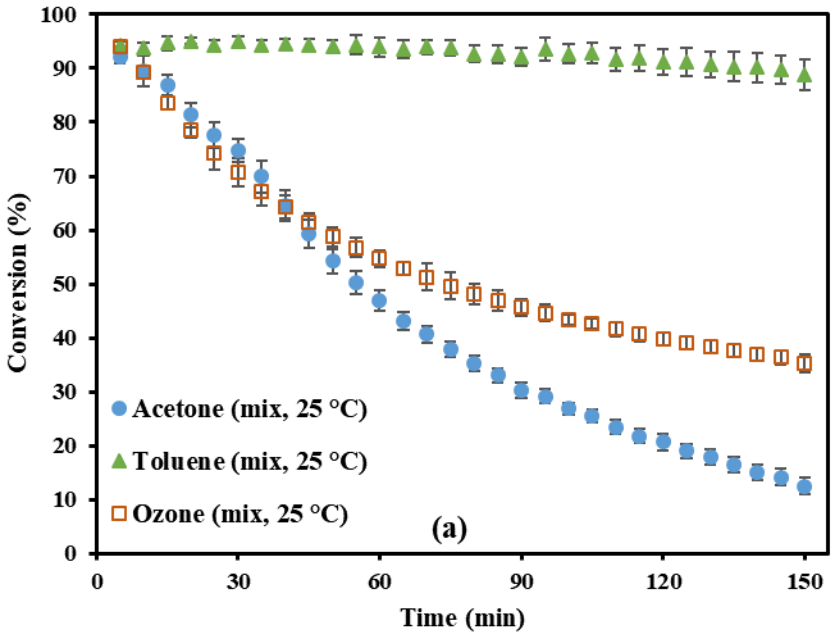
Conversion (%)
Time (min)
Acetone (mix, 25 °C)
Toluene (mix, 25 °C)
Ozone (mix, 25 °C)
(a)

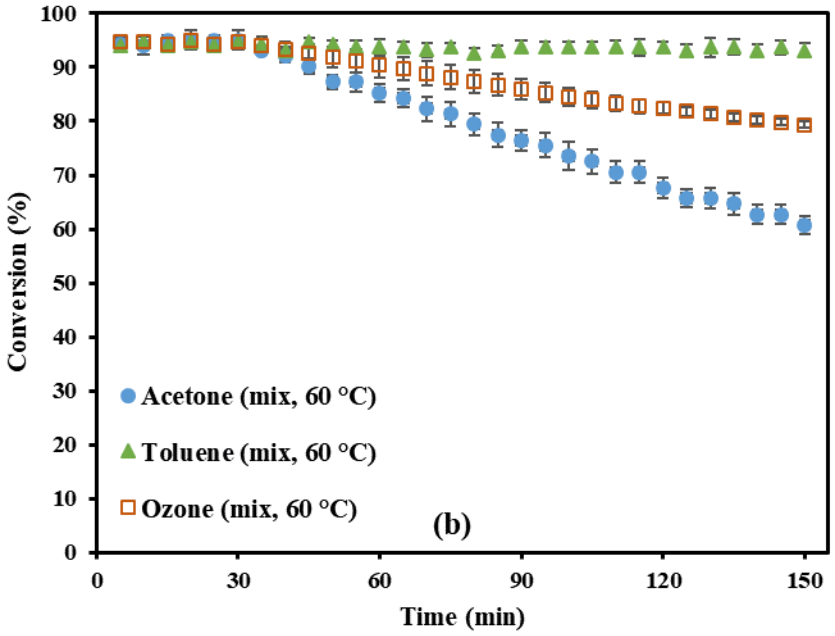
Conversion (%)
Time (min)
Acetone (mix, 60 °C)
Toluene (mix, 60 °C)
Ozone (mix, 60 °C)
(b)

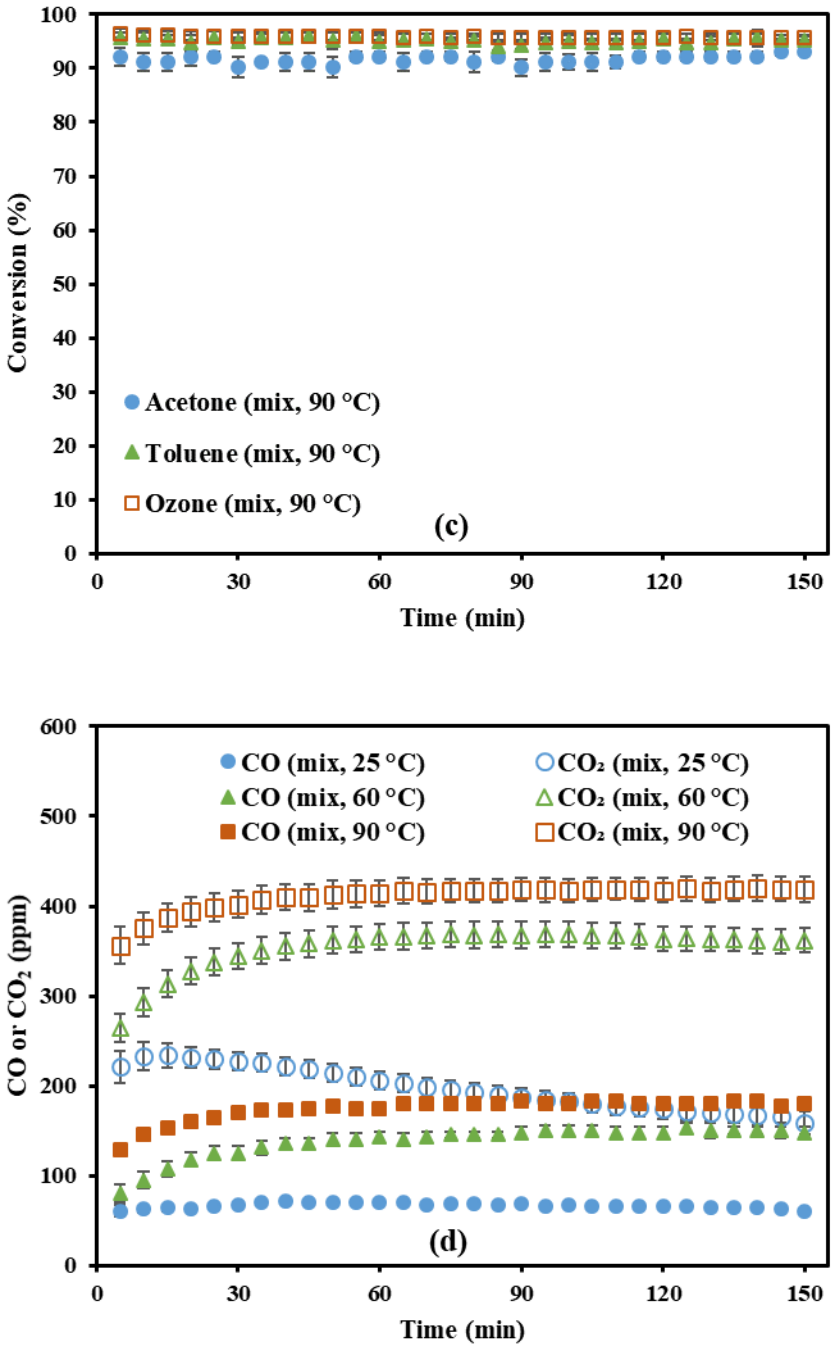

Fig. 6.1. Catalytic ozonation of mixture VOCs on MnO_x/γ-alumina, (a) conversions at 25 °C; (b) conversions at 60 °C; (a) conversions at 90 °C; (d) CO and CO_2 concentrations in the exhaust stream; WHSV = 350 L h^{-1} g^{-1}, [O_3] = 1200 ppmv, [toluene] = 65 ppmv, and [acetone] = 65 ppmv; error bars are standard errors.

In the mixture-25 reaction, toluene conversion was significantly higher than acetone conversion. After 150 min, toluene conversion was about 89%, while ozone conversion was almost 35%. However, acetone conversion drastically dropped to 13%. Carbon monoxide concentration was relatively constant at 65 ppmv, while carbon dioxide concentration decreased gradually and reached 159 ppmv after 150 min of reaction. Similar to the mixture-25, in the mixture-60 reaction, toluene conversion was higher than acetone conversion. Toluene conversion was relatively constant at around 93%. However, acetone and ozone conversions gradually declined and reached 61% and 79% after 150 min of the reaction, respectively.

Carbon monoxide and carbon dioxide concentrations in the exhaust stream of the mixture-60 reaction were 148 and 362 ppmv, respectively. These values were significantly higher than those of the mixture-25 reaction. A stable removal of both acetone and toluene was achieved by increasing the reaction temperature to 90 °C. In the mixture-90 reaction, toluene, acetone and ozone conversions were 95%, 93%, and 96%, respectively. Carbon monoxide and carbon dioxide concentrations in the exhaust stream of the mixture-90 reaction increased initially and reached constant values of 180 and 420 ppmv, respectively.

Fig. 6.2 compares catalytic ozonation of single VOCs with that of mixture of acetone and toluene at three reaction temperatures of 25, 60, and 90 °C. Significant differences were observed. Toluene conversion in the mixture-25 was higher than that of the single compound (toluene-25). Contrarily, acetone conversion in the mixture-25 was lower than that of the single compound (acetone-25). A similar pattern was observed at 60 °C. However, at 90 °C toluene and acetone conversions in catalytic ozonation of the mixture were comparable with those in catalytic ozonation of the single compounds.

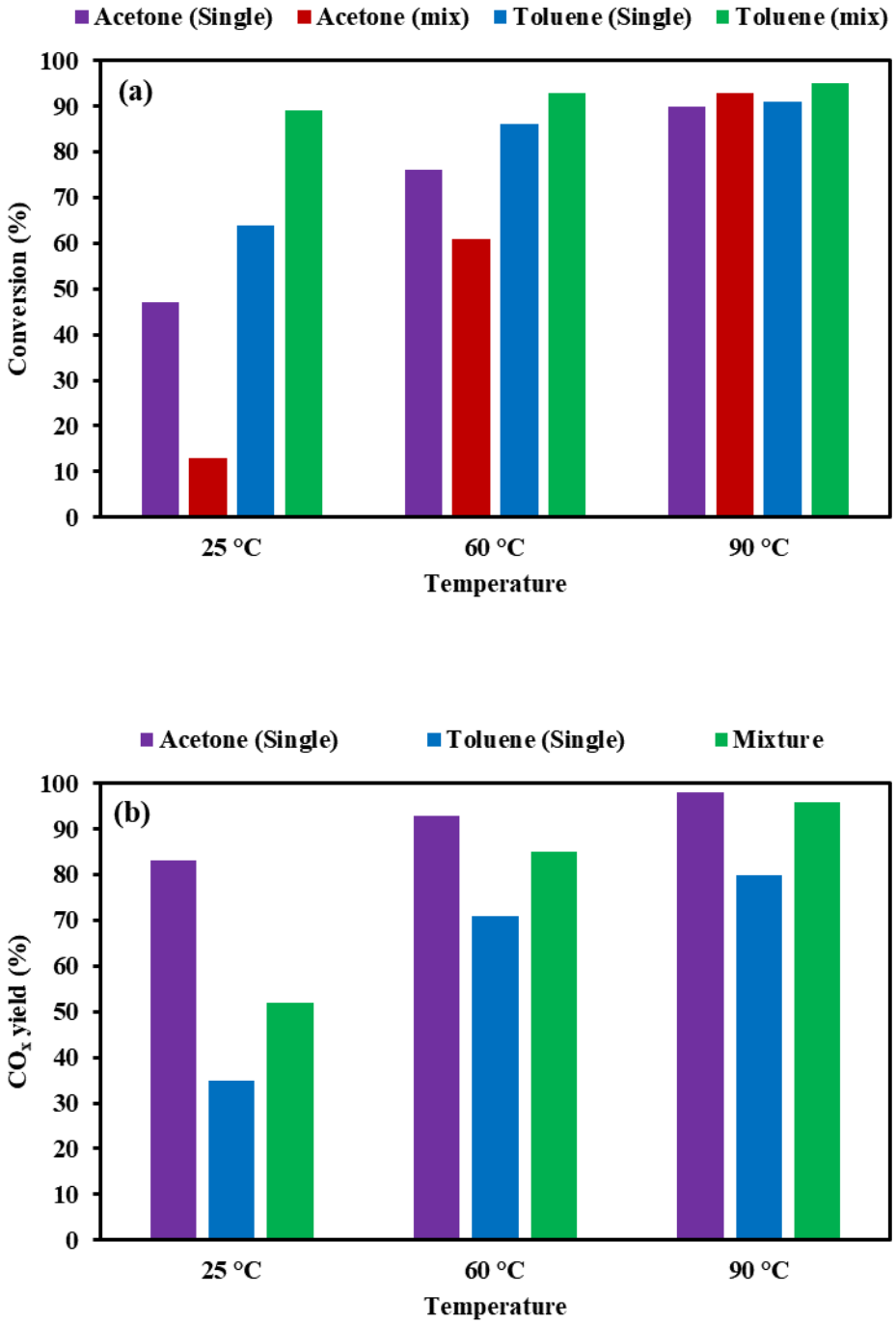

Fig. 6.2. Comparison of catalytic ozonation of single VOCs and mixture VOCs on MnO_x/γ-alumina, (a) conversions of VOCs (b) average CO_x yields.

Increase of temperature in catalytic ozonation of either single VOCs or the mixture of VOCs enhanced the VOCs conversion and CO_x yield. Also, the gap between toluene and acetone conversions decreased by increase of temperature from 25 to 90 °C. At all temperatures, CO_x yields for catalytic ozonation of the mixture of VOCs were lower than CO_x yields of the single acetone removal and higher than those of the single toluene removal. In other words, the overall CO_x yield was improved compared to catalytic ozonation of single toluene.

The results indicate that there were considerable mixture effects in catalytic ozonation of toluene and acetone. Catalytic ozonation in the mixture was favourable for toluene conversion, while it was repressive for acetone conversion.

Kolar et al. [123] studied synergic effect of catalytic combustion and ozone for removal of a mixture of 2-methylbutanal and 3-methylbutanal at 160 °C. Ozone helped to decrease the temperature required for total degradation of these compounds. However, at this relatively high reaction temperature ozone reacted with the VOCs mainly in the gas phase [123]. At high temperatures ozone is thermally decomposed before reaching the catalyst [124]. Studies [8,91,92,125] on catalytic oxidation (without ozone) of mixture of VOCs have suggested that competitive adsorption on the catalyst plays an important role in determining the reactivity of VOCs. Therefore, competitive adsorption may explain the observed mixture effects in the catalytic ozonation of toluene and acetone as well. However, breakthrough curves of adsorption of toluene and acetone as a mixture on MnO_x/γ-alumina at 25 °C (Fig. 6.3) showed that in the absence of ozone, acetone is adsorbed better on the catalyst. Interestingly, after about 20 minutes of adsorption of the mixture of toluene and acetone, toluene concentration in the exhaust stream became higher than its concentration in the inlet stream. This indicates that acetone competes

with toluene for adsorption and forces the initially adsorbed toluene molecules to be gradually desorbed. Similar trends were observed at 60 and 90 °C. Therefore, better reactivity of toluene in the catalytic ozonation of the mixture cannot be attributed to competitive adsorption of VOCs on the catalyst.

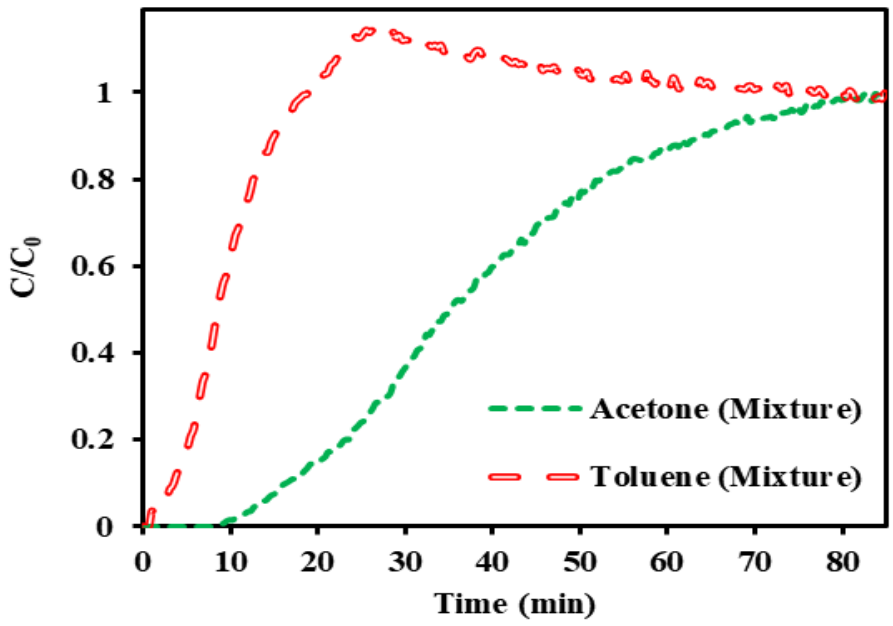

Fig. 6.3. Breakthrough curves of adsorption of toluene and acetone as a mixture on MnO_x/γ-alumina at 25 °C.

Activation energies of catalytic ozonation reactions can better explain why catalytic ozonation in the mixture is favourable for toluene conversion. Apparent activation energy of catalytic ozonation of toluene (33 kJ $mole^{-1}$) is lower than apparent activation energy of catalytic ozonation of acetone (40 kJ $mole^{-1}$). This is a significant advantage for catalytic ozonation of

toluene and indicates that tendency to react with active oxygen species (resulted from catalytic decomposition of ozone) is a more important factor than ability to be adsorbed on the catalyst in the absence of ozone. Similarly, Burgos et al. [126] have studied catalytic oxidation (without ozone) of mixtures of 2-propanol, toluene, and methyl ethyl ketone on $Pt/Al_2O_3/Al$ monoliths and have reported that competition of VOCs to react with chemisorbed oxygen atoms is more important than competitive adsorption of VOCs on the catalyst [126].

6.2. In situ DRIFTS of catalytic ozonation of mixture of VOCs

In situ diffuse reflectance infrared Fourier transform spectroscopy was used to monitor surface of the MnO_x/γ-alumina catalyst and understand the formation of products during catalytic ozonation. DRIFTS spectra for catalytic ozonation of mixture of VOCs at 25, 60, and 90 °C are depicted in Fig. 6.4. Appendix D presents a summary of the functional groups observed in the DRIFTS spectra [19,26,112].

The intensity of the peak at around 1600 cm^{-1}, corresponding to COO^- stretching of surface carboxylates, varied in different reactions. As discussed earlier for single acetone, the peak at 1600 cm^{-1} appeared during adsorption of acetone on the catalyst (see Fig. 5.4 in "*5.4. In situ DRIFTS of catalytic ozonation of acetone*"). On the other hand, for single toluene, adsorption on the catalyst did not change spectra of the fresh catalyst, while an intense peak at 1600 cm^{-1} appeared immediately after addition of ozone (see Fig. 4.7 in section "*4.5. In situ DRIFTS of catalytic ozonation of toluene*").

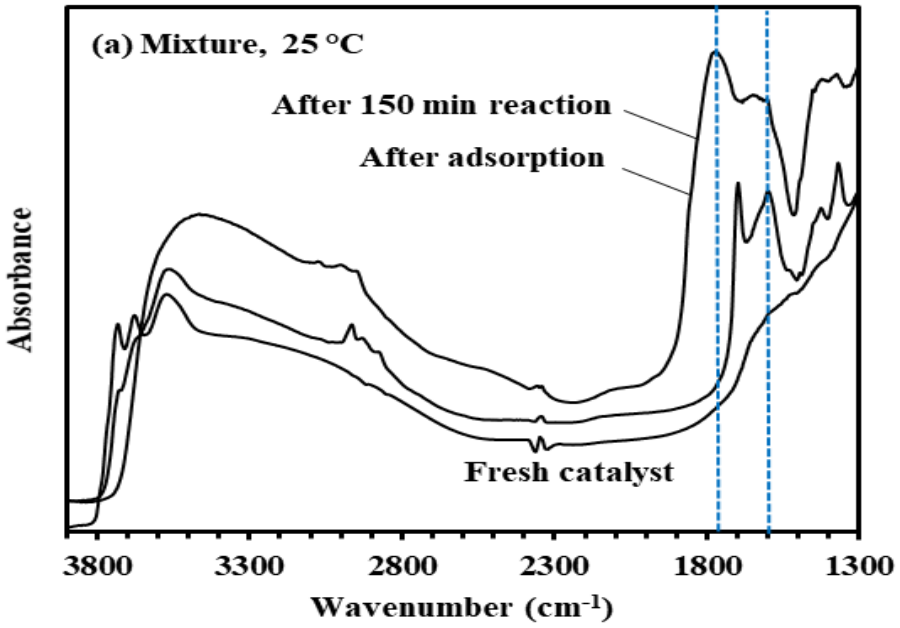
(a) Mixture, 25 °C
After 150 min reaction
After adsorption
Fresh catalyst
Absorbance
3800
3300
2800
2300
1800
1300
Wavenumber (cm-1)

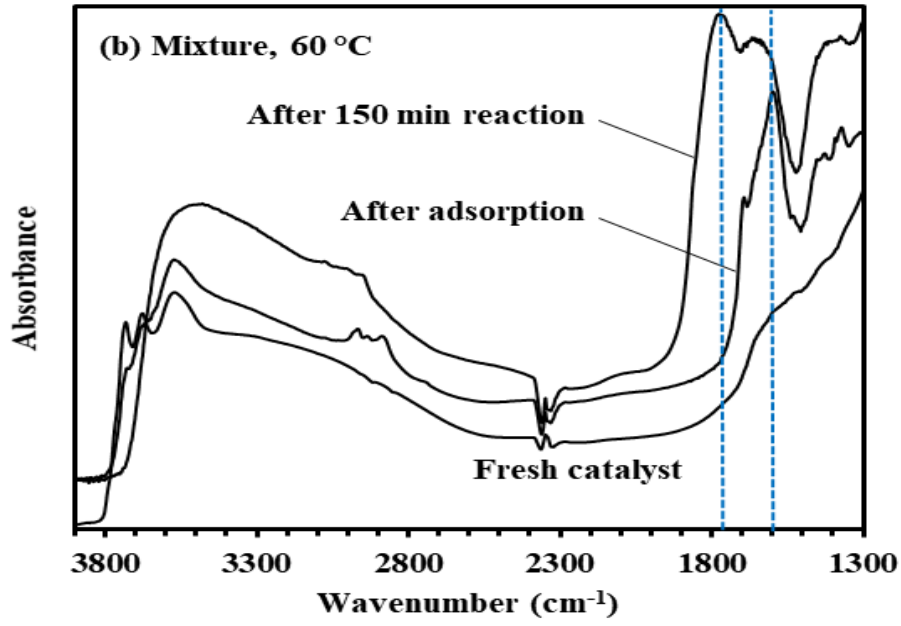
(b) Mixture, 60 °C
After 150 min reaction
After adsorption
Fresh catalyst
Absorbance
3800
3300
2800
2300
1800
1300
Wavenumber (cm-1)

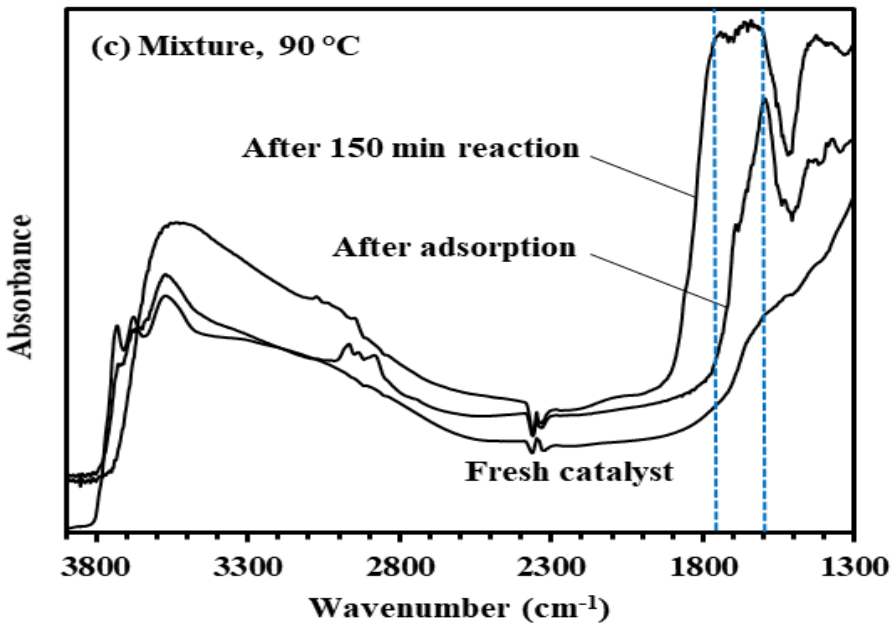

Fig. 6.4. In situ DRIFTS spectra of catalytic ozonation of mixture of toluene and acetone over MnO_x/γ-alumina at (a) 25 °C, (b) 60 °C, and (c) 90 °C; WHSV = 350 L h^{-1} g^{-1}, [O_3] = 1200 ppmv, [toluene] = 65 ppmv, and [acetone] = 130 ppmv.

DRIFTS spectrum after adsorption of the mixture of acetone and toluene at 25 °C (Fig. 6.4a) was similar to that of single acetone adsorption. Once ozone was introduced to the reaction systems, the intensity of the peak at around 1600 cm^{-1} increased significantly. This indicates that partial oxidation of toluene and acetone to surface carboxylates is an essential step in catalytic ozonation of these VOCs. Increase of temperature to 60 (Fig. 6.4a) and 90 °C (Fig. 6.4c) significantly increased intensity of the peak at 1600 cm^{-1}, indicating that more oxidation to surface carboxylates occurred at higher temperatures. This observation is consistent with the improved VOC conversions at 60 and 90 °C. The peak at around 1720 (C=O stretching) and the broad band from 2400 to 3750 cm^{-1} (OH stretching) were other significant bands. These bands

appeared later during the reaction and their intensities increased with time. These bands are assigned to compounds such as carboxylic acids, ketones and alcohols that formed on the surface of the catalyst during catalytic ozonation of VOCs.

6.3. Temperature programmed analysis on the spent catalyst

Thermo-gravimetric analysis was carried out under nitrogen flow to monitor variation in weight of the spent catalysts with increase of temperature to 790 °C. Fig. 6.5s depicts profiles of the weight change of the spent catalysts used in catalytic ozonation of mixture of VOCs. The spent catalysts of 25, 60, and 90 °C reactions lost 20%, 12%, and 6% of their weights, respectively. Fig. 6.5b compares weight losses during thermo-gravimetric analysis used for catalytic ozonation of single VOCs with those of the mixture of acetone and toluene. Catalysts used for catalytic ozonation of single toluene showed the most intense weight losses at each temperature. While, catalysts used for catalytic ozonation of single acetone showed the least intense weight losses. This is consistent with the observed CO_x yields (see Fig. 6.2b). For instance, although toluene-25 reaction showed higher VOC removal rate than acetone-25, considerably lower CO_x yield of toluene-25 resulted in build-up of significant amount of products on the catalyst.

Less intense weight losses were observed for catalysts used at higher temperatures. The catalysts used at 90 ° showed the least weight losses, followed by the catalysts used at 60 and 25 °C. This is in agreement with the observed CO_x yields as well. Higher reaction temperatures increased conversion of the VOCs to CO_x, which led to deposition of less products on the catalyst.

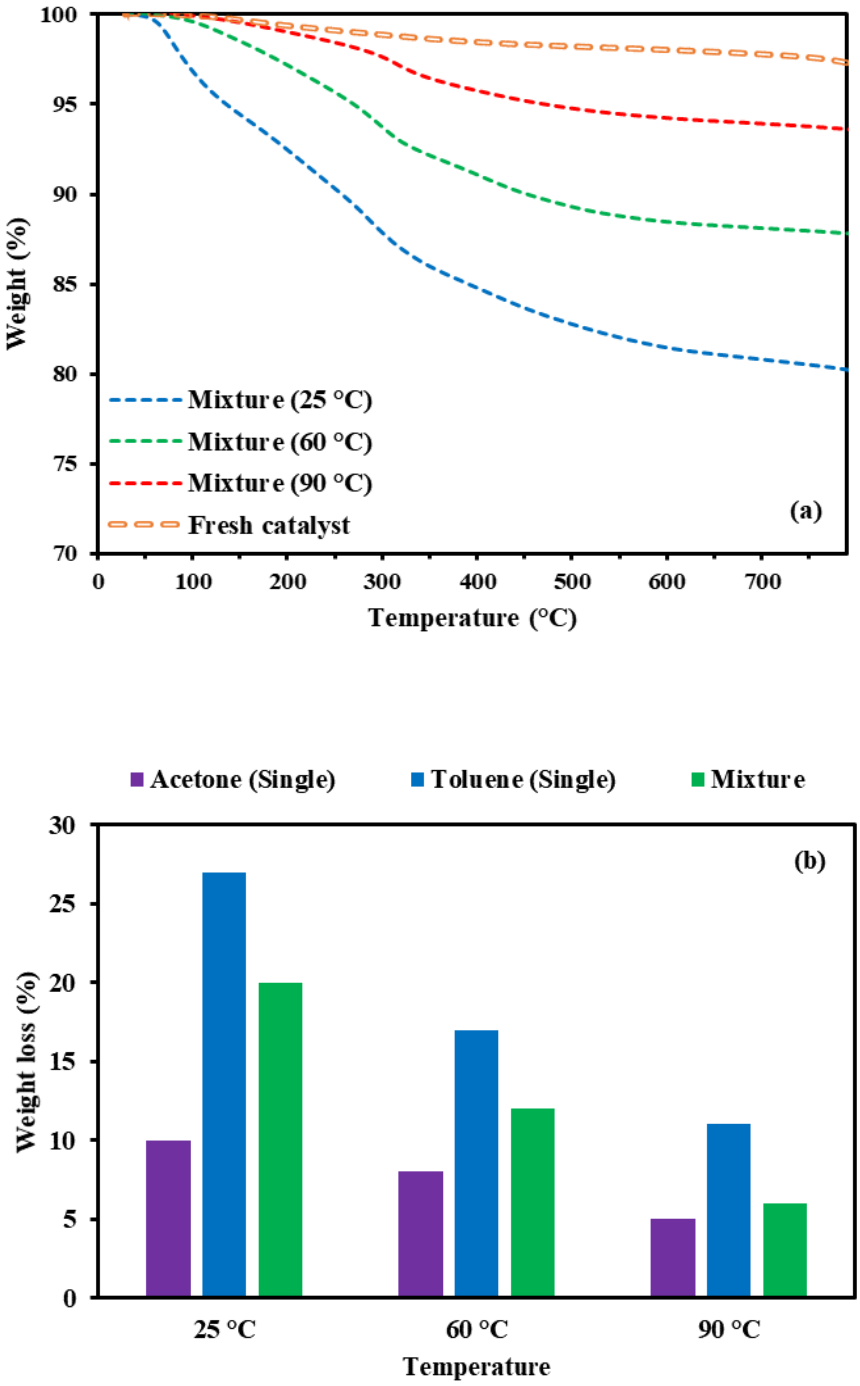

Fig. 6.5. Thermo-gravimetric analysis of MnO_x/γ-alumina, (a) weight loss profile of the catalysts used in catalytic ozonation of the mixture toluene acetone; (b) comparison of weight losses of the catalysts used in catalytic ozonation of single VOCs and the mixture of VOCs.

Temperature programmed oxidation (TPO) was performed at a heating rate of 10 °C/min under 350 mL/min of oxygen-nitrogen (20-80 v%) flow. Fig. 6.6 shows the profiles of carbon dioxide and carbon monoxide concentrations during TPO of the catalysts used in catalytic ozonation of the mixture of toluene and acetone. TPO of the mixture-25, mixture-60, and mixture-90 catalysts, produced maximum CO_2 concentrations of 1160, 750, and 370 ppmv, respectively. Also, TPO analyses produced maximum CO concentrations of 257, 127, and 41 ppmv for the mixture-25, mixture-60, and mixture-90 catalysts, respectively. The TPO profiles showed that a significant amount of accumulated carbonaceous materials was oxidized at around 325 °C.

TPO results were used to calculate the overall carbon balance of the reaction systems. The carbon distribution breakdown is presented in Table 6.1. The results in Table 6.1 showed a good carbon balance (greater than 96%) for all reactions. For the mixture-25 catalyst, total amount of the evolved CO_x during TPO was 1.8 times higher than the evolved CO_x during TPO of the mixture-60 catalyst. Also, total amount of the evolved CO_x during TPO for the mixture-25 catalyst was 3.5 times higher than that for the mixture-90 catalyst. This indicates that higher amount of carbonaceous materials accumulated on the spent catalysts in the 25 °C reactions compared to the 60 and 90 °C reactions.

In addition, the total amount of the evolved CO_x during TPO for the catalysts used in removal of the single toluene (see Table 4.5) were higher than that for the catalysts used in removal of single acetone (see Table 5.4). This can be attributed to higher number of carbons in the structure of toluene compared to acetone. Also, this observation is consistent with lower CO_x yields during catalytic ozonation of toluene (see Fig. 6.2b).

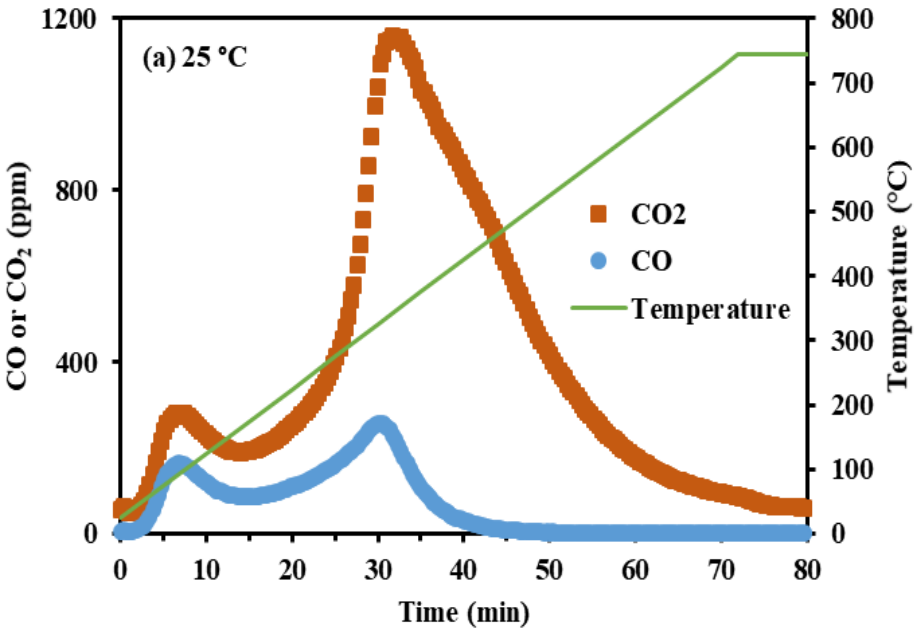
(a) 25 °C
CO2
CO
Temperature
CO or CO2 (ppm)
Temperature (°C)
Time (min)
0
400
800
1200
0
100
200
300
400
500
600
700
800
0
10
20
30
40
50
60
70
80

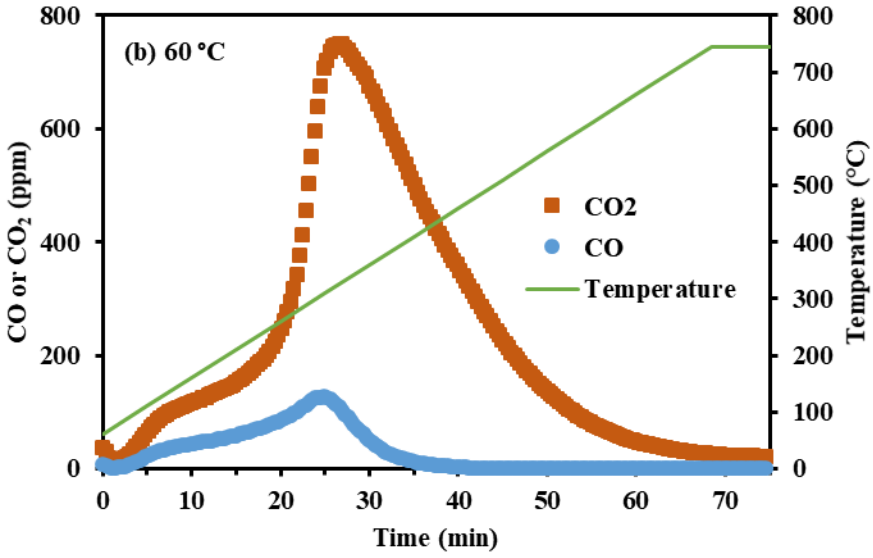
(b) 60 °C
CO2
CO
Temperature
CO or CO2 (ppm)
Temperature (°C)
Time (min)
0
200
400
600
800
0
100
200
300
400
500
600
700
800
0
10
20
30
40
50
60
70

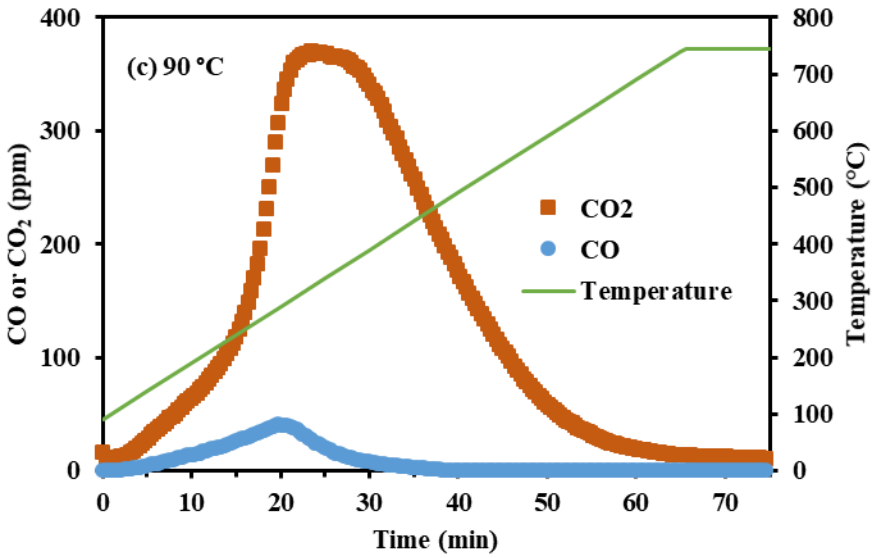

Fig. 6.6. Variation of carbon dioxide and carbon monoxide concentrations during TPO analysis of the spent MnO_x/γ-alumina used in catalytic ozonation of mixture of acetone and toluene at (a) 25 °C, (b) 60 °C, and (c) 90 °C.

Table 6.1. Carbon distribution breakdown (numbers are in mg) and the overall carbon balance for catalytic ozonation of the mixture of VOCs over MnO_x/γ-alumina.

	25 °C reaction	60 °C reaction	90 °C reaction
Total carbon in [a]	26.24	22.89	21.77
Total carbon out before TPO [b]	19.23	18.94	19.96
Total carbon evolved during TPO [c]	6.10	3.42	1.74
Total Carbon out	25.33	22.36	21.70
Carbon balance (%)	96.53	97.68	99.68

[a] During reaction and catalyst saturation with VOCs.
[b] As CO_x and unreacted VOCs.
[c] As evolved CO_x during TPO.

6.4. Identification of carbonaceous deposits by GC-MS

During the reaction, carbonaceous species build up on the catalyst and cause a decline in the catalyst activity. In order to identify the carbonaceous species accumulated on the catalyst during catalytic ozonation, the spent catalysts were contacted with dichloromethane and the resulting extracts were analyzed with GC-MS. For the mixture-25, a number of organic compounds were identified such as formic acid, acetic acid, acetol, formyl acetate, acetic anhydride, acetoxyacetic acid, β-isoamylene oxide, and isopropyl methyl ketone. These compounds are listed in order of increasing the number of carbon atoms in their structures. Compounds found for the mixture-25 were the same as those of the toluene-25 (see section 4.7). This is in contrast to the remarkably high conversion of toluene in the mixture-25 reaction, indicating that oxidation of toluene was severely incomplete. Moreover, this indicates that low CO_x yield for the mixture-25 reaction (Fig. 6.2b) was mainly due to poor oxidation of toluene.

As discussed earlier, for the acetone-25 (see section 5.6), compounds such as acetic acid, acetic anhydride, β-isoamylene oxide, and isopropyl methyl ketone were identified on the spent catalyst. These compounds are among the compounds found for the mixture-25 and toluene-25 catalysts as well.

For the toluene-60 catalyst, the identified compounds were formic acid, acetic acid, acetic anhydride, β-isoamylene oxide, isopropyl methyl ketone. However, a number of compounds that were found for the toluene-25 catalyst, including acetol, formyl acetate, and acetoxyacetic acid were not found for the toluene-60 catalyst. In addition, for the acetone-60 catalyst only acetic acid and isopropyl methyl ketone were found. This suggests that increase of temperature

improved oxidation of VOCs to CO_x. This is consistent with the reported CO_x yields (Fig. 6.2b). Interestingly, for the mixture-60 catalyst, only formic acid, acetic acid and isopropyl methyl ketone were identified on the spent catalyst; while, acetic anhydride and β-isoamylene oxide were not detected. This confirms that catalytic ozonation in the mixture was favourable for toluene conversion to CO_x.

For the mixture-90 catalyst, none of the above compounds were found by GC-MS analysis (similar to toluene-90 and acetone-90). In another attempt, the mixture-25 catalyst, was heated to 425 °C under 350 ml/min of nitrogen flow. Then the catalyst was washed with dichloromethane and the resulting extract was analyzed with GC-MS. The results did not show any extracted compounds. This indicates that all the mentioned carbonaceous materials were mostly desorbed by heating the spent catalyst to 425 °C.

As discussed earlier, difference in reactivity of toluene and acetone in the mixture can be attributed to the difference in the apparent activation energies. Moreover, accumulation of the numerous carbonaceous materials, which are produced from the severely incomplete oxidation of toluene, affects acetone conversion negatively. This causes the acetone conversion in the mixture-25 to be lower than that of the acetone-25.

In addition, the majority of the identified compounds for the mixture-25 and mixture-60 catalysts are polar. Acetone is polar as well, while toluene is non-polar. Dipole moment of acetone is 2.88 D, whereas toluene has a dipole moment of 0.38 D [127]. One may conclude that non-polar compounds are more reactive in catalytic ozonation, although further research with a wide variety of VOCs is required to validate this conclusion.

6.5. Catalyst regeneration

As discussed in section 6.4, heating the mixture-25 catalyst to 425 °C under nitrogen was enough to desorb the majority of the deposited carbonaceous products. Also, according to the thermo-gravimetric analysis (see Fig. 6.5) for the mixture-25 catalyst, almost 80% of the observed weight loss occurred by heating the spent catalyst to 425 °C under nitrogen flow. This suggests that heating the spent catalyst up to 425 °C may be adequate for catalyst regeneration.

To investigate this possibility, the catalyst that was used in catalytic ozonation of mixture of VOCs at 25 °C (mixture-25) was heated to 425 °C under 350 ml/min N_2 flow and was used for a second catalytic ozonation reaction. All other reaction conditions were the same. Fig. 6.7 compares VOCs and ozone conversions, and CO and CO_2 concentrations obtained from use of the fresh and regenerated catalysts.

Performances of the fresh and regenerated catalysts in catalytic ozonation of the mixture of toluene and acetone were comparable. This confirms that heating the spent catalyst to 425 °C was enough to regenerate the spent catalyst and regain high catalytic activity. Interestingly, CO and CO_2 concentrations were significantly higher for the regenerated catalyst in the first 30 minutes of the reaction. Higher CO_x concentration in the first 30 minutes can be attributed to the oxidation of the carbonaceous materials that accumulated in the first catalytic ozonation reaction and were not desorbed by heating the catalyst to 425 °C.

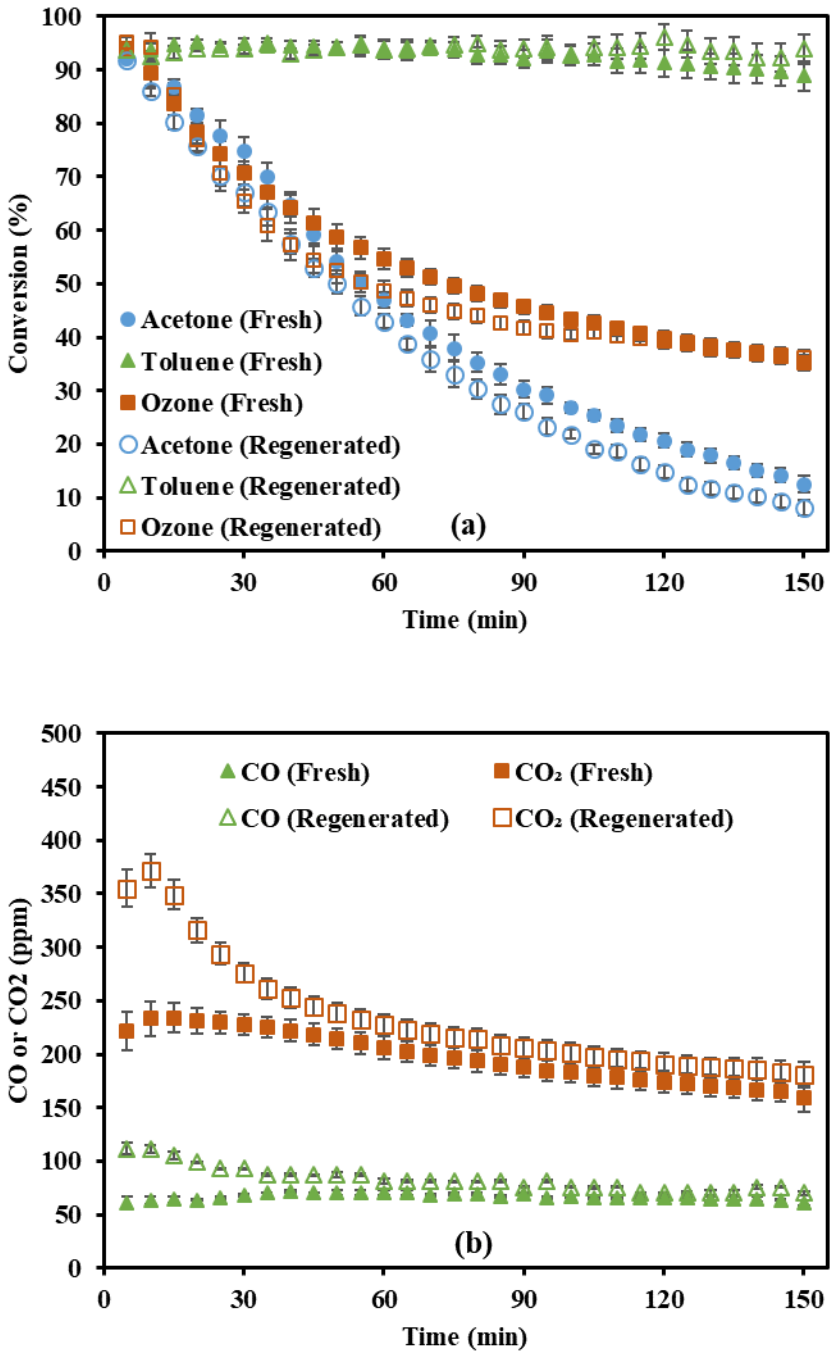

Fig. 6.7. Catalytic ozonation of mixture VOCs at 25 °C by using fresh and regenerated MnO_x/γ-alumina, (a) VOCs and ozone conversions; (b) CO and CO_2 concentrations in the exhaust stream; WHSV = 350 L h^{-1} g^{-1}, [O_3] = 1200 ppmv, [toluene] = 65 ppmv, and [acetone] = 65 ppmv; error bars are standard errors.

As discussed in Chapter 4 and Chapter 5, in situ studies during temperature programmed desorption under nitrogen flow showed that surface carboxylates remain on the surface of the catalyst even after heating the catalyst up to 425 °C (see Fig. 4.10 and Fig. 5.9). Therefore, the surface carboxylates were present from the beginning of the second catalytic ozonation reaction (by using the regenerated catalyst). Regaining high catalytic activity despite the presence of the surface carboxylates indicates that the surface carboxylates do not cause deactivation of the MnO_x/γ-alumina catalyst. This is similar to the conclusion made in section "*4.8. Role of surface carboxylates*".

6.6. Summary

VOCs in both indoor and outdoor environments are usually present as mixtures of different compounds. Despite this, low temperature catalytic ozonation of mixture of VOCs has not been reported in the literature. In this chapter, catalytic ozonation of a binary mixture of toluene and acetone was investigated. Considerable mixture effects were observed in catalytic ozonation of toluene and acetone. Catalytic ozonation in the mixture was favourable for toluene conversion, and repressive for acetone conversion. In the absence of ozone, acetone was adsorbed better on the catalyst. Also, in situ DRIFTS spectrum after adsorption of the mixture of acetone and toluene was similar to that of single acetone adsorption. Despite this, in the presence of ozone, toluene removal in the mixture at 25 °C was about seven times higher than acetone removal.

Undesired products found on the catalyst used for catalytic ozonation of the mixture at 25 °C were the same as those of the catalytic ozonation of toluene. This was despite the remarkably high conversion of toluene in the catalytic ozonation of the mixture, indicating that oxidation of toluene in the mixture was severely incomplete. The catalyst deactivation caused by the undesired products was reversible. Heating the spent catalyst to 425 °C under nitrogen was enough to regenerate the spent catalyst and regain high catalytic activity.

Studies on catalytic oxidation (without ozone) of mixture of VOCs have suggested that competitive adsorption on the catalyst plays an important role in determining the reactivity of VOCs. However, breakthrough curves of adsorption of toluene and acetone as a mixture on MnO_x/γ-alumina showed that in the absence of ozone, acetone is adsorbed better on the catalyst. Therefore, better reactivity of toluene in the catalytic ozonation of the mixture cannot be attributed to competitive adsorption of VOCs on the catalyst. Favourable reaction towards toluene removal can be assigned to lower apparent activation energy of catalytic ozonation of toluene. In other words, tendency to react with active oxygen species (resulted from catalytic decomposition of ozone) is a more important factor than ability to be adsorbed on the catalyst in the absence of ozone. Also, repressive reaction towards acetone removal can be attributed to oppressive effect on acetone conversion caused by accumulation of carbonaceous materials that resulted from severely incomplete oxidation of toluene. Increase of temperature from 25 to 60 and 90 °C increased removal of both VOCs and enhanced CO_x yield. Also, increasing the reaction temperature decreased the gap between toluene and acetone conversions.

Chapter 7:
Conclusions and recommendations for future work

7.1. Summary of the thesis

In this thesis research, catalytic ozonation of single VOCs and a binary mixture of VOCs over γ-alumina-supported manganese oxide catalyst was investigated. VOCs are important indoor and outdoor air pollutants that have adverse health effects on humans. The most common methods for removal of VOCs from air are adsorption, photocatalytic oxidation, non-thermal plasma, biological treatment, catalytic oxidation and ozone-assisted catalytic oxidation (i.e. catalytic ozonation). Among these, catalytic ozonation has gained increasing attention in the recent years due to its advantages over catalytic oxidation. Compared to catalytic oxidation, the reaction temperature for catalytic ozonation is significantly lower. In addition, catalysts based on transition metal oxides have high efficiencies in removal of VOCs by catalytic ozonation, eliminating the need for expensive noble metals that are commonly used in catalytic oxidation of VOCs by oxygen.

As discussed in Chapter 2, catalysts based on manganese oxides are the most active catalysts for removal of VOCs in gas phase in the presence of ozone. Catalytic ozonation with manganese oxide-based catalysts has been used for oxidation of a variety of VOCs in air at temperatures below 100 °C. Catalytic ozonation of VOCs using manganese oxide supported on γ-alumina have shown higher VOC removal rates than catalysts supported on silica, titania, and

zirconia. Therefore, alumina supported manganese oxide catalyst was used for catalytic ozonation of acetone and toluene. Acetone and toluene have different chemical properties and both are common VOCs in indoor and outdoor environments.

Literature review on catalytic ozonation of VOCs showed that topics such as effect of operating conditions, comparison of transition metal oxides, comparison of supports, effect of water vapor, effect of manganese loading, and effect of noble metals have been studied extensively. On the other hand, catalytic ozonation of a mixture of VOCs and identifying the role of reaction intermediates are among the remaining knowledge gaps. Therefore, the objectives of this work were to investigate the nature and roles of intermediates that are formed on the surface of the catalyst, and to study catalytic ozonation of a mixture of toluene and acetone.

Alumina supported manganese oxide catalyst was prepared by dry impregnation method and was used in an atmospheric reactor to carry out catalytic ozonation of toluene and acetone. In situ diffuse reflectance infrared Fourier transform spectroscopy, X-ray spectroscopy techniques, and a number of temperature programmed analyses were used to achieve the objectives of this investigation. Details of experimental setup and reaction conditions were discussed in Chapter 3.

As discussed in Chapter 4, XANES and XPS studies showed that Mn_2O_3 was the dominant manganese oxide phase of the MnO_x/γ-alumina catalyst. Absorption energy of Mn *K-edge* of the catalyst was determined as 6553.86 eV. Mn_2O_3 was used to estimate the amplitude reduction factor (S_o^2) for EXAFS analyses. Mn_2O_3 has two Mn sites with occupancies of 25% and 75%. Aggregate FEFF calculation was used to integrate the two Mn sites into one single site for EXAFS analysis. An amplitude reduction factor of 0.754 was obtained for Mn_2O_3. Fitting

EXAFS data of the MnO_x/γ-alumina catalyst found 5.58 Mn atoms at the second Mn shell at interatomic distance of ca. 3.12 Å. Also, 1.5, 3.0, and 1.7 oxygen atoms were found at the first Mn shell at interatomic distances of ca. 1.88, 1.97 and 2.23 Å, respectively.

Catalytic ozonation of toluene was conducted on MnO_x/γ-alumina catalyst at 25 and 90 °C. At 90 °C, a stable reaction was observed; however, at 25 °C, a decline in toluene and ozone conversions was observed. Kinetic studies over MnO_x/γ-alumina showed that reaction orders for toluene and ozone were 0.181 and 0.469, respectively. The apparent activation energy of the reaction was estimated as 33 kJ $mole^{-1}$. Rapid catalyst deactivation was observed at both 25 and 90 °C when using pure γ-alumina (without manganese) as catalyst indicating the important role of the manganese in the catalytic activity of the MnO_x/γ- alumina catalyst. During catalytic ozonation of toluene, surface carboxylates were observed on MnO_x/γ-alumina and pure γ-alumina; however, they were not formed on pure manganese oxide. Alumina not only acts as a reservoir for toluene, but also it interacts effectively with toluene, in the presence of ozone, to create surface carboxylate intermediates. Based on these observations, a reaction pathway was proposed for catalytic ozonation of toluene on MnO_x/γ-alumina.

Catalytic ozonation of acetone was discussed in Chapter 5. Similar to toluene, a stable catalyst activity was observed at 90 °C, while a gradual decline in conversions was observed at 25 °C. An apparent activation energy of 40 kJ $mole^{-1}$ was obtained for catalytic ozonation of acetone over alumina-supported manganese oxide catalyst. Also, reaction orders of 0.109 and 0.506 were obtained for acetone and ozone, respectively. In situ DRIFTS studies showed that acetone interacted with the surface of the alumina-supported manganese oxide catalyst mainly via its carbonyl group. Surface carboxylates such as surface acetate were produced during

acetone adsorption and catalytic ozonation on both MnO_x/γ-alumina and pure γ-alumina as a result of interaction of alumina with the adsorbed acetone. The presence of Mn sites was necessary to achieve further oxidation of carboxylates on the surface of the catalyst. Temperature programmed oxidation of the spent MnO_x/γ-alumina catalysts showed that higher amount of carbonaceous materials accumulated on the spent catalyst in the 25 °C reaction compared to the 90 °C reaction. Increase of temperature to 625 °C under oxygen-nitrogen (without ozone) flow was enough to remove all the deposited carbonaceous materials.

Catalytic ozonation of a binary mixture of toluene and acetone was discussed in Chapter 6. Remarkable mixture effects were observed in catalytic ozonation of toluene and acetone. Catalytic ozonation in the mixture was favourable for toluene conversion, and repressive for acetone conversion. In the absence of ozone, acetone was adsorbed better on the catalyst. Also, in situ DRIFTS spectrum after adsorption of the mixture of acetone and toluene was similar to that of single acetone adsorption. Despite this, in the presence of ozone, toluene removal in the mixture at 25 °C was about seven times higher than acetone removal. Undesired products found on the catalyst used for catalytic ozonation of the mixture at 25 °C were the same as those of the catalytic ozonation of toluene. This was despite the remarkably high conversion of toluene in the catalytic ozonation of the mixture, indicating that oxidation of toluene in the mixture was severely incomplete. The catalyst deactivation caused by the undesired products was reversible. Heating the spent catalyst to 425 °C under nitrogen was enough to regenerate the spent catalyst and regain high catalytic activity. Increase of reaction temperature from 25 to 60 and 90 °C increased removal of both VOCs and enhanced CO_x yield. Also, increasing the reaction temperature decreased the gap between toluene and acetone conversions.

7.2. Conclusions

The following are the main conclusions from this work that were obtained based on the defined research objectives:

- Surface carboxylates form during catalytic ozonation of acetone and toluene on the alumina supported manganese oxide catalyst, even though these VOCs have significantly different chemical properties. The surface carboxylates form on alumina sites of the catalyst at both 25 °C (with catalyst deactivation) and 90 °C (with stable catalytic activity).

- Pure γ-alumina cannot further oxidize surface carboxylates and the presence of manganese sites is necessary for further oxidation of the surface carboxylates.

- The surface carboxylates are present from the beginning of the first catalytic ozonation reaction (using fresh MnO_x/γ-alumina catalyst) and from the beginning of the second catalytic ozonation reaction (by using the regenerated MnO_x/γ-alumina catalyst). Regaining high catalytic activity despite the presence of the surface carboxylates indicates that the surface carboxylates do not cause deactivation of the MnO_x/γ-alumina catalyst.

- At 25 °C, undesired products such as acetic acid and formic acid accumulate on the surface of the MnO_x/γ-alumina catalyst and decrease the catalyst activity. However, at 90 °C, the undesired products are quickly oxidized to carbon dioxide and carbon monoxide. Therefore, a stable catalytic activity is observed at 90 °C.

- Catalytic ozonation in the mixture is favourable for toluene conversion, and repressive for acetone conversion. Increase of the reaction temperature increases removal of both VOCs, enhances CO_x yield, and decreases the gap between toluene and acetone conversions.

- Favourable reaction towards toluene removal can be attributed to lower apparent activation energy of catalytic ozonation of toluene. Tendency to react with active oxygen species, generated from catalytic decomposition of ozone, is a more important factor than competitive adsorption of VOCs on the catalyst in the absence of ozone. Also, accumulation of the numerous carbonaceous materials, resulted from the severely incomplete oxidation of toluene, affects acetone conversion negatively.

7.3. Recommendations for future work

Catalytic ozonation has been used to remove a variety of VOCs such as aromatics, aldehydes, chlorinated VOCs, ketones, alcohols, and cycloalkanes. Despite the recent developments, catalytic ozonation is still facing some important challenges and it is far from a perfect method for removal of VOCs. The main advantage of catalytic ozonation is lower reaction temperature compared to catalytic oxidation. However, the required temperature for stable operation of catalytic ozonation is still higher than the room temperature. The ultimate goal for catalytic ozonation is achieving a stable catalytic activity at room temperature. Here are

a number of recommendations for the future work that will help to further understand and improve catalytic ozonation of VOCs:

- Investigating effective removal of small carboxylic acids such as acetic acid and formic acid

Small carboxylic acids such as acetic acid and formic acid are the most recalcitrant compounds to be removed by catalytic ozonation. Unfortunately, these compounds are produced during catalytic ozonation of many VOCs. As discussed in this work, accumulation of these compounds on the surface of catalyst is the main cause of catalyst deactivation at room temperature. Therefore, effective removal of these compounds should be one of the main goals of future catalyst improvement/optimization studies. It is believed that a catalytic ozonation system capable of oxidizing small carboxylic acids at room temperature will have significantly higher chance to perform stably for a long time at room temperature.

- Conducting theoretical study of the catalytic ozonation of VOCs using density functional theory

Theoretical studies of the reaction using density functional theory (DFT) can help to better understand the catalytic ozonation mechanism. Presence of highly active oxygen species and very quick reactions make it very challenging to study reaction mechanism experimentally. Therefore, a theoretical or a combined theoretical-experimental study can further elucidate the reaction mechanism. DFT studies have been used to in similar topics such as homogenous reaction of ozone with benzene, and catalytic oxidation of hydrocarbons [128–130].

- Using manganese based catalyst promoted by a limited amount of cobalt to improve carbon dioxide selectivity

Although manganese based catalysts have shown the highest activity in catalytic ozonation of VOCs, these catalysts do not have a good selectivity towards carbon dioxide and usually a considerable amount of carbon monoxide is produced as well. Cobalt is the second most active transition metal catalyst in the catalytic ozonation of VOCs and it has shown excellent activity in conversion of carbon monoxide to carbon dioxide. Therefore, manganese based catalyst promoted by a limited amount of cobalt (a dual function catalyst) has a potential to increase the selectivity toward carbon dioxide without decreasing activity of the original catalyst.

- Investigating catalytic ozonation of a variety of VOC mixtures with a wide range of polarity

Investigating catalytic ozonation of a binary mixture of VOCs showed that studies on a single compound cannot fully represent the catalyst application. Some compounds may have positive or negative effects on removal of other VOCs in the mixture. Commercial application of catalytic ozonation will require simultaneous removal of a wide variety of VOCs. Also, as mentioned in Chapter 7, polarity of VOCs may affect their reactivity in the catalytic ozonation. Therefore, further studies on catalytic ozonation of VOCs with a large number of compounds is necessary.

- Investigating removal of biological air contaminates by catalytic ozonation

Catalytic ozonation, as an air treatment technique, should be able to treat biological air contaminates such as bacteria and viruses as well. Non-catalytic ozone treatment has been successfully used for removal of biological contaminants from air [131,132]. Ozone has been

more effective than UV radiation in removal of microorganisms such as Escherichia coli, Pseudomonas aeruginosa, and Staphylococcus aureus [133]. Most probably a more effective removal of biological air contaminates can be achieved by catalytic ozonation compared to non-catalytic ozone treatment.

List of references

[1] C.D. Cooper, F.C. Alley, Air Pollution Control: A Design Approach, 3rd ed., Waveland Press, Illinois, 2002.

[2] J. Namieśnik, T. Górecki, B. Kozdroń-Zabiega ła, J. Łukasiak, Indoor air quality (IAQ), pollutants, their sources and concentration levels, Build. Environ. 27 (1992) 339–356. doi:http://dx.doi.org/10.1016/0360-1323(92)90034-M.

[3] J.A. Hoskins, Health Effects due to Indoor Air Pollution, Indoor Built Environ. 12 (2003) 427–433. doi:10.1177/1420326X03037109.

[4] Y. Huang, S.S.H. Ho, Y. Lu, R. Niu, L. Xu, J. Cao, S. Lee, Removal of indoor volatile organic compounds via photocatalytic oxidation: A short review and prospect, Molecules. 21 (2016) 56–76. doi:10.3390/molecules21010056.

[5] S. Wang, H.M. Ang, M.O. Tade, Volatile organic compounds in indoor environment and photocatalytic oxidation: State of the art, Environ. Int. 33 (2007) 694–705. doi:10.1016/j.envint.2007.02.011.

[6] United States Environmental Protection Agency, Volatile Organic Compounds' Impact on Indoor Air Quality, (2017). https://www.epa.gov/indoor-air-quality-iaq/volatile-organic-compounds-impact-indoor-air-quality (accessed July 26, 2017).

[7] B. Guieysse, C. Hort, V. Platel, R. Munoz, M. Ondarts, S. Revah, Biological treatment of indoor air for VOC removal: Potential and challenges, Biotechnol. Adv. 26 (2008) 398–

410. doi:http://dx.doi.org/10.1016/j.biotechadv.2008.03.005.

[8] J.E. Colman Lerner, M.A. Peluso, A. Porta, H.J. Thomas, J.E. Sambeth, Catalytic removal of a mixture of volatile organic compounds present in indoor air at various work sites over Pt, MnOx and Pt/MnOx supported monoliths, React. Kinet. Mech. Catal. 114 (2015) 395–407. doi:10.1007/s11144-014-0827-7.

[9] R. Chauveau, G. Grevillot, S. Marsteau, C. Vallieres, Values of the mass transfer coefficient of the linear driving force model for VOC adsorption on activated carbons, Chem. Eng. Res. Des. 91 (2013) 955–962. doi:10.1016/j.cherd.2012.09.019.

[10] E.F. Mohamed, G. Awad, C. Andriantsiferana, A.I. El-Diwany, Biofiltration technology for the removal of toluene from polluted air using Streptomyces griseus, Environ. Technol. 37 (2016) 1197–1207. doi:10.1080/09593330.2015.1107623.

[11] A. Rodrigues, J.-M. Tatibouet, E. Fourre, Operando DRIFT Spectroscopy Characterization of Intermediate Species on Catalysts Surface in VOC Removal from Air by Non-thermal Plasma Assisted Catalysis, Plasma Chem. Plasma Process. 36 (2016) 901–915. doi:10.1007/s11090-016-9718-1.

[12] I. Banu, C.M. Manta, G. Bercaru, G. Bozga, Combustion kinetics of cyclooctane and its binary mixture with o-xylene over a Pt/gamma-alumina catalyst, Chem. Eng. Res. Des. 102 (2015) 399–406. doi:10.1016/j.cherd.2015.07.012.

[13] H. Einaga, S. Yamamoto, N. Maeda, Y. Teraoka, Structural analysis of manganese oxides supported on SiO2 for benzene oxidation with ozone, Catal. Today. 242 (2015) 287–293.

doi:10.1016/j.cattod.2014.05.018.

[14] M.-S. Li, S.C. Wu, Y.-H. Shih, Characterization of volatile organic compound adsorption on multiwall carbon nanotubes under different levels of relative humidity using linear solvation energy relationship., J. Hazard. Mater. 315 (2016) 35–41. doi:10.1016/j.jhazmat.2016.04.004.

[15] X. Fan, T.L. Zhu, M.Y. Wang, X.M. Li, Removal of low-concentration BTX in air using a combined plasma catalysis system, Chemosphere. 75 (2009) 1301–1306. doi:10.1016/j.chemosphere.2009.03.029.

[16] Y. Cheng, H. He, C. Yang, G. Zeng, X. Li, H. Chen, G. Yu, Challenges and solutions for biofiltration of hydrophobic volatile organic compounds, Biotechnol. Adv. 34 (2016) 1091–1102. doi:10.1016/j.biotechadv.2016.06.007.

[17] S.-C. Jung, Y.-K. Park, H.Y. Jung, U. Il Kang, J.W. Nah, S.C. Kim, Effects of calcination and support on supported manganese catalysts for the catalytic oxidation of toluene as a model of VOCs, Res. Chem. Intermed. 42 (2016) 185–199. doi:10.1007/s11164-015-2333-6.

[18] H.S. Liang, H.C. Wang, M.B. Chang, Low-Temperature Catalytic Oxidation of Monochlorobenzene by Ozone over Silica-Supported Manganese Oxide, Ind. Eng. Chem. Res. 50 (2011) 13322–13329. doi:10.1021/ie202216m.

[19] E. Rezaei, J. Soltan, N. Chen, Catalytic oxidation of toluene by ozone over alumina supported manganese oxides: Effect of catalyst loading, Appl. Catal. B Environ. 136–137

(2013) 239–247. doi:http://dx.doi.org/10.1016/j.apcatb.2013.01.061.

[20] E. Rezaei, J. Soltan, Low temperature oxidation of toluene by ozone over MnOx/γ-alumina and MnOx/MCM-41 catalysts, Chem. Eng. J. 198–199 (2012) 482–490. doi:http://dx.doi.org/10.1016/j.cej.2012.06.016.

[21] H. Huang, X. Ye, W. Huang, J. Chen, Y. Xu, M. Wu, Q. Shao, Z. Peng, G. Ou, J. Shi, X. Feng, Q. Feng, H. Huang, P. Hu, D.Y.C. Leung, Ozone-catalytic oxidation of gaseous benzene over MnO2/ZSM-5 at ambient temperature: Catalytic deactivation and its suppression, Chem. Eng. J. 264 (2015) 24–31. doi:http://dx.doi.org/10.1016/j.cej.2014.11.072.

[22] D.-Z. Zhao, C. Shi, X.-S. Li, A.-M. Zhu, B.W.-L. Jang, Enhanced effect of water vapor on complete oxidation of formaldehyde in air with ozone over MnOx catalysts at room temperature, J. Hazard. Mater. 239 (2012) 362–369. doi:10.1016/j.jhazmat.2012.09.009.

[23] H. Einaga, S. Futamura, Comparative study on the catalytic activities of alumina-supported metal oxides for oxidation of benzene and cyclohexane with ozone, React. Kinet. Catal. Lett. 81 (2004) 121–128. doi:10.1023/B:REAC.0000016525.91158.c5.

[24] D. Jin, Z. Ren, Z. Ma, F. Liu, H. Yang, Low temperature chlorobenzene catalytic oxidation over MnOx/CNTs with the assistance of ozone, Rsc Adv. 5 (2015) 15103–15109. doi:10.1039/c4ra16687f.

[25] H. Einaga, N. Maeda, Y. Teraoka, Effect of catalyst composition and preparation conditions on catalytic properties of unsupported manganese oxides for benzene oxidation

with ozone, Appl. Catal. B-Environmental. 142 (2013) 406–413. doi:10.1016/j.apcatb.2013.05.041.

[26] H. Einaga, S. Futamura, Catalytic oxidation of benzene with ozone over alumina-supported manganese oxides, J. Catal. 227 (2004) 304–312. doi:http://dx.doi.org/10.1016/j.jcat.2004.07.029.

[27] H. Einaga, S. Futamura, Oxidation behavior of cyclohexane on alumina-supported manganese oxides with ozone, Appl. Catal. B-Environmental. 60 (2005) 49–55. doi:10.1016/j.apcath.2005.02.017.

[28] H. Einaga, A. Ogata, Benzene oxidation with ozone over supported manganese oxide catalysts: Effect of catalyst support and reaction conditions, J. Hazard. Mater. 164 (2009) 1236–1241. doi:http://dx.doi.org/10.1016/j.jhazmat.2008.09.032.

[29] J.E. Colman Lerner, E.Y. Sanchez, J.E. Sambeth, A.A. Porta, Characterization and health risk assessment of VOCs in occupational environments in Buenos Aires, Argentina, Atmos. Environ. 55 (2012) 440–447. doi:10.1016/j.atmosenv.2012.03.041.

[30] E. Gallego, F.J. Roca, J.F. Perales, G. Sanchez, P. Esplugas, Characterization and determination of the odorous charge in the indoor air of a waste treatment facility through the evaluation of volatile organic compounds (VOCs) using TD-GC/MS, Waste Manag. 32 (2012) 2469–2481. doi:10.1016/j.wasman.2012.07.010.

[31] C. Walgraeve, K. Demeestere, J. Dewulf, K. Van Huffel, H. Van Langenhove, Diffusive sampling of 25 volatile organic compounds in indoor air: Uptake rate determination and

application in Flemish homes for the elderly, Atmos. Environ. 45 (2011) 5828–5836. doi:10.1016/j.atmosenv.2011.07.007.

[32] European Union Publications Office, Directive 2004/42/CE of the European Parliament and the Council, 2004. http://eur-lex.europa.eu/legal-content/EN/TXT/?uri=celex:32004L0042.

[33] World Health Organization, Indoor air quality: organic pollutants, Copenhagen, Denmark, 1989.

[34] United States Environmental Protection Agency, Technical Overview of Volatile Organic Compounds, (2017). https://www.epa.gov/indoor-air-quality-iaq/technical-overview-volatile-organic-compounds (accessed July 26, 2017).

[35] P. Wolkoff, G.D. Nielsen, Organic compounds in indoor air - their relevance for perceived indoor air quality?, Atmos. Environ. 35 (2001) 4407–4417. doi:10.1016/S1352-2310(01)00244-8.

[36] C.J. Weschler, Changes in indoor pollutants since the 1950s, Atmos. Environ. 43 (2009) 153–169. doi:10.1016/j.atmosenv.2008.09.044.

[37] S.C. Hodgson, R.J. Casey, S.W. Bigger, J. Scheirs, Review of volatile organic compounds derived from polyethylene, Polym. Plast. Technol. Eng. 39 (2000) 845–874. doi:10.1081/PPT-100101409.

[38] S.K. Mishra, L. Ajello, D.G. Ahearn, H.A. Burge, V.P. Kurup, D.L. Pierson, D.L. Price, R.A. Samson, R.S. Sandhu, B. Shelton, R.B. Simmons, K.F. Switzer, Environmental

mycology and its importance to public health, J. Med. Vet. Mycol. 30 (1992) 287–305.

[39] J. Ten Brinke, S. Selvin, A.T. Hodgson, W.J. Fisk, M.J. Mendell, C.P. Koshland, J.M. Daisey, Development of new volatile organic compound (VOC) exposure metrics and their relationship to “sick building syndrome” symptoms, INDOOR AIR-INTERNATIONAL J. INDOOR AIR Qual. Clim. 8 (1998) 140–152.

[40] C. Reed, Y.-K. Lee, S.T. Oyama, Structure and Oxidation State of Silica-Supported Manganese Oxide Catalysts and Reactivity for Acetone Oxidation with Ozone, J. Phys. Chem. B. 110 (2006) 4207–4216. doi:10.1021/jp054288w.

[41] W.H. Chen, J.S.S. Zhang, Z.B. Zhang, Performance of air cleaners for removing multiple volatile organic compounds in indoor air, in: ASHRAE Trans. 2005, Vol 111, Pt 1, 2005: pp. 1101–1114.

[42] J. Van Durme, J. Dewulf, K. Demeestere, C. Leys, H. Van Langenhove, Post-plasma catalytic technology for the removal of toluene from indoor air: Effect of humidity, Appl. Catal. B-ENVIRONMENTAL. 87 (2009) 78–83. doi:10.1016/j.apcatb.2008.08.015.

[43] J. Van Durme, J. Dewulf, C. Leys, H. Van Langenhove, Combining non-thermal plasma with heterogeneous catalysis in waste gas treatment: A review, Appl. Catal. B-ENVIRONMENTAL. 78 (2008) 324–333. doi:10.1016/j.apcatb.2007.09.035.

[44] M.C. Delhomenie, M. Heitz, Biofiltration of air: A review, Crit. Rev. Biotechnol. 25 (2005) 53–72. doi:10.1080/07388550590935814.

[45] J. Mo, Y. Zhang, Q. Xu, J.J. Lamson, R. Zhao, Photocatalytic purification of volatile

organic compounds in indoor air: A literature review, Atmos. Environ. 43 (2009) 2229–2246. doi:10.1016/j.atmosenv.2009.01.034.

[46] S.T. Oyama, Chemical and catalytic properties of ozone, Catal. Rev. Eng. 42 (2000) 279–322. doi:10.1081/CR-100100263.

[47] C. Domeno, A. Rodriguez-Lafuente, J.M. Martos, R. Bilbao, C. Nerin, VOC Removal and Deodorization of Effluent Gases from an Industrial Plant by Photo-Oxidation, Chemical Oxidation, and Ozonization, Environ. Sci. Technol. 44 (2010) 2585–2591. doi:10.1021/es902735g.

[48] E.C. Moretti, A.I. of Chemical Engineers. Center for Waste Reduction Technologies, Practical solutions for reducing volatile organic compounds and hazardous air pollutants, Center for Waste Reduction Technologies, American Institute of Chemical Engineers, 2001.

[49] N.P. Cheremisinoff, Chapter 7 - Prevention and Control Hardware, in: N.P. Cheremisinoff (Ed.), Handb. Air Pollut. Prev. Control, Butterworth-Heinemann, Woburn, 2002: pp. 389–497. doi:https://doi.org/10.1016/B978-075067499-7/50008-0.

[50] F.I. Khan, A.K. Ghoshal, Removal of Volatile Organic Compounds from polluted air, J. Loss Prev. Process Ind. 13 (2000) 527–545. doi:10.1016/S0950-4230(00)00007-3.

[51] N. C, Kirk–Othmer Encyclopedia of Chemical Technology, Kirk–Othmer Encycl. Chem. Technol. (1981).

[52] W.J. Orville-Thomas, A bond-order/bond-length relation for oxygen-oxygen bonds, J.

Mol. Spectrosc. 3 (1959) 588–591. doi:http://dx.doi.org/10.1016/0022-2852(59)90053-0.

[53] W. Von Siemens, Ueber die elektrostatische Induction und die Verzoegerung des Stroms in Flaschendraehten, Poggendorffs Ann Phys Chem. 102 (1857) 66–122.

[54] J.A. Wojtowicz, Kirk-Othmer Encyclopedia of Chemical Technology, Kirk–Othmer Encycl. Chem. Technol. (1996) 953–994. doi:10.1002/0471238961.

[55] R. Atkinson, W.P.L. Carter, Kinetics and mechanisms of the gas-phase reactions of ozone with organic compounds under atmospheric conditions, Chem. Rev. 84 (1984) 437–470. doi:10.1021/cr00063a002.

[56] C.T. Pate, R. Atkinson, J.N.P. Jr., The gas phase reaction of O3 with a series of aromatic hydrocarbons, J. Environ. Sci. Heal. . Part A Environ. Sci. Eng. 11 (1976) 1–10. doi:10.1080/10934527609385750.

[57] I. Spasova, P. Nikolov, D. Mehandjiev, Ozone decomposition over alumina-supported copper, manganese and copper-manganese catalysts, OZONE-SCIENCE Eng. 29 (2007) 41–45. doi:10.1080/01919510601111665.

[58] R. Radhakrishnan, S.T. Oyama, Ozone decomposition over manganese oxide supported on ZrO2 and TiO2: A kinetic study using in situ laser Raman spectroscopy, J. Catal. 199 (2001) 282–290. doi:10.1006/jcat.2001.3167.

[59] C. Heisig, W.M. Zhang, S.T. Oyama, Decomposition of ozone using carbon-supported metal oxide catalysts, Appl. Catal. B-ENVIRONMENTAL. 14 (1997) 117–129. doi:10.1016/S0926-3373(97)00017-9.

[60] R. Radhakrishnan, S.T. Oyama, J.G. Chen, K. Asakura, Electron Transfer Effects in Ozone Decomposition on Supported Manganese Oxide, J. Phys. Chem. B. 105 (2001) 4245–4253. doi:10.1021/jp003246z.

[61] R.M. Heck, R.J. Farrauto, Catalytic Air Pollution Control: Commercial Technology, Van Nostrand Reinhold, New York, 1995.

[62] A. Naydenov, D. Mehandjiev, Complete oxidation of benzene on manganese dioxide by ozone, Appl. Catal. A Gen. 97 (1993) 17–22. doi:http://dx.doi.org/10.1016/0926-860X(93)80063-V.

[63] H. Einaga, A. Ogata, Catalytic Oxidation of Benzene in the Gas Phase over Alumina-Supported Silver Catalysts, Environ. Sci. Technol. 44 (2010) 2612–2617. doi:10.1021/es903095j.

[64] H. Einaga, Y. Teraoka, A. Ogata, Catalytic oxidation of benzene by ozone over manganese oxides supported on USY zeolite, J. Catal. 305 (2013) 227–237. doi:http://dx.doi.org/10.1016/j.jcat.2013.05.016.

[65] D. Andreeva, T. Tabakova, L. Ilieva, A. Naydenov, D. Mehanjiev, M. V Abrashev, Nanosize gold catalysts promoted by vanadium oxide supported on titania and zirconia for complete benzene oxidation, Appl. Catal. A Gen. 209 (2001) 291–300. doi:http://dx.doi.org/10.1016/S0926-860X(00)00766-3.

[66] P. Konova, M. Stoyanova, A. Naydenov, S. Christoskova, D. Mehandjiev, Catalytic oxidation of VOCs and CO by ozone over alumina supported cobalt oxide, Appl. Catal.

A-GENERAL. 298 (2006) 109–114. doi:10.1016/j.apcata.2005.09.027.

[67] M. Stoyanova, P. Konova, P. Nikolov, A. Naydenov, S. Christoskova, D. Mehandjiev, Alumina-supported nickel oxide for ozone decomposition and catalytic ozonation of CO and VOCs, Chem. Eng. J. 122 (2006) 41–46. doi:10.1016/j.cej.2006.05.018.

[68] H.C. Wang, H.S. Liang, M.B. Chang, Chlorobenzene oxidation using ozone over iron oxide and manganese oxide catalysts, J. Hazard. Mater. 186 (2011) 1781–1787. doi:10.1016/j.jhazmat.2010.12.070.

[69] M. Sugasawa, A. Ogata, Effect of Different Combinations of Metal and Zeolite on Ozone-Assisted Catalysis for Toluene Removal, OZONE-SCIENCE Eng. 33 (2011) 158–163. doi:10.1080/01919512.2010.547431.

[70] H. Einaga, S. Futamura, Effect of water vapor on catalytic oxidation of benzene with ozone on alumina-supported manganese oxides, J. Catal. 243 (2006) 446–450. doi:http://dx.doi.org/10.1016/j.jcat.2006.07.021.

[71] Y. Liu, X.-S. Li, C. Shi, J.-L. Liu, A.-M. Zhu, B.W.-L. Jang, Ozone catalytic oxidation of adsorbed benzene over AgMn/HZSM-5 catalysts at room temperature, Catal. Sci. Technol. 4 (2014) 2589–2598. doi:10.1039/c3cy01102j.

[72] Y. Liu, X. Li, J. Liu, C. Shi, A. Zhu, Ozone catalytic oxidation of benzene over AgMn/HZSM-5 catalysts at room temperature: Effects of Mn loading and water content, CHINESE J. Catal. 35 (2014) 1465–1474. doi:10.1016/S1872-2067(14)60070-X.

[73] D. Mehandjiev, A. Naydenov, G. Ivanov, Ozone decomposition, benzene and CO

oxidation over NiMnO3-ilmenite and NiMn2O4-spinel catalysts, Appl. Catal. A Gen. 206 (2001) 13–18. doi:http://dx.doi.org/10.1016/S0926-860X(00)00570-6.

[74] D. Mehandjiev, K. Cheshkova, A. Naydenov, V. Georgesku, Catalytic oxidation of Co and C6H6 on alumina-supported Cu-Cr and Co-Cr oxide catalysts in the presence of ozone, React. Kinet. Catal. Lett. 76 (2002) 287–293. doi:10.1023/A:1016536011704.

[75] E. Rezaei, J. Soltan, N. Chen, J. Lin, Effect of noble metals on activity of MnOx/γ-alumina catalyst in catalytic ozonation of toluene, Chem. Eng. J. 214 (2013) 219–228. doi:http://dx.doi.org/10.1016/j.cej.2012.10.044.

[76] H. Einaga, N. Maeda, S. Yamamoto, Y. Teraoka, Catalytic properties of copper-manganese mixed oxides supported on SiO2 for benzene oxidation with ozone, Catal. TODAY. 245 (2015) 22–27. doi:10.1016/j.cattod.2014.09.018.

[77] J.R. Kastner, R. Ganagavaram, P. Kolar, A. Teja, C. Xu, Catalytic ozonation of propanal using wood fly ash and metal oxide nanoparticle impregnated carbon, Environ. Sci. Technol. 42 (2008) 556–562. doi:10.1021/es0707512.

[78] H. Einaga, M. Harada, A. Ogata, Relationship Between the Structure of Manganese Oxides on Alumina and Catalytic Activities for Benzene Oxidation with Ozone, Catal. Letters. 129 (2009) 422–427. doi:10.1007/s10562-008-9814-9.

[79] E. Rezaei, J. Soltan, EXAFS and kinetic study of MnOx/γ-alumina in gas phase catalytic oxidation of toluene by ozone, Appl. Catal. B Environ. 148–149 (2014) 70–79. doi:http://dx.doi.org/10.1016/j.apcatb.2013.10.041.

[80] M. Hu, Z. Yao, K.N. Hui, K.S. Hui, Novel mechanistic view of catalytic ozonation of gaseous toluene by dual-site kinetic modelling, Chem. Eng. J. 308 (2017) 710–718. doi:10.1016/j.cej.2016.09.086.

[81] C. Reed, Y. Xi, S.T. Oyama, Distinguishing between reaction intermediates and spectators: A kinetic study of acetone oxidation using ozone on a silica-supported manganese oxide catalyst, J. Catal. 235 (2005) 378–392. doi:http://dx.doi.org/10.1016/j.jcat.2005.08.014.

[82] H.-H. Kim, M. Sugasawa, H. Hirata, Y. Teramoto, K. Kosuge, N. Negishi, A. Ogata, Ozone-Assisted Catalysis of Toluene with Layered ZSM-5 and Ag/ZSM-5 Zeolites, Plasma Chem. Plasma Process. 33 (2013) 1083–1098. doi:10.1007/s11090-013-9487-z.

[83] S. Ichikaw, Dashpure TM□(Model DE-10TU) Air Cleaner Specifications, (1998).

[84] V. Ragaini, C.L. Bianchi, G. Forcella, A. Gervasini, No Title, in: L. Bonati (Ed.), Trends Ecol. Phys. Chem., Elsevier, Amsterdam, The Netherlands, 1993: pp. 275–280.

[85] J.A. Rodberg, J.F. Miller, G.E. Keller, J.E. Woods, CIB/ASHRAE Healthy Buildings, (1991).

[86] R. Radhakrishnan, S.T. Oyama, Y. Ohminami, K. Asakura, Structure of MnOx/Al2O3 catalyst: A study using EXAFS, in situ laser raman spectroscopy and ab initio calculations, J. Phys. Chem. B. 105 (2001) 9067–9070. doi:10.1021/jp004480s.

[87] Y. Xi, C. Reed, Y.-K. Lee, S.T. Oyama, Acetone Oxidation Using Ozone on Manganese Oxide Catalysts, J. Phys. Chem. B. 109 (2005) 17587–17596. doi:10.1021/jp052930g.

[88] J. Zhao, X.D. Yang, Photocatalytic oxidation for indoor air purification: a literature review, Build. Environ. 38 (2003) 645–654. doi:10.1016/S0360-1323(02)00212-3.

[89] G. Chen, Y. Chi, C. Pan, J. Yan, M. Ni, Methane-benzene binary mixture destruction in a reverse flow catalytic reactor, J. Mater. Cycles Waste Manag. 13 (2011) 219–224. doi:10.1007/s10163-011-0021-1.

[90] C. He, P. Li, J. Cheng, Z.-P. Hao, Z.-P. Xu, A Comprehensive Study of Deep Catalytic Oxidation of Benzene, Toluene, Ethyl Acetate, and their Mixtures over Pd/ZSM-5 Catalyst: Mutual Effects and Kinetics, Water Air Soil Pollut. 209 (2010) 365–376. doi:10.1007/s11270-009-0205-7.

[91] V.P. Santos, M.F.R. Pereira, J.J.M. Orfao, J.L. Figueiredo, Mixture effects during the oxidation of toluene, ethyl acetate and ethanol over a cryptomelane catalyst, J. Hazard. Mater. 185 (2011) 1236–1240. doi:10.1016/j.jhazmat.2010.10.036.

[92] F.N. Aguero, B.P. Barbero, L. Gambaro, L.E. Cadus, Catalytic combustion of volatile organic compounds in binary mixtures over MnOx/Al2O3 catalyst, Appl. Catal. B-Environmental. 91 (2009) 108–112. doi:10.1016/j.apcatb.2009.05.012.

[93] G. Bunker, Elements of XAFS, (n.d.). http://gbxafs.iit.edu/training/xafsoverview.pdf.

[94] M. Newville, Fundamentals of X-ray Absorption Fine Structure, (2004).

[95] D.T. Jiang, N. Chen, W. Sheng, Wiggler-base hard x-ray spectroscopy beamline at CLS, in: Choi, JY and Rah, S (Ed.), SYNCHROTRON Radiat. INSTRUMENTATION, PTS 1 2, 2007: p. 800+.

[96] B. Ravel, M. Newville, ATHENA, ARTEMIS, HEPHAESTUS: data analysis for X-ray absorption spectroscopy using IFEFFIT, J. Synchrotron Radiat. 12 (2005) 537–541. doi:doi:10.1107/S0909049505012719.

[97] J.J. Rehr, R.C. Albers, Theoretical approaches to x-ray absorption fine structure, Rev. Mod. Phys. 72 (2000) 621–654. doi:10.1103/RevModPhys.72.621.

[98] M. Newville, IFEFFIT: interactive XAFS analysis and FEFF fitting, J. Synchrotron Radiat. 8 (2001) 322–324. doi:10.1107/S0909049500016964.

[99] R. Azargohar, S. Nanda, J.A. Kozinski, A.K. Dalai, R. Sutarto, Effects of temperature on the physicochemical characteristics of fast pyrolysis bio-chars derived from Canadian waste biomass, Fuel. 125 (2014) 90–100. doi:10.1016/j.fuel.2014.01.083.

[100] B. Berglund, G. Clausen, Total Volatile Organic Compounds (TVOC) in Indoor Air Quality Investigations, 1977.

[101] H.Q. Trinh, Y.S. Mok, Plasma-catalytic oxidation of acetone in annular porous monolithic ceramic-supported catalysts, Chem. Eng. J. 251 (2014) 199–206. doi:10.1016/j.cej.2014.04.071.

[102] M.P. Heynderickx, J.W. Thybaut, H. Poelman, D. Poelman, G.B. Marin, Kinetic modeling of the total oxidation of propane over CuO-CeO2/gamma-Al2O3, Appl. Catal. B-ENVIRONMENTAL. 95 (2010) 26–38. doi:10.1016/j.apcatb.2009.11.018.

[103] M. Newville, Fundamentals of XAFS, (2004).

[104] B. Ravel, Introduction to EXAFS Experiments and Theory, (2000). http://cars9.uchicago.edu/~ravel/course/basics.pdf.

[105] B. Ravel, Path degeneracy and EXAFS analysis of disordered materials, J. Synchrotron Radiat. 21 (2014) 1269–1274. doi:10.1107/S1600577514014982.

[106] A. Longo, L.F. Liotta, G. Di Carlo, F. Giannici, A.M. Venezia, A. Martorana, Structure and the Metal Support Interaction of the Au/Mn Oxide Catalysts, Chem. Mater. 22 (2010) 3952–3960. doi:10.1021/cm100697b.

[107] C. Shi, Y. Wang, A. Zhu, B. Chen, C. Au, MnxCo3−xO4 solid solution as high-efficient catalysts for low-temperature oxidation of formaldehyde, Catal. Commun. 28 (2012) 18–22. doi:http://dx.doi.org/10.1016/j.catcom.2012.08.003.

[108] L. Liping, Z. Jianguo, Y. Lixian, F. Mingli, W. Junliang, H. Bichun, Y. Daiqi, Room Temperature Catalytic Ozonation of Toluene over MnO2/Al2O3, Chinese J. Catal. 32 (2011) 904–916. doi:10.1016/S1872-2067(10)60216-1.

[109] S. Toby, L.J. de Burgt, F.S. Toby, Kinetics and chemiluminescence of ozone-aromatic reactions in the gas phase, J. Phys. Chem. 89 (1985) 1982–1986. doi:10.1021/j100256a034.

[110] J. Bedia, J.M. Rosas, J. Rodriguez-Mirasol, T. Cordero, Pd supported on mesoporous activated carbons with high oxidation resistance as catalysts for toluene oxidation, Appl. Catal. B-ENVIRONMENTAL. 94 (2010) 8–18. doi:10.1016/j.apcatb.2009.10.015.

[111] A.C.C. Rodrigues, Gas-phase toluene oxidation over platinum-containing mixed oxides,

React. Kinet. Catal. Lett. 93 (2008) 343–350. doi:10.1007/s11144-008-5258-x.

[112] J. Coates, Interpretation of infrared spectra, a practical approach, in: R.A. Meyers (Ed.), Encycl. Anal. Chem., John Wiley & Sons Ltd., Chichester, 2000: pp. 10815–10837. doi:DOI: 10.1002/9780470027318.a5606.

[113] S.L.T. Andersson, Reaction networks in the catalytic vapor-phase oxidation of toluene and xylenes, J. Catal. 98 (1986) 138–149. doi:http://dx.doi.org/10.1016/0021-9517(86)90304-0.

[114] G. Busca, F. Cavani, F. Trifirò, Oxidation and ammoxidation of toluene over vanadium-titanium oxide catalysts: A Fourier transform infrared and flow reactor study, J. Catal. 106 (1987) 471–482. doi:http://dx.doi.org/10.1016/0021-9517(87)90260-0.

[115] B. Irigoyen, A. Juan, S. Larrondo, N. Amadeo, The adsorption of toluene on V–Sb oxides. Theoretical aspects, Surf. Sci. 523 (2003) 252–266. doi:http://dx.doi.org/10.1016/S0039-6028(02)02434-2.

[116] U. Menon, V. V Galvita, G.B. Marin, Reaction network for the total oxidation of toluene over CuO–CeO2/Al2O3, J. Catal. 283 (2011) 1–9. doi:http://dx.doi.org/10.1016/j.jcat.2011.05.024.

[117] C. Hu, Catalytic combustion kinetics of acetone and toluene over Cu0.13Ce0.87Oy catalyst, Chem. Eng. J. 168 (2011) 1185–1192. doi:10.1016/j.cej.2011.02.006.

[118] L.M. Gandia, A. Gil, S.A. Korili, Effects of various alkali-acid additives on the activity of a manganese oxide in the catalytic combustion of ketones, Appl. Catal. B-

ENVIRONMENTAL. 33 (2001) 1–8. doi:10.1016/S0926-3373(01)00155-2.

[119] X. Hu, C. Li, C. Yang, Studies on lattice oxygen utilization during catalytic conversion of n-heptane activated by V2O5/Al2O3, Chem. Eng. J. 263 (2015) 113–118. doi:10.1016/j.cej.2014.11.035.

[120] U. Rodemerck, E. V Kondratenko, T. Otroshchenko, D. Linke, Unexpectedly high activity of bare alumina for non-oxidative isobutane dehydrogenation, Chem. Commun. (2016). doi:10.1039/C6CC06442F.

[121] J. March, Advanced organic chemistry: reactions, mechanisms, and structure, 4th ed., John Wiley & Sons Ltd., 1992.

[122] C.W. Kwong, C.Y.H. Chao, K.S. Hui, M.P. Wan, Catalytic Ozonation of Toluene Using Zeolite and MCM-41 Materials, Environ. Sci. Technol. 42 (2008) 8504–8509. doi:10.1021/es801087f.

[123] P. Kolar, J.R. Kastner, Low-temperature catalytic oxidation of aldehyde mixtures using wood fly ash: Kinetics, mechanism, and effect of ozone, Chemosphere. 78 (2010) 1110–1115. doi:10.1016/j.chemosphere.2009.12.033.

[124] A. Gervasini, G.C. Vezzoli, V. Ragaini, VOC removal by synergic effect of combustion catalyst and ozone, Catal. TODAY. 29 (1996) 449–455. doi:10.1016/0920-5861(95)00319-3.

[125] B. de Rivas, J.I. Gutierrez-Ortiz, R. Lopez-Fonseca, J.R. Gonzalez-Velasco, Analysis of the simultaneous catalytic combustion of chlorinated aliphatic pollutants and toluene over

ceria-zirconia mixed oxides, Appl. Catal. A-GENERAL. 314 (2006) 54–63. doi:10.1016/j.apcata.2006.08.005.

[126] N. Burgos, M. Paulis, M.M. Antxustegi, M. Montes, Deep oxidation of VOC mixtures with platinum supported on Al2O3/Al monoliths, Appl. Catal. B-ENVIRONMENTAL. 38 (2002) 251–258. doi:10.1016/S0926-3373(01)00294-6.

[127] D.R. Lide, CRC Handbook of Chemistry and Physics, 85th ed., Taylor & Francis, Boca Raton, FL, 2004.

[128] Z. Wen, Z. Wang, J. Zhou, K. Cen, A Theoretical Study on the Mechanism and Kinetic of the Reaction between Ozone and Benzene, OZONE-SCIENCE Eng. 31 (2009) 393–401. doi:10.1080/01919510903157879.

[129] Y.-H. Chin, C. Buda, M. Neurock, E. Iglesia, Reactivity of Chemisorbed Oxygen Atoms and Their Catalytic Consequences during CH4–O2 Catalysis on Supported Pt Clusters, J. Am. Chem. Soc. 133 (2011) 15958–15978. doi:10.1021/ja202411v.

[130] M. García-Diéguez, Y.-H. (Cathy) Chin, E. Iglesia, Catalytic reactions of dioxygen with ethane and methane on platinum clusters: Mechanistic connections, site requirements, and consequences of chemisorbed oxygen, J. Catal. 285 (2012) 260–272. doi:http://dx.doi.org/10.1016/j.jcat.2011.09.036.

[131] C.D. Bertol, K.P. Vieira, L.G. Rossato, J. V D'Avila, Microbiological Environmental Monitoring After the Use of Air Purifier Ozone Generator, OZONE-SCIENCE Eng. 34 (2012) 225–230. doi:10.1080/01919512.2012.679871.

[132] J.J. Gaware, P. V Joshi, V. Abrol, Modelling of sterilization and air exchange rates for indoor environment: An application to effect of ozone concentration on room bacteria, INDIAN J. Chem. Technol. 10 (2003) 680–683.

[133] K. Klanova, A. Lajcikova, Use of ozone to reduce bacteria and moulds in the air and on surfaces, INDOOR BUILT Environ. 15 (2006) 81–84. doi:10.1177/1420326X06062344.

[134] B.C. Smith, Fundamentals of Fourier Transform Infrared Spectroscopy, 2nd ed., CRC Press, Boca Raton, FL, 2011.

[135] H.S. Fogler, Elements of chemical reaction engineering, 4th ed., Prentice Hall PTR, Upper Saddle River, NJ, 2006.

Appendix A:
Preliminary comparison of catalytic ozonation of toluene, acetone and benzene

Preliminary catalytic ozonation investigations were conducted on three VOCs including toluene, benzene, and acetone. Preliminary studies showed very similar results for catalytic ozonation of toluene and benzene. This was probably due to similar structure of toluene and benzene. Therefore, acetone and toluene were chosen as model compounds for the main body of this thesis.

A.1. Experimental

Alumina supported manganese oxide catalyst was prepared with the same method that was discussed in Section "*3.1. Catalyst preparation*". Also, experiments were conducted by using a setup similar to Fig 3.3 with the difference that instead of the FTIR analyzer, a GC-MS system was used for gas analysis. CHNS analysis (Vario EL III, Elementar Americas Inc.) was utilized to determine weight percentage of carbon, as adsorbed pollutant and accumulated products, on the catalysts.

When exhaust gas (containing residual ozone and VOC) from the reactor passes through the GC-MS system, unwanted reactions occur due to residence time in the column and relatively high temperatures in the injector, column and detector sections of the GC. Unwanted non-

catalytic reactions between ozone and each model compound were observed during blank tests using the empty reactor, with a maximum conversion of 18, 18, and 15.5% for toluene, benzene and acetone, respectively. The non-catalytic conversion was subtracted from the total conversion by assuming a first order reaction between ozone and each VOC in the gas phase. For this reason, the FTIR system was used for the main body of this work (except these preliminary experiments). The FTIR system provided fast analyses with negligible unwanted reactions between compounds.

A.2. Results and discussion

Fig. A.1 shows conversion of VOC by catalytic oxidation using $MnO_x/\gamma\text{-}Al_2O_3$ (10 wt%) catalyst in the absence of ozone. The data points in Fig. A.1 were obtained under steady state conditions. Catalytic oxidation (without ozone) required operating temperatures higher than 200 °C for removal of acetone, benzene and toluene. Acetone was oxidized much faster than toluene and benzene in the catalytic oxidation and even its complete removal was achieved at 290 °C.

To study catalytic ozonation of toluene, benzene, and acetone, a continuous VOC removal experiment was conducted for each VOC and the results are presented in Fig. A.2. Catalytic ozonation was started at 25 °C and after 150 min the operating temperature was increased to 40 °C without changing the catalyst or feed flow rate. After 120 min, the reaction temperature was increased to 60 °C and kept constant for another 120 min. Then, the reaction temperature was increased to 75 °C. After 90 min, the temperature was increased to 90 °C and the reaction was allowed to continue for another 60 min.

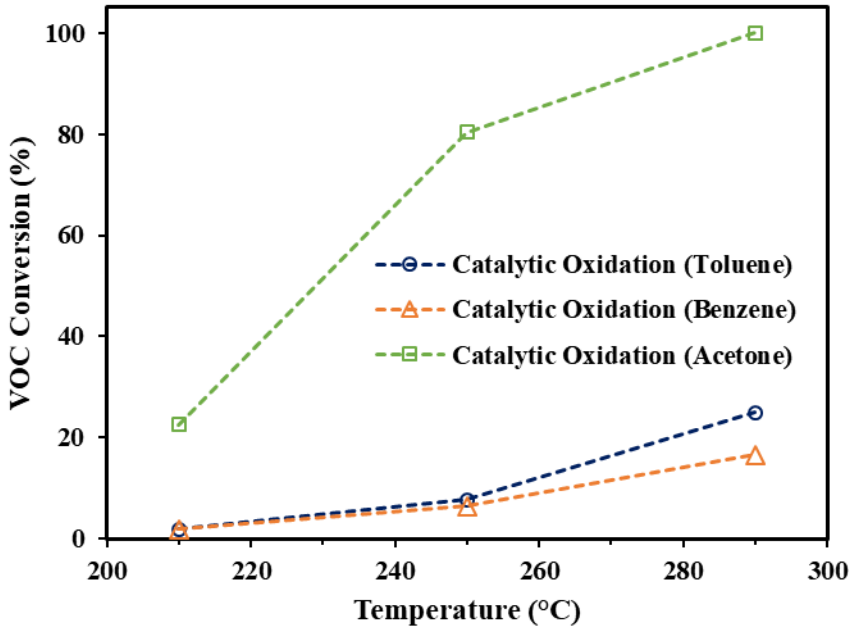

Fig. A.1. Performance of catalytic oxidation in removal of single VOC (120 ppmv) streams of toluene, benzene and acetone; WHSV = 300 L h^{-1} g^{-1}.

A rapid catalyst deactivation occurred at 25 °C and this reduced the VOC conversion dramatically. Temperature increase to 40 °C increased the conversion temporarily, followed by another rapid catalyst deactivation. The temporary rise in conversion is believed to be due to desorption of some VOC and reaction intermediates from the catalyst surface, which led to better adsorption of newly introduced VOC and slightly improved conversion. The increase in conversion was quickly suppressed by continuous deactivation of the catalyst. A similar but more significant conversion rise occurred when the reaction temperature was increased to 60 °C. Further increase of temperature to 75 °C and 90 °C, led to higher conversions for all VOCs.

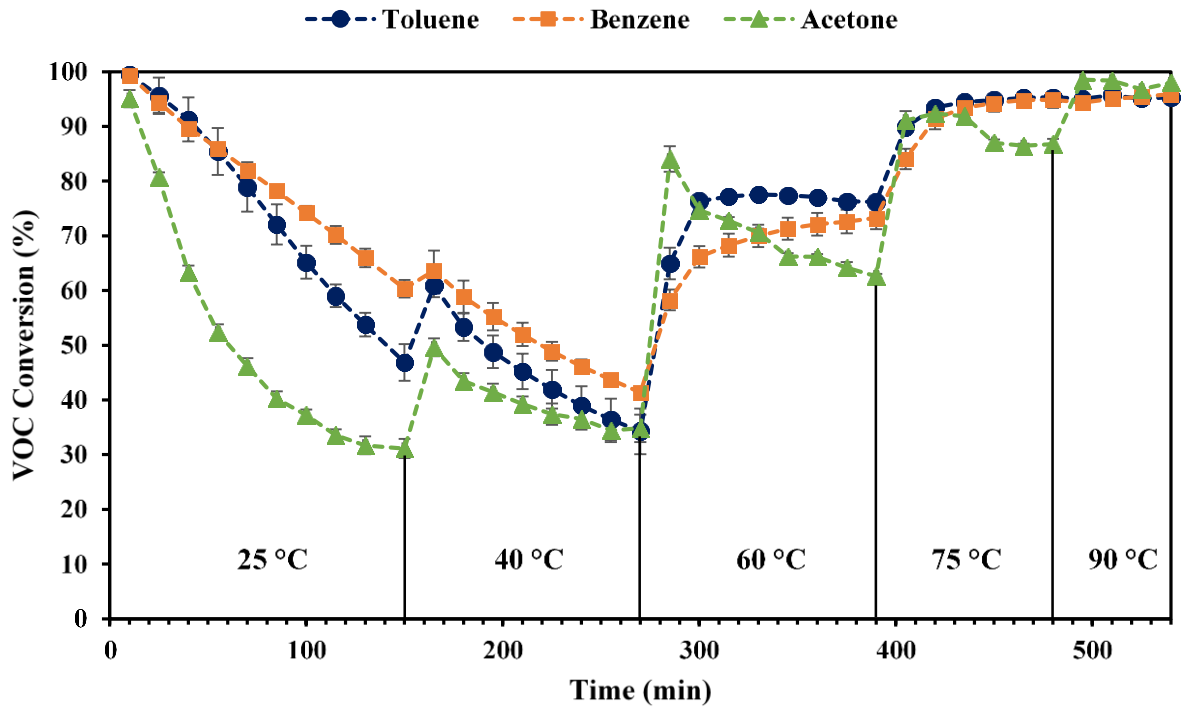

Fig. A.2. Continuous catalytic ozonation of single VOC (120 ppmv) streams of toluene, benzene and acetone at 25 - 90 °C on MnO_x/γ-alumina. WHSV = 300 L h^{-1} g^{-1}, [O_3] = 1100 ppmv; error bars are standard errors.

Another important observation is that the catalyst was regenerated and regained its activity by increase in temperature, indicating that the deactivation was reversible. In other word, the catalyst can be regenerated without changing the gas flow and only by increasing the reaction temperature in the presence of ozone.

Fig. A.3 shows carbon content on the catalysts used for catalytic ozonation of single VOCs at 25 °C. The amount of the measured carbon in these samples includes adsorbed VOCs

and the accumulated carbonaceous products on the catalyst. Carbon content of the fresh catalyst was negligible. Carbon content of the catalyst used for catalytic ozonation of acetone was noticeably less than that of benzene and toluene. The lower carbon contents on the spent catalysts for acetone ozonation may be attributed to the fewer carbon atoms in the chemical structure of acetone. Acetone has three carbon atoms in its structure, while toluene and benzene have 7 and 6 carbon atoms, respectively. Another reason can be deposition of less carbonaceous products on the surface of the catalyst due to significantly lower conversion of acetone at 25 °C, compared to those of toluene and benzene.

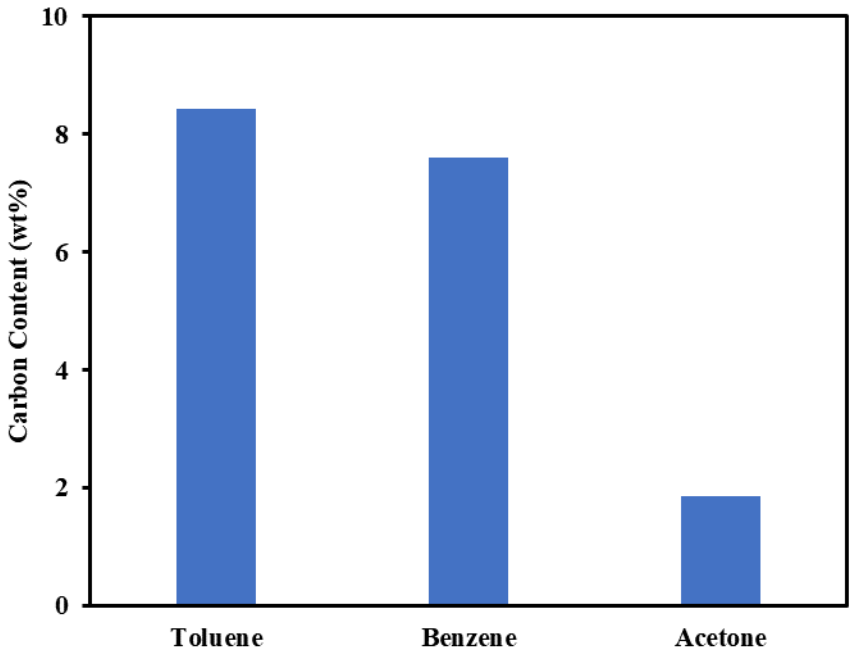

Fig. A.3. Carbon content on the catalysts used for catalytic ozonation of single VOC (120 ppmv) streams of toluene, benzene and acetone at 25 °C; WHSV = 300 L h^{-1} g^{-1}, [O_3] = 1100 ppmv.

Based on the obtained results, it was concluded that toluene and benzene behave very similarly during the catalytic ozonation reaction. In addition, as discussed in Chapter 2 benzene is a mutagenic compound, which needs extra caution during handling and experiments. Therefore, experiments for the main body of the thesis were performed using toluene and acetone only.

As a part of the preliminary studies, catalytic ozonation of a mixture of acetone and benzene at 25 °C was investigated. For this experiment, 240 ppmv of total VOCs was used (120 ppmv of each VOC) and ozone concentration was doubled to 2200 ppmv. Fig. A.4 shows the profiles of conversion of VOCs and ozone versus reaction time.

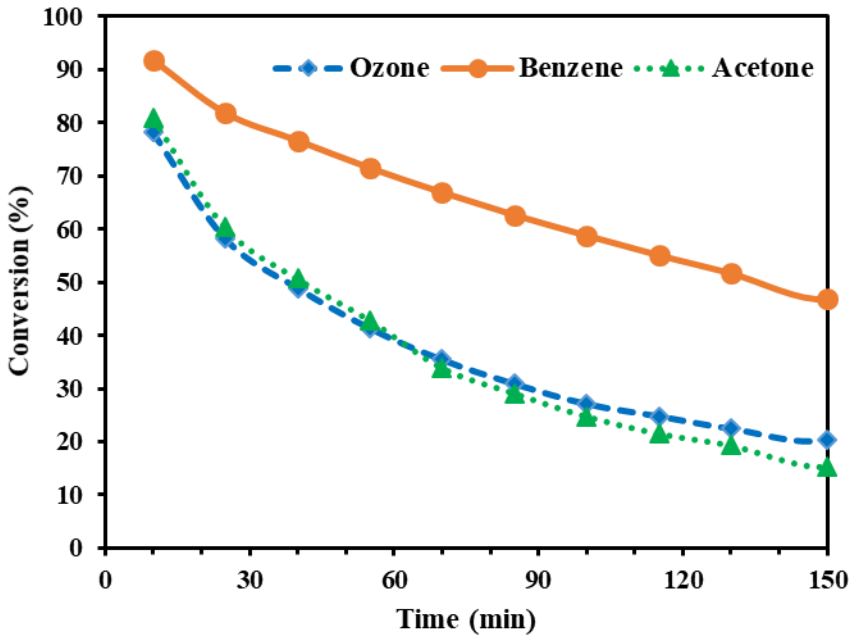

Fig. A.4. Catalytic ozonation of a mixture of acetone and benzene (each 120 ppmv) at 25 °C; WHSV = 300 L h^{-1} g^{-1}, $[O_3]$ = 2200 ppmv.

It can be seen that acetone conversion in the mixture was significantly less than conversion of benzene. Catalytic ozonation of acetone in the mixture with toluene was also repressive for acetone (See Chapter 6). This confirms that the choice of acetone and toluene for the main body of this work was appropriate.

Appendix B:
Calibration data for gas analyses

Concentrations of acetone, toluene, carbon dioxide, and carbon monoxide in the gas stream were analyzed by passing the stream through a long-path gas cell (PIKE, volume 0.1 L, 2.4 m optical length, KBr window), coupled with a Nicolet iS50 FTIR spectrometer. Deuterated L-alanine doped triglycine sulfate (DLaTGS) detector was employed. Spectra were collected at a resolution of 4 cm^{-1} in the range of 4000-400 cm^{-1}.

Calibration curves based on either peak height or peak area can be used for FTIR analyses [134], and both were reliable in quantification of the gases used in this work. The following figures show calibration curves for acetone, toluene, carbon monoxide, and carbon dioxide by using peak height of the peaks at 1737, 729, 2174, and 2361 cm^{-1}, respectively.

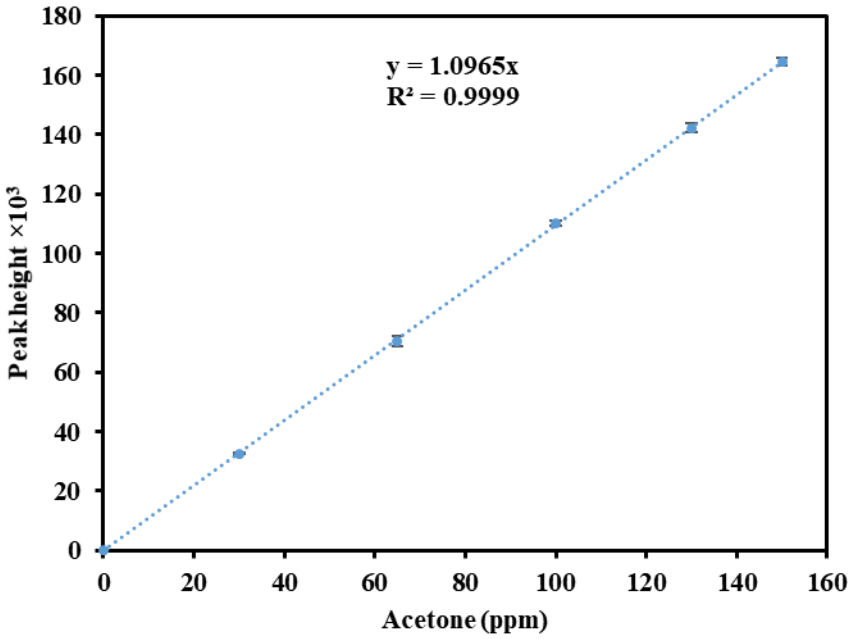

Fig. B.1. Acetone calibration based on peak height at 1737 cm^{-1}; error bars are standard errors.

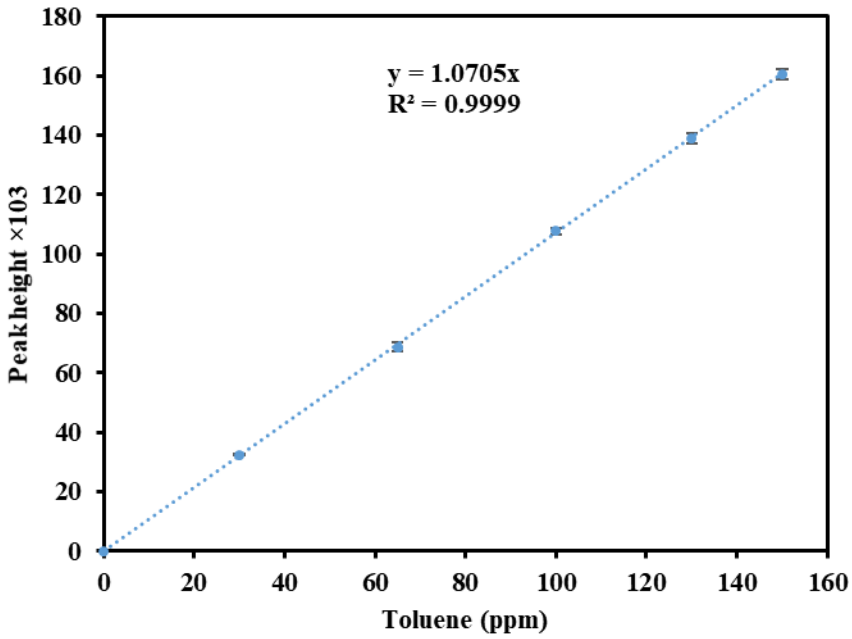

Fig. B.2. Toluene calibration based on peak height at 729 cm^{-1}; error bars are standard errors.

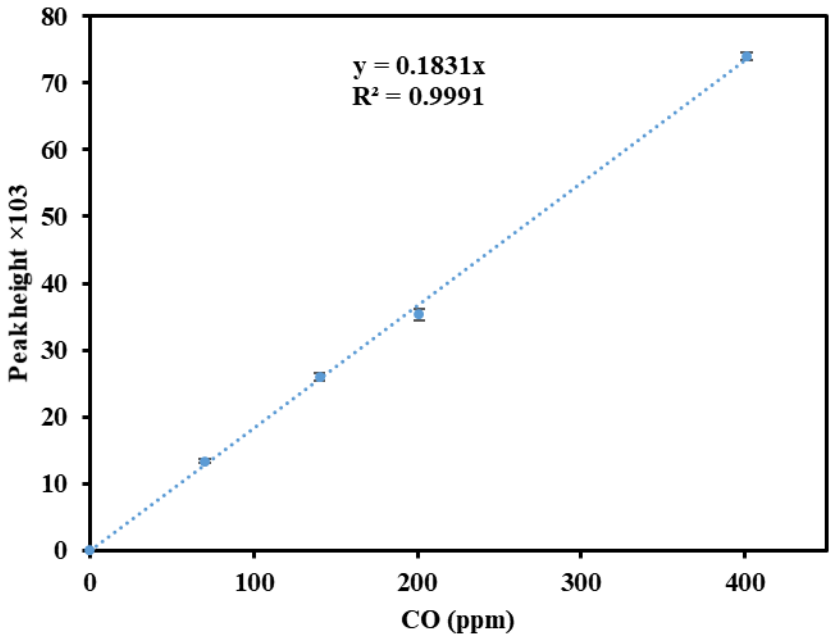

Fig. B.3. CO calibration based on peak height at 2174 cm^{-1}; error bars are standard errors.

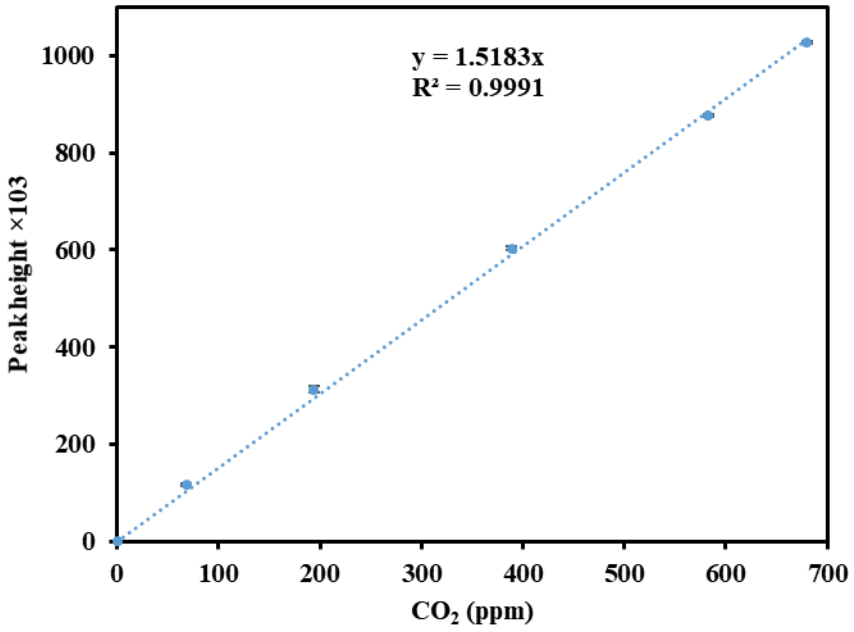

Fig. B.4. CO_2 calibration based on peak height at 2361 cm^{-1}; error bars are standard errors.

Appendix C:
Mass transfer calculations and effect of particle size

Mear's criterion was used to investigate whether external mass transfer is limiting the reaction rate [135]. Based on Mear's criterion if

$$C_M = \frac{-r'_A \rho_b R n}{k_c C_A} < 0.15 \quad \text{(C.1)}$$

then external mass transfer effects are negligible. Parameters in Eq. (C.1) are defined as follows:

$-r'_A$: reaction rate of A (mole kg^{-1} s^{-1})

ρ_b : catalyst bed bulk density (kg m^{-3})

R : radius of the catalyst particle (m)

n : reaction order

k_c : external mass transfer coefficient (m s^{-1})

C_A : bulk concentration of A in the gas phase (mole m^{-3})

The external mass transfer coefficient (k_c) can be calculated by using Frossling equation [135]:

$$Sh = 2 + 0.6 Re^{1/2} Sc^{1/3} \quad \text{(C.2)}$$

where, Sh is Sherwood number, Re is Reynolds number, and Sc is Schmidt number. These dimensionless numbers are defined as:

$$Sh = \frac{k_c d_p}{D_{AB}} \tag{C.3}$$

$$Re = \frac{\rho_g U_g d_p}{\mu_g} \tag{C.4}$$

$$Sc = \frac{\mu_g}{\rho_g D_{AB}} \tag{C.5}$$

Parameters in Eqs. (C.1), (C.2), and (C.3) are defined as follows:

d_p : catalyst particle diameter (m)

D_{AB} : diffusivity coefficient of A in B ($m^2\ s^{-1}$)

ρ_g : density of the gas phase ($kg\ m^{-3}$)

μ_g : viscosity of the gas phase ($kg\ m^{-1}\ s^{-1}$)

U_g : superficial gas velocity ($m\ s^{-1}$)

Chemical and physical parameters used for calculations are presented in Table C.1. Catalytic ozonation reactions at atmospheric pressure and 90 °C were considered for this sample calculation. The following results are obtained for catalytic ozonation of toluene:

$Re = 3.08$ $Sc = 1.91$ $Sh = 3.31$ $k_c = 0.19\ m\ s^{-1}$

Therefore, the Mear's criterion is satisfied as $C_M = 0.028 < 0.15$.

Table C.1. Chemical and physical parameters used for the mass transfer calculations.

Parameter	Unit	Value
d_p	m	2.08×10^{-4}
ρ_g	kg m^{-3}	0.97
μ_g	kg m^{-1} s^{-1}	2.17×10^{-5}
U_g	m s^{-1}	3.31×10^{-2}
R	m	1.04×10^{-4}
ρ_b	kg m^{-3}	500
C_A	mole m^{-3}	0.53×10^{-2}
D_{AB} for toluene	m^2 s^{-1}	1.17×10^{-5}
D_{AB} for acetone	m^2 s^{-1}	1.67×10^{-5}
$-r'_A$ for toluene	mole kg^{-1} s^{-1}	2.69×10^{-3}
$-r'_A$ for acetone	mole kg^{-1} s^{-1}	1.14×10^{-3}

Similarly, the following results are obtained for catalytic ozonation of acetone:

$Re = 3.08$ $Sc = 1.34$ $Sh = 3.16$ $k_c = 0.25$ m s^{-1}

Therefore, the Mear's criterion is satisfied as $C_M = 0.005 < 0.15$. Hence, external mass transfer effects can be neglected.

Using a small enough catalyst particle size eliminates internal mass transfer limitations [135]. For this purpose, different particle sizes in the range of 0.080 to 0.417 mm were examined for the catalytic ozonation reactions. The results are depicted in Fig. C.1 and Fig. C.2.

It can be seen that activity of the catalyst activity for catalytic ozonation of acetone declines when particle size is larger than 0.355 mm. On the other hand, the catalyst for catalytic ozonation of toluene decreases when particle size is larger than 0.208 mm. Therefore, catalyst particle size of smaller than 0.208 mm was used for all catalytic ozonation reactions.

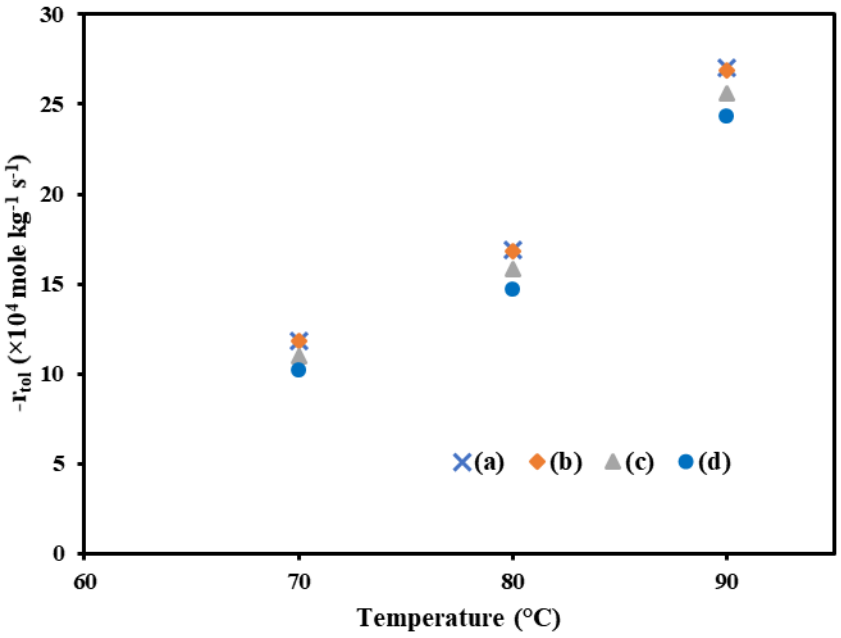

Fig. C.1. Effect of particle size on the catalyst activity in catalytic ozonation of toluene; (a) <0.080 mm, (b) 0.080-0.208 mm, (c) 0.208-0.355 mm, (d) 0.355-0.417 mm.

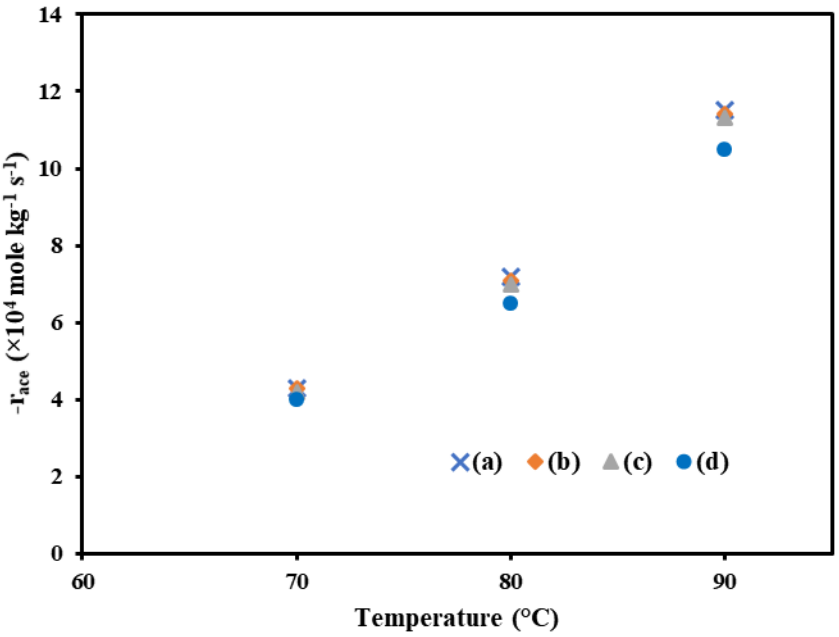

Fig. C.2. Effect of particle size on the catalyst activity in catalytic ozonation of acetone; (a) <0.080 mm, (b) 0.080-0.208 mm, (c) 0.208-0.355 mm, (d) 0.355-0.417 mm.

Appendix D:
FTIR functional groups

Table D.1. Significant bands observed during in situ DRIFTS studies of catalytic ozonation of VOCs and the corresponding functional groups.

Significant band (cm^{-1})	Assigned functional groups
1308 - 1393	Methyl C-H bending, and antisymmetric and symmetric COO^- stretching of carboxylates
1410-1429	C-H asymmetric deformation vibration
1453	Aromatic ring stretching
1462	Methyl and methylene C-H bending
1498	Aromatic ring stretching
1570-1605	antisymmetric and symmetric COO^- stretching of carboxylates
1702-1740	C=O stretching of ketones and carboxylic acids
1854	C=O stretching of anhydrides
2350	Adsorbed carbon dioxide
2871 - 2988	Saturated C-H stretching
3008 - 3072	Unsaturated C-H and aromatic C-H stretching
2400 - 3750	OH stretching of alcohols, carboxylic acids and water

Appendix E:

Permissions to use the published papers

This Agreement between Mr. Mostafa Aghbolaghy ("You") and Springer ("Springer") consists of your license details and the terms and conditions provided by Springer and Copyright Clearance Center.

Your confirmation email will contain your order number for future reference.

Printable details.

License Number	4166021032678
License date	Aug 11, 2017
Licensed Content Publisher	Springer
Licensed Content Publication	Catalysis Letters
Licensed Content Title	Role of Surface Carboxylates in the Gas Phase Ozone-Assisted Catalytic Oxidation of Toluene
Licensed Content Author	Mostafa Aghbolaghy
Licensed Content Date	Jan 1, 2017
Type of Use	Thesis/Dissertation
Portion	Full text
Number of copies	1
Author of this Springer article	Yes and you are the sole author of the new work
Order reference number	
Title of your thesis / dissertation	Catalytic ozonation of acetone and toluene on alumina-supported manganese oxide
Expected completion date	Nov 2017
Estimated size(pages)	180
Requestor Location	Mr. Mostafa Aghbolaghy 57 Campus Dr. College of Engineering Saskatoon, SK S7N 5A9 Canada Attn: Mr. Mostafa Aghbolaghy
Billing Type	Invoice
Billing address	Mr. Mostafa Aghbolaghy 57 Campus Dr. College of Engineering Saskatoon, SK S7N 5A9 Canada Attn: Mr. Mostafa Aghbolaghy
Total	0.00 CAD

Fig. E.1. Permission to use the published paper “Role of Surface Carboxylates in the Gas Phase Ozone-Assisted Catalytic Oxidation of Toluene”.

Fig. E.2. Permission to use the published paper “The Role of Surface Carboxylates in Catalytic Ozonation of Acetone on Alumina-Supported Manganese Oxide”.